Me 163

ACTA POLYTECHNICA SCANDINAVICA

MECHANICAL ENGINEERING SERIES No. 163

Numerical Modeling of the Drying, Devolatilization and Char Conversion Processes of Black Liquor Droplets

MIKA PETTERI JÄRVINEN

Helsinki University of Technology
Department of Mechanical Engineering
Otakaari 4, FIN-02015 HUT
FINLAND

Dissertation for the degree of Doctor of Science in Technology to be presented with due permission of the Department of Mechanical Engineering, Helsinki University of Technology, for public examination and debate in Auditorium K216 at Helsinki University of Technology (Espoo, Finland) on the 13th of December, 2002, at 12 o'clock noon.

ESPOO 2002

Järvinen, M., P., **Numerical Modeling of the Drying, Devolatilization and Char Conversion Processes of Black Liquor Droplets**, Acta Polytechnica Scandinavica, Mechanical Engineering Series No. 163, Espoo 2002, 77 p., Published by the Finnish Academy of Technology, ISBN 951-666-617-5 ja ISSN 0001-687X

Keywords: Black liquor combustion, numerical modeling, drying, devolatilization, char conversion

ABSTRACT

In this work a detailed physical single particle combustion model for black liquor was developed. As a difference to previous models, intra-particle mass transfer during drying and devolatilization was considered, in addition to heat transfer. Relevant chemical reactions and experimentally observed physical combustion phenomena e.g. swelling were implemented. The model was widely tested against experimental data. Char conversion mechanisms were studied in laboratory reactor and furnace conditions addressing the relevant reaction mechanisms needed for developing simplified particle combustion sub-models for use in combination with CFD (Computational Fluid Dynamics).

The model succeeded well in predicting experimentally observed combustion behavior. Release rates and yields of mass and carbon were well predicted for the cases studied. The model also succeeded well in predicting particle temperatures during combustion. Values for particle thermal conductivity, devolatilization heat, swelling and shrinkage parameters could be obtained by sensitivity analysis and experimental verification.

A novel char conversion mechanism was found by the model, referred to as auto-gasification. Char conversion may take place already during devolatilization as H_2O and CO_2 flow out from the particle interior and pass through the hot, pyrolyzed particle surface. This auto-gasification mechanism could not be fully validated experimentally. However, an excellent correlation with experimental data was obtained when this mechanism was included.

It was shown that char conversion mechanisms for black liquor essentially differ from those for other fuels. It was observed that at typical recovery boiler temperatures and gas compositions dominating char conversion mechanisms are H_2O gasification, CO_2 gasification and carbonate reduction, under non-convective conditions. When convective effects are present, the role of direct char oxidation increases. For high slip velocity conditions, the overlapping of devolatilization and char oxidation is an issue as O_2 can reach the particle surface more easily. The concept of envelope flame under furnace conditions should be re-evaluated.

The results from this study suggest that the development of a simplified CFD particle combustion model requires the proper understanding of physical and chemical processes taking place in the particle during combustion. In order to transfer the experimental observations to furnace conditions, the relevant mechanisms that take place need to be understood before the important ones can be selected for CFD-based modeling.

PREFACE

This work has been carried out at the Laboratory of Energy Engineering and Environmental Protection, Helsinki University of Technology. Work has been funded by the National Technology Agency of Finland, Tekes (year 1998: as a separate Tekes project 244/401/97, years 1999-2002: as a Tekes/CODE-Technology Program, project 103), Andrizt-Ahlstrom Corporation, Walter Ahlström Foundation and the Academy of Finland (Project No. 53606) and Helsinki University of Technology. These all are acknowledged for making this work possible.

I especially want to thank the instructors and co-authors Dr. Ron Zevenhoven and Dr. Esa Vakkilainen for many valuable discussions and the time that they gave me. Professor Carl-Johan Fogelholm is acknowledged for giving me the possibility to do this interesting research work at the laboratory, many useful comments and also for helping to keep up the schedule. I wish to thank my co-author Mikaél Forssén from Åbo Akademi, for many valuable discussions on experimental work and possibilities for model validation. I hope that this work will continue for bringing the experimental work and modeling more closer to each other. I also thank my colleagues Ari Kankkunen and Pasi Miikkulainen for being always ready for listening and commenting my ideas and other non-organized hum that just appeared in my mind.

There are no words for expressing my gratitude to my parents and grandmother for giving me the support and best guidance for life. I also like to thank other members of my family and friends for their support.

Finally, I thank my wife Paula for her love and support. She helped me to remember the basic things in life and gave me an irresistible reason to use my time more effectively.

Mika Järvinen

Espoo 18th November, 2002

CONTENTS

NOMENCLATURE

A	diffusion matrix, -
A_s	specific surface area, m^2/g
a	stoichiometric matrix
A	frequency factor, 1/s
a_R	Rosseland mean absorption coefficient, 1/m
B_0	permeability, m^2
B	parameter in flame models, -
Bi	Biot number = $(aL_c)/?$
c	concentration, $mole/m^3$
$\dot{c}_i$	source term for chemical species j, mol/m^3 s
C_p	molar heat capacity, J/mol K
d	pore/particle diameter, m
$Đ_{i,j}$	molecular diffusion coefficient, m^2/s
$D_{i,j}$	effective diffusion coefficient, m^2/s
$Đ_K$	Knudsen diffusion coefficient, m^2/s
D_K	effective Knudsen flow parameter, m^2/s
Da	Damkohler number
E	activation energy, J/mol
e	m/m_0 during devolatilization, -
G	iteration residual vector
h	heat transfer coefficient, W/m^2K
h_m	mass transfer coefficient, m/s
H	molar enthalpy, J/mol
J	Jakobian matrix
K	equilibrium constant, -
k	specific reaction rate, unit depends on reaction order
k_r'''	reaction rate per particle volume, 1/s
L_c	characteristic length, m
M	molecular mass, g/mol
$\dot{m}$	mass flow rate, kg/s
N, $\dot{N}$	mole amount, molar flux, mol, mol/s
Nu	Nusselt number = $(ad)/?$
p	pressure, Pa
P	pyrolysable matter
Pe	Peclet number
Q, $\dot{Q}$	heat, heat flux, J, W
r	radial coordinate, m
R	reaction rate vector, heat resistance, mol/m^3 s, K/W
R_u	universal gas constant, J/mol K
Re	Reynolds number
s	swelling number
S	interfacial area, m^2
Sh	Sherwood number = $(hd)/D_{AB}$
T	absolute temperature, K
t	time, s
u	velocity, m/s

x	mole fraction, -
X	conversion, -
y	mass fraction, -

Greek letters

α	heat transfer coefficient, W/m^2 K
β	volumetric swelling coefficient, -
G	under-relaxation parameter of iteration
Δh	specific reaction heat, J/kg
Δx	correction of iterative method for variable x
Δr	radial space increment, m
Δt	time step, s
e	emissivity, -
h	effectiveness factor
l	thermal conductivity, W/m K
m	dynamical viscosity, Pas
x	coefficient, -
r	density, kg/m^3
s	Stefan-Bolzman constant = 5.67 10-8 W/m^{2}K^4
t	tortuosity, -
f	porosity, -
f_1	Thiele number
ψ	weighed rate, mol/m^3 s

Subscripts

b	boiling
BL	black liquor
c	char, convection
dry	drying
e	effective
g	gas
K	Knudsen
p	devolatilization
r	reaction, radiation
s	solid, surface

1 INTRODUCTION

1.1 Kraft recovery boiler processes and principles of black liquor combustion

Black liquor is a by-product of chemical pulping. Black liquor is often called a waste although it contains valuable energy and most importantly, converted expensive inorganic cooking chemicals. There are several processes which have been developed for recovering the organic combustion heat and chemicals as effectively as possible. The most common process is called the kraft pulping process where Na_2S and NaOH are used as cooking chemicals.

In the US, 80 000 000 tons of black liquor (calculated for 25% water content liquor) is burnt in recovery boilers every year. That corresponds to over 1% of the US total heat and power generation, Macek (1999). In Northern Europe, black liquor plays even a more important role. In Finland and Sweden black liquor combustion covers 7 and 4.5% of the total heat and power generation, respectively. This corresponds in both cases to roughly 30% of the heat and power generated from biofuels, Asplund (1997).

The principles of kraft pulping are shown in Figure 1.1. First, wood fibers are separated from the wood by chemical cooking. The active chemicals in the Kraft process are NaOH and Na_2S. The fibers are then washed and the this pulp is used to make paper products. The residual material is called weak black liquor, containing 80-85% water, inorganic chemicals and the rest of the organic material from wood. After a significant evaporation, the water content of liquor is 20-25%. This strong black liquor is then sprayed into the recovery boiler furnace for releasing the organic combustion heat and to recover the inorganic chemicals. Na_2CO_3 is converted later back to NaOH by the caustizing process.

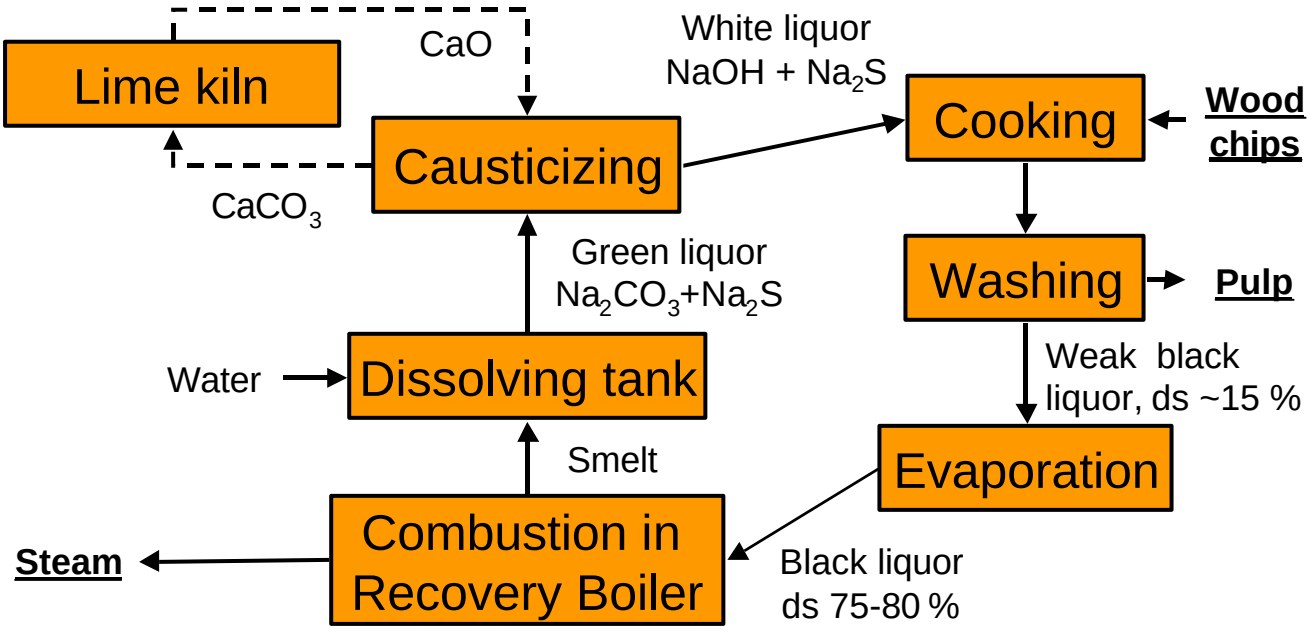

Figure 1.1. Schematic of the kraft pulping process

The liquor is usually sprayed into the recovery furnace using splashplate nozzles that produce large droplets, with a mass median droplet size of 3-5 mm, Kankkunen (2001). Subsequent to spraying, black liquor droplets go through drying, devolatilization and char conversion stages of combustion, see Figure 1.2., Hupa *et al.* (1987), Adams *et al.* (1997).

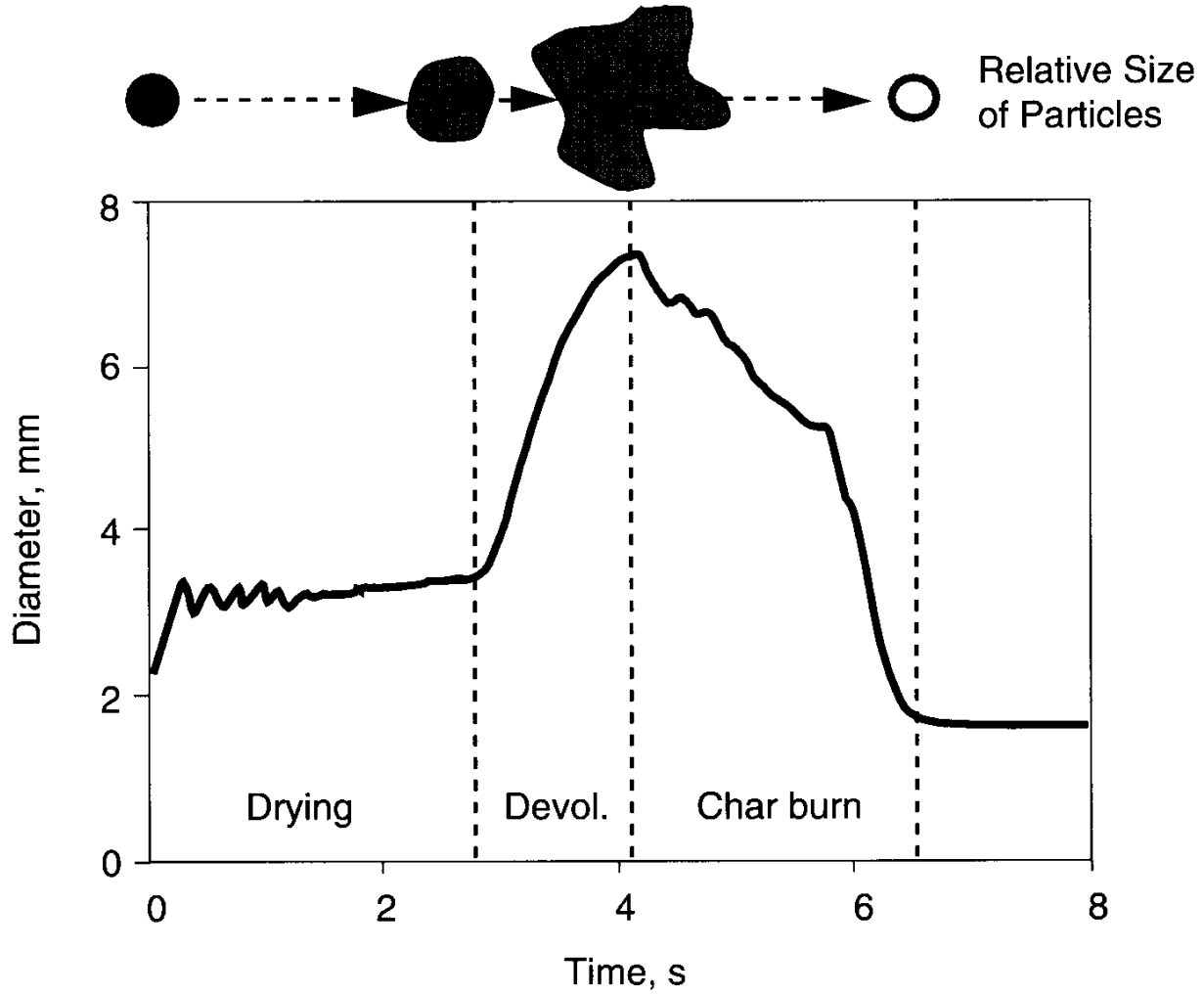

Figure 1.2. Stages of black liquor combustion, Hupa *et al.* (1987).

Black liquors swells significantly during devolatilization. Its diameter may increase by a factor of 3-4, which affects the flight path and rate of conversion processes. In order to have a good efficiency of chemical reduction and effective boiler operation, most of the droplets should hit the char bed located at the furnace bottom dry and containing organic material that is required for chemical reduction, droplet (a), Figure 1.3. If all char is burned from the droplets during in-flight combustion i.e. droplet size is too small, the desirable species sulfide, Na_2S, will be partly oxidized and the reduction efficiency of the furnace will decrease, droplet (b). Still smaller droplets are entrained with flue gases up to the heat transfer surfaces of the boiler, causing fouling and increased emissions of the boiler, droplet (c).

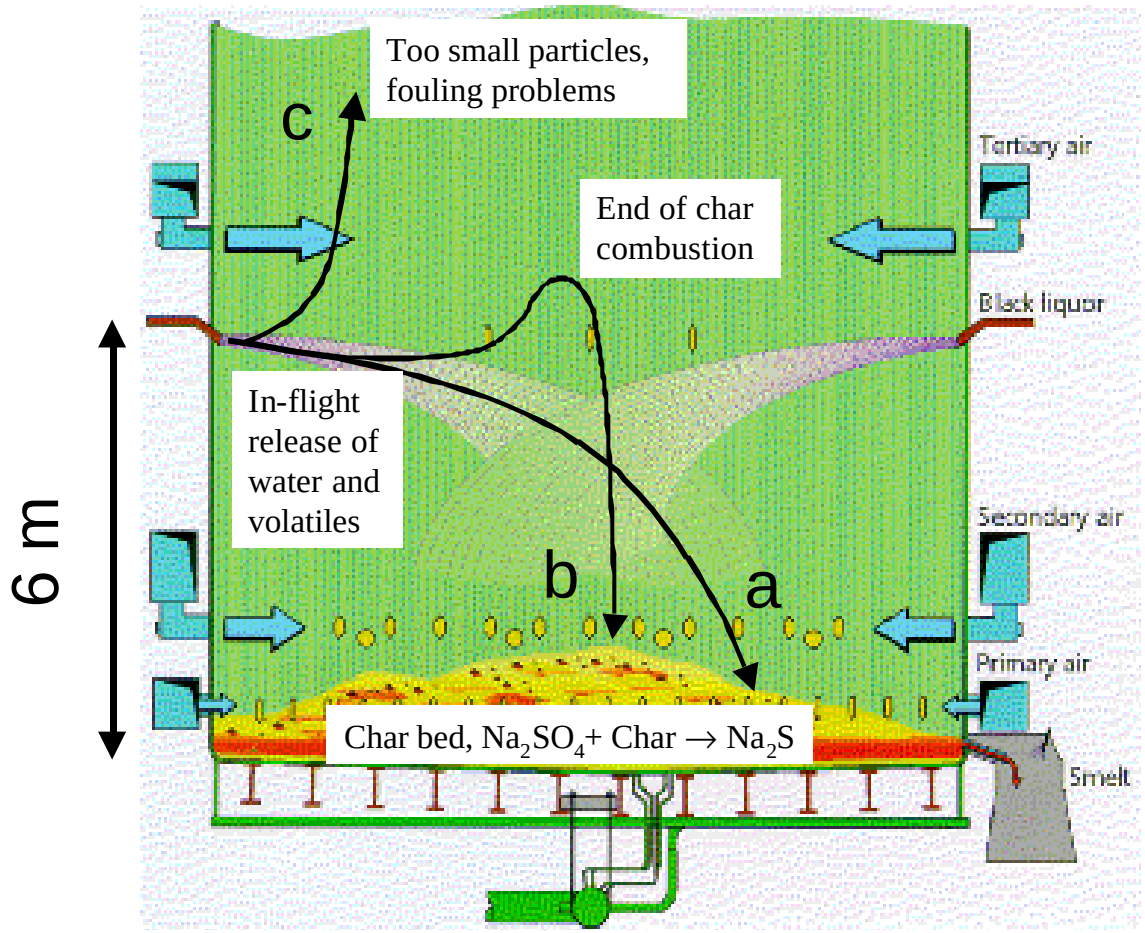

Figure 1.3. Lower furnace recovery boiler processes

1.2 Modeling of black liquor combustion

The large, 3-5 mm droplet size of black liquor makes the combustion modeling very challenging. It was first noted by Frederick (1990a) that black liquor particles are so large that the temperature distribution inside the particle should be considered. The first model to accurately account for this behavior was presented by Saastamoinen (1993a). Verrill (1995a) presented a similar single particle model to consider temperature distribution inside the particle, and this model was used also in CFD calculations, Verrill *et al.* (1995b), Wessel *et al.* (1997).

Black liquor combustion in a recovery boiler has been modeled since 1980 by Merriam (1980). The simplest approach is to assume that the flow field remains constant. The trajectory of particles and the release locations of different species can then be easily calculated. This method is called the *fixed flow field approach*. Its greatest benefit is that complex particle combustion models can be used and calculation times are short. More detailed information on furnace-scale combustion can be obtained by solving simultaneously for the gas flow and trajectories of the particles and release of species from them by using a CFD solver. In this case, the single particle combustion sub-model needs to be very simple as the solution for the reacting, non-isothermal flow field itself is very time consuming.

Combustion of black liquor has been experimentally studied since the 1980's, Hupa *et al.* (1987). At first, the general combustion characteristics were studied. Swelling behavior, total release

fraction of different species and the duration of different combustion stages were well defined under laboratory scale reactor conditions. On the basis of these data, the first simple black liquor combustion models could be developed. As understanding increased, models were further developed. The rate expressions for char gasification and inorganic reactions were experimentally determined. As on-line analysis systems developed we obtained valuable information on the rate of different processes, and the fraction of pyrolysable and fixed carbon, sulfur and nitrogen could be identified. Recently, for the very first time, valuable data on the release of carbon, sulfur and nitrogen species were obtained by simultaneously recording the particle swelling, Forssén *et al.* (2001), Paper IV.

It should be realized that the flow conditions in a furnace are very different from a laboratory scale reactor. In the early stages of combustion the slip velocity between the particle and gas being far from stagnant might well exceed 10-20 m/s. As can be realized, this will have a huge effect on the heat and mass transfer processes at the particle scale. Slip velocity will decrease as devolatilization swelling takes place but still, significant convective effects will be present. This work will concentrate on developing a method that can be used to transfer the experimental observations to a furnace environment. Internal heat and mass transfer as well as the description of the external heat and mass transfer will be studied in detail.

1.3 Outline of the work

What was known scientifically prior to this work is reviewed in Chapter 2. This information is summarized in Chapter 3. On the basis of this, the research problem for this work was formulated. A new one-dimensional heat and mass transfer model in porous media with reacting internal flow is presented in Chapter 4 and the application of this to black liquor is shown in Chapter 5. Chapters 6 and 7 focus on the experimental validation and verification of the model. Chapter 8 presents the most important results and findings from this work. Finally, Chapter 9 concludes and gives the main recommendations from this work.

In addition to this summarizing introductory part, most of the work done is presented in the following seven appendix papers.

I. Järvinen, M., Zevenhoven, R. and Vakkilainen, E. Auto-gasification of Large Black Liquor Droplets. Apollonia '99 Joint Meeting of 4th Workshop on Transport Phenomena in Two-Phase Flow and EFCE Working Party on Multiphase Fluid Flow. September 11-16, Sozopol, pp.17-22.

II. Järvinen Mika, Zevenhoven Ron, Vakkilainen Esa and Forssén Mikael. Black Liquor devolatilization and Swelling – Detailed Droplet Model and Experimental Validation. Accepted for publication in Biomass and Bioenergy (2002).

III. Järvinen, M. P., Zevenhoven, R. and Vakkilainen, E. K. Importance of Different Char Conversion Mechanisms in Black Liquor Combustion – A Detailed Modeling Approach, Presented at the International Chemical Recovery Conference 2001, Whistler, Canada.

IV. Forssén, M. and Järvinen, M. Liquor-to-liquor differences in combustion and gasification processes: Simultaneous measurements of swelling and CO_2, CO, SO_2 and NO formation reveals new data for mathematical models. Presented at the International Chemical Recovery Conference 2001, Whistler, Canada.

V. Järvinen, M. P., Zevenhoven R., Forssén, M. and Vakkilainen E. K. Effective thermal conductivity and Internal Thermal Radiation in Porous Black Liquor Solids. Accepted for publication in Combustion Science and Technology (2002)

VI. Järvinen, M. P., Zevenhoven R. and Vakkilainen E. K. Auto-Gasification of a Biofuel. Accepted for publication in Combustion and Flame (2002).

VII. Mika Järvinen, Ron Zevenhoven, Esa Vakkilainen, (2002) Implementation of a detailed black liquor combustion model for furnace calculations. Published in IFRF Combustion Journal, Article No. 200206, June 2002. http://www.journal.ifrf.net/articles.html

The disputant has been the leading author in Papers I-III and V-VII. Before paper I was written, the disputant had personally developed the first version of the detailed numerical heat and mass transfer/combustion model and written the Fortran 77 simulation code. Discussions with co-authors Vakkilainen and Zevenhoven helped in selecting the chemical expressions and physical sub-models. Vakkilainen and Zevenhoven also contributed comments for all the papers.

Based on detailed numerical simulations, a new char conversion mechanism referred as "auto-gasification" was presented in Paper I. Surface char layer is gasified by the out-flowing H_2O and CO_2. This paper neglected the inorganic reactions. The disputant carried out all the simulations and wrote most of the paper.

In Paper II, the role of swelling and non-homogeneous internal structure on devolatilization and auto-gasification was studied. The disputant acted as the leading author, wrote most of the text and carried out all the simulations. For this paper, inorganic reactions were implemented for the model by the disputant. The new experiments carried out for this paper were partly planned in co-operation with Åbo Akademi University, but the actual tests were done by M. Forssén, at ÅA. Forssén also actively contributed his comments on the paper.

In Paper III, the dominating char conversion mechanisms in a stagnant recovery boiler environment were studied. The model was also validated with temperature measurements and swelling/size reduction data available from the literature. The disputant was the leading author for this paper.

Paper IV was mainly written by Forssén, the disputant wrote the modeling part and carried out the combustion simulations for comparison with experiments in 3-21% O_2/N_2. A role for overlapping devolatilization and char conversion was shown by the disputant's combustion simulations.

Paper V studied the role of intra-particle thermal radiation. The paper was mainly written by the disputant, some of the experimental results from Paper IV, were used for validation. The parameters for internal thermal radiation model were isolated by fitting the model for experimental carbon release and swelling data. Forssén took the microscopic photographs of pore structure, the disputant carried out the image analysis procedures for clarifying the pore structure. Forssén also actively commented on the paper.

Paper VI discussed the same phenomena as Paper I. At this point, the model was validated and compared with experimental data. The auto-gasification was analyzed in greater detail and relevant mechanisms were generally discussed. The disputant acted as the leading author.

Finally, in the Paper VII, the detailed model was implemented to a flight path calculation procedure to see the effect of continuously changing boundary conditions and to study the requirements for developing a simplified CFD sub-model. A simplified CH_4/CO oxidation scheme was implemented into the model and also, a localized gas oxidation model was developed for furnace calculations. The disputant acted as the leading author for this paper, and he implemented all the new sub-models and carried out all the calculations and simulations.

2 LITERATURE REVIEW

The purpose of this chapter is to review the relevant literature and work prior to this thesis. We will start with a review of the general combustion behavior of black liquor. As the experimental work is the basis for important validation and verification of some model parameters, we will also concentrate on this aspect of the study. The different experimental configurations will be reviewed and their application to modeling work will be critically discussed. The existing single particle combustion models developed for black liquor will be examined, including their properties, assumptions and relevancy to the modeling of different combustion conditions.

2.1 Black liquor as a fuel

The purpose of this section is to present the general combustion characteristics of black liquor and to compare black liquor properties with other fuels. Table 2.1 shows a comparison of black liquor, wood and two coals in terms of elemental composition and the most important combustion properties that also affect the selection of a modeling approach.

Table 2.1. Comparison of black liquor with other fuels

	Black liquor	***Wood Pine***	***Coal Gardanne***	***Coal Göttelborn***
C, dry	38.2 [1]	48.9 [4]	48.0 [4]	72.4 [4]
H, dry	3.4 [1]	6.0 [4]	3.2 [4]	4.8 [4]
O, dry	31.1 * [1]	43.8 ** [4]	19.7 ** [4]	11.1 ** [4]
S, dry	5.2 [1]	0.06 [4]	4.2 [4]	1.0 [4]
Na, dry	19.8 [1]	0.003 [4]	0.03 [4]	0.04 [4]
K, dry	1.9 [1]	0.051 [4]	0.07 [4]	0.2 [4]
Cl, dry	0.1 [1]	<0.01 [4]	0.09 [4]	0.09 [4]
N, dry	0.1 [1]	0.17 [4]	1.2 [4]	1.5 [4]
Moisture, %	15-30 [1]	40	30 [5]	1 [4]
Ash, % dry	40 [1]	0.5 [4]	31.4 [4]	18.1 [4]
Fuel ratio	0.25 [1]	0.09 [4]	0.47 [4]	1.58 [4]
Relative reactivity*	9900 [2]	30 [4]	15 [4]	1 [4]
Swelling, d/d_0	3-4 [1]	-	-	-
Particle size, mm	3-5 [3]	0.1-100	0.01-50 [5]	
HHV, MJ/kg	14 [1]	19.1 [4]	18.7 [4]	30 [4]

[1] Adams *et al.* (1997), [2] Li *and van Heiningen* (1991), [3] Kankkunen *et al.* 2001, [4] Zevenhoven *and Hupa* (1997), [5] Bartok and Sarofim (1991), *H_2O gasification at 900 °C, reactivity normalized to Göttelborn Coal, * by difference, ** measured

As Table 2.1 shows, black liquor contains a large amount of inorganic matter (Na, K, S) i.e. the chemicals from the pulping process. As the sodium effectively catalyzes gasification reactions, the reactivity of black liquor is many magnitudes higher than for other fuels.

Another important factor is the swelling behavior, the diameter of the particle may increase by a factor of 3-4 during devolatilization. This effectively increases the external reaction surface area, which affects the rate of external heat and mass transfer controlled processes. Also, swelling opens pore volume for internal mass transfer, internal reactions and also for internal thermal radiation. What should be noted is that the sprayed droplets are not initially spherical, Kankkunen *et al.*

(2001) and do not keep their original shape during swelling, although only spherical particles are considered in this work.

Black liquor water content is relatively high, but lower than for wood. In modern recovery boilers the water content of the black liquor burned approaches 15-20%, which means that problems related to this (*e.g.* risk of water smelt explosion) will be smaller. As Table 2.1 also shows, the fuel ratio (char/volatile matter) of black liquor is very low which means that most of the organics will burn in the gas phase. This increases the rate of combustion and makes the conversion of larger particles more effective.

For black liquor combustion the particle size is typically 3-5 mm in modern recovery boilers, Kankkunen *et al.* (2001). For pulverized wood combustion particle size is very small, Saastamoinen (2000) and very large for combustion on a grate for small scale applications (logs). For pulverized coal combustion, particle size is 10-100 µm and if burned in a stoker furnace, particles of 10-50 mm are used, Bartok and Sarofim (1991). Small pulverized particles may be approximated as being isothermal which greatly simplifies their single particle modeling. For example, single particle combustion sub-models for CFD use can then be more easily developed. For thermally large particles, internal heat transfer and also mass transfer needs to be considered which considerably complicates the model requirements and development.

From the boiler operation point of view black liquor is a very difficult fuel as it has high ash content and more importantly, black liquor ash has a very low melting point that may give rise to severe boiler fouling problems, Adams *et al.* (1997).

2.2 Experimental validation for black liquor combustion models

The development of a proper black liquor combustion model is not possible without experimental work. The observations on swelling behavior, extremely reactive char and other typical black liquor combustion properties could not be theoretically verified. When validating the developed combustion models, experimental results are required. Different experimental setups are developed for studying specific properties. For example, a laminar entrained flow reactor LEFR could be well suited to determining devolatilization kinetics as the particle size is thermally small $Bi < 0.1$ and small time increments can be used. However, these results can not be used to validate the combustion behavior of 2-5 mm particles as the physical mechanisms are completely different. Opposed to this, intrinsic reaction kinetics can not be derived from larger particles as they are not isothermal and the role of chemical or physical phenomenon can not be isolated.

When validating a model, it should be assured that the model and experimental geometry and set-up are similar enough, i.e. we actually model the same phenomena that has been experimentally studied. For example, the temperature of the thermal radiation source can be different from the convective one or the thermal delays are not well established. Data should not be used before the experimental procedure has been understood.

2.2.1 Small particles, determination of chemical kinetics

Small particle size is required for determining reaction kinetics. Particles should be thermally small (Bi<0.1). Mass transfer resistances should also be absent. For larger particles, heat and mass transfer are controlling and the kinetics cannot be experimentally determined. There are several

experimental configurations that use small particle size. The laminar entrained flow reactor (LEFR), Shricharoenchaikul *et al.* (1995), grid heater (GH), McKeough *et al.* (1995) and the packed bed reactor (PBR), Li and van Heiningen (1990a) are the most used for black liquor. The LEFR and GH are primarily used for studying the kinetics of devolatilization and the release rates of different species during devolatilization. In a LEFR, heating rate is defined by the particles size and temperature history needs to be calculated. In a grid heater, heating rate is predetermined, however, the temperature of the particles can not be fully controlled due to the limited heat transfer rate between the grid and particles, Saastamoinen (1993a). The PBR is primarily used to study the rate of gasification. As the focus of this work is more on larger particles, these reactor types are not discussed in greater detail here.

For a typical droplet size distribution, the mass fraction of 0.1 mm particles formed in spraying is roughly 1% (mean size 6.5 mm, square root normal distribution). These small particles can be a very important source of boiler fouling problems and important for furnace radiation. It was also suggested by Tamminen *et al.* (2001), Verrill *et al.* (1998) and Kochesfahani *et al.* (2001) that a much more significant fraction of small particles (Intermediate Sized Particles, ISP, 1-100 µm) are also formed during combustion. The secondary combustion of these should also be considered in furnace modeling.

2.2.2 Large particles, determination of physical behavior

The mean droplet size in modern kraft recovery boilers is 3-5 mm, Kankkunen (2001). The combustion time of these large droplets can be in the order of tens of seconds. There are two main experimental approaches used for studying these large droplets: a) a droplet can be suspended from a wire or set into a crucible and inserted into a reactor for a predetermined time or b) a free fall reactor can be used where residence time is controlled by adjusting the length of the particle's flight path. As the particles are very large, free fall reactor dimensions need to very large to obtain residence times of 5-10 s. No such facilities are currently available and the fixed position approach is more common. The droplets are usually attached to a small metal hook (diameter 0.1-0.3 mm), Hupa *et al.* (1987). The maximum particle size that can be used is 2-2.5 mm, larger droplets will not stay attached to a hook as their particle viscosities are significantly reduced when they are heated to their boiling points. The effect of the metal hook on particle heat transfer rate was studied by Saastamoinen (1993a) and Verrill *et al.* (1995a), it was approximated that a maximum 20 % of total heat transfer can result from conduction through the wire.

The purpose of this chapter is to critically discuss the performance of available laboratory reactors for determining particle combustion behavior and to produce validation data for modeling purposes. Figures 2.1.-2.5. show the schematics of the reactors used for model validation in this work.

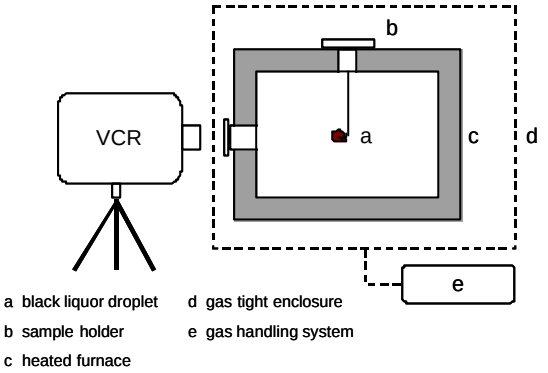

Figure 2.1. Muffle furnace reactor, Hupa *et al.* (1987)

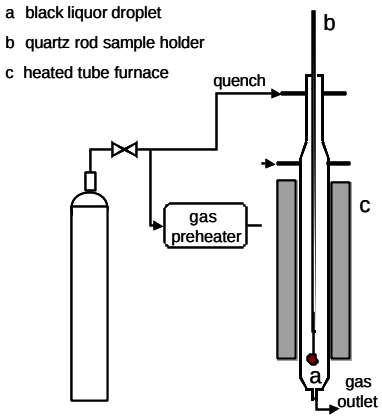

Figure 2.3. Tube furnace reactor, Whitty (1997)

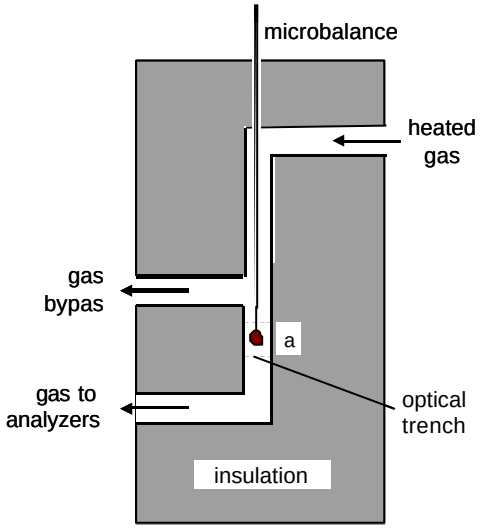

Figure 2.2. Single particle reactor, Kulas (1990)

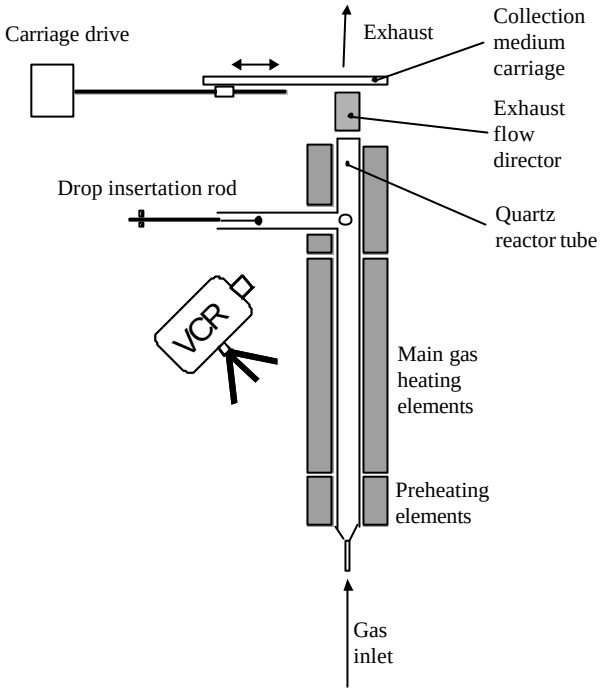

Figure 2.4. Drop tube furnace, Verrill and Nichols (1994)

A muffle furnace, Figure 2.1, has been used extensively by Åbo Akademi for determining the combustion behavior of 1.5-2.5 mm particles, *e.g.* Hupa *et al.*(1987), Frederick *et al.* (1990a, 1990b, 1993, 1994b, 1994c). The duration of different combustion stages, swelling behavior and mass loss and the release of species at predetermined time intervals (for example 1, 2, 5, 10 20 and 40 sec) are measured. Differences between liquors are well established and a new fuel specific approach was developed using this reactor type. This type of reactor can be well used for modeling purposes as the boundary conditions can be defined for a one-dimensional single particle combustion model. The furnace walls can be assumed to be isothermal, which makes the calculation of radiation heat transfer more reliable. Also, as the dimension of the furnace is much larger than the particle size, the emissivity of the furnace walls has no effect on the thermal radiation heat transfer rate.

The single particle reactor, Figure 2.2., is somewhat different from the muffle furnace, Kulas (1990). A droplet is inserted into a gas channel (50x50 mm cross section) where its swelling behavior can be monitored. The gas velocity can be controlled to simulate in-flight conditions. The temperature of the furnace wall near the particle is measured. As the size of the channel is much larger than the particle, furnace wall emissivity has no major effect on the heat transfer rate. Furnace walls were heated up only by the flowing gas, so their temperature control and adjustment was difficult. However, based on wall temperature measurement, the radiation heat flux to the particle can be estimated, Frederick (1990a). The flow conditions in the reactor were also discussed by Frederick (1990a) and the source of flow disturbances were addressed. Released gases can be led to analyzers for measuring the total amount of released species. One disadvantage of this reactor configuration was that the time required for inserting the particle into the reactor was long (few seconds). The particle will then be exposed to hot and oxidizing conditions before the actual experimental condition is reached. To solve this problem, the whole transient experiment should be modeled, including the insert period, particle removal from the reactor and cool down.

The tube furnace reactor, Figure 2.3., was developed to be used with on-line gas analyzers, Whitty (1997). The release of CO_2, CO, SO_2 and NO are recorded and by the means of reactor modeling (a de-convolution procedure), the release rate at the position of the droplet can be back-calculated. By using the tube furnace reactor, devolatilization release and a fixed yield of carbon, sulfur and nitrogen species could be obtained. This is very usable information for modeling purposes. The disadvantages of this reactor configuration is that we can get no information on the particles swelling during devolatilization and particle size reduction while the char is converted. Heat transfer is also very complex in this reactor type. The furnace walls are close to the particle surface and therefore, the emissivity of the quartz reactor surface may play a role in the values measured. Boundary conditions for the droplet are difficult to adjust. Most importantly, a particle is lowered into the furnace through an inlet gas channel by using a 10-12 mm quartz rod which is initially at room temperature. The rod acts as a time dependent boundary condition that is very difficult to model. However, as this reactor type is used for studying char gasification these factors have no effect on its application and the reactor produces very valuable information. Also, when comparing and identifying differences between fuels, devolatilization conditions are the same for all particles and therefore, this reactor can be well used for this purpose.

Another very sophisticated drop reactor furnace was used by Verrill and Nichols (1994) for studying the formation inorganic emissions during black liquor pyrolysis, Figure 2.4. The drop furnace consisted of a packed, tubular gas heater and a custom-fabricated quartz reactor tube, 6.5 cm inner diameter. Individual drops of black liquor are formed on a nickel-chrome wire and inserted into the furnace. The drop insertation rod places the liquor drops rapidly and precisely at the center of the reactor tube. Observations of drop combustion in the furnace can be recorded on videotape at 30 frames per second. Times for each stage of combustion are calculated from the elapsed video images. This experimental configuration also consisted of an aerosol collection equipment that could be used to determine the amount of aerosols and other solid material such as small fragments separated by physical ejection, released during combustion. The collected material could be analyzed in detail for composition, size and structure.

To combine the properties of muffle furnace and tube furnace, a new reactor system shown in Figure 2.5, was developed at Åbo Akademi 2000 by Forssén (Paper IV). The new quartz reactor is installed into the muffle furnace and gases are led to on-line gas analyzers. Incoming gases are heated up to their final temperature before they reach the particle. As the particle is recorded on video during the experiment, droplet swelling and release of different species can be measured simultaneously. This reactor type is most optimal for obtaining validation data for modeling

purposes. As will be shown later in this work, excellent data for verifying sub-models of detailed single particle combustion model is generated. Also, more accurate data on the mechanisms of devolatilization swelling and particle shrinkage can be obtained as the release rates and particle dimensions can be combined.

The combustion of larger particle has also been studied in a free fall reactor, Figure 2.6, Macek (1999). An identical reactor was also used by Clay *et al.* (1987). In this configuration, particles of strictly controlled size are fed from the top of the reactor. Heated gas is fed from the reactor bottom, the gas flow is then opposite to particles' flow direction. The particle size range used here is 1.6-2.7 mm. The maximum residence time of particles is 1-1.5 sec, which basically means that only the drying and devolatilization stages of combustion may be studied. This reactor best simulates the in-furnace combustion. Unfortunately, particles can not be continuously observed in this reactor type.

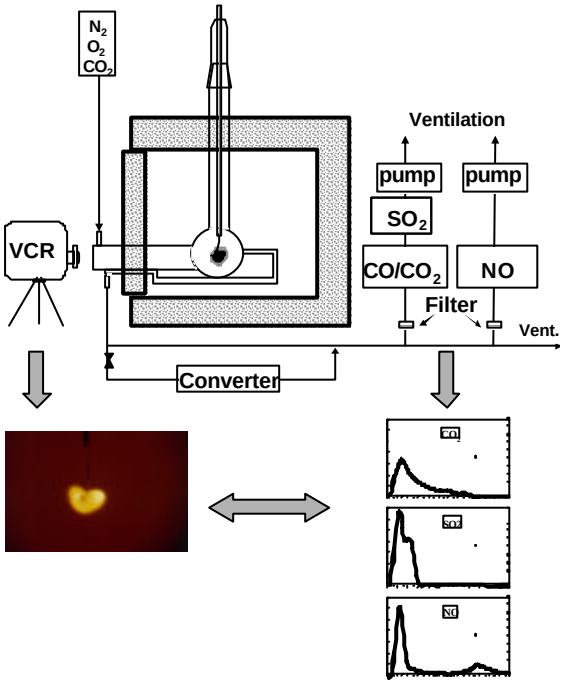

Figure 2.5. New ÅA reactor configuration, Paper IV

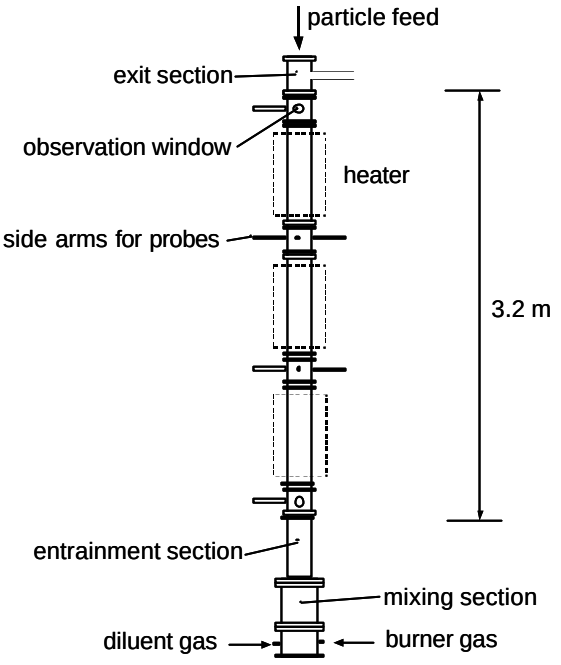

Figure 2.6. Free fall reactor, Macek (1999)

2.3 Combustion models for black liquor

Several models have been presented for black liquor combustion. Two main categories can be distinguished: a) isothermal particle models and b) non-isothermal models. These are reviewed here with respect to physical heat and mass transfer models, drying and devolatilization models and char conversion mechanisms. The applicability of models for CFD calculations is also discussed.

In the case of thermally large particles ($Bi > 0.1$) intra-particle heat transfer needs to be solved for drying and devolatilization, Figure 2.6, model H1. Without simplifications, simultaneous mass transfer should also be calculated. However, mass transfer during drying and devolatilization is not typically calculated as gas-solid interactions are neglected. For the char combustion stage, mass transfer needs to be considered to describe the transport of oxidizer to the particle, Figure 2.6,

model M1. The equations needed for this complete model are the conservation equations of species and enthalpy.

$$-\frac{1}{S}\frac{\partial}{\partial r}\overline{\dot{N}}+\overline{\dot{c}}=\frac{\partial \overline{c}}{\partial t} \tag{2.1}$$

$$-\frac{1}{S}\frac{\partial}{\partial r}\left(\sum_{j=1}^{n}\left\{\dot{N}_j H_{m,j}\right\}-lS\frac{\partial T}{\partial r}+\dot{Q}_r\right)=\frac{\partial}{\partial t}\sum_{j=1}^{n}\left\{c_j H_{m,j}\right\} \tag{2.2}$$

Proper boundary conditions for these need to be defined. These depend mainly on the existing conditions. Also, secondary parameters need to be defined i.e. transport properties, thermodynamic properties. These all are functions of temperature, gas composition etc. Source terms are defined by the processes taking place in the particle e.g. drying, devolatilization and char conversion. As the overall problem defined by all this is very complex, no analytical solution can be obtained and therefore, a numerical solution must be found. However, as the numerical solution of these equations requires large amount of calculation time this kind of approach can not be used for CFD purposes. There are several assumptions available that can be used to greatly simplify the combustion model. Figure 2.7 presents the general approaches for modeling heat and mass transfer in particle combustion.

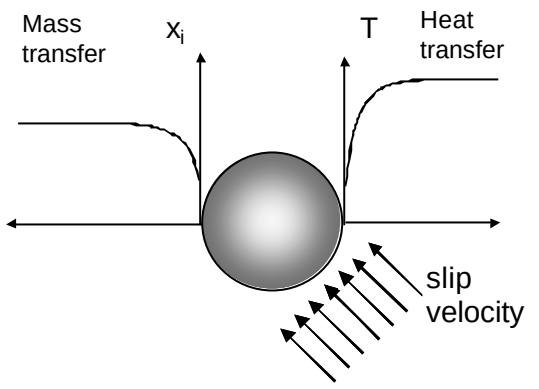

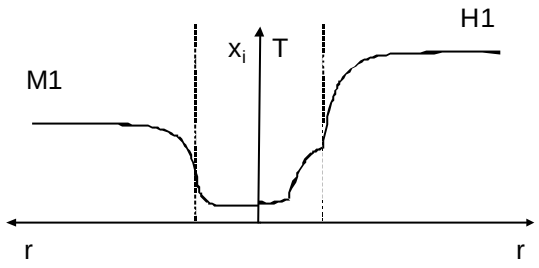

M1. Finite intrinsic reaction rate, external and internal mass transfer both important

H1. Internal and external heat transfer both important, Bi > 0.1.

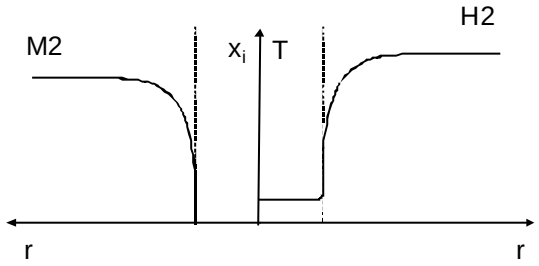

M2. Surface reaction/external diffusion control, suitable for large and non-porous particles

H2. Rough approximation for thermally large particles.

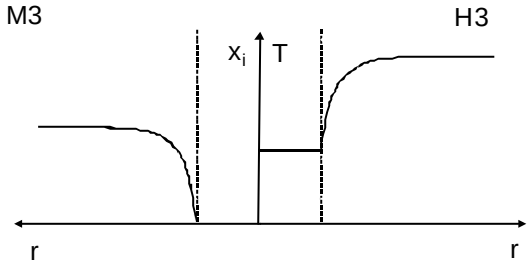

M3. Infinite surface reaction rate, external diffusion control, suitable for large and reactive particles, extreme case of M2.

H3. Internal heat transfer very effective, $R_{h,i} \rightarrow 0$. Suitable for small particles, Bi<0.1.

Figure 2.8. Descriptions of the particle heat and mass transfer models, temperature and gas concentration profiles, assumptions, application ranges.

Simplifications for heat transfer

Instead of the complete solution of Eq. 2.2. for heat transfer in thermally large particles, internal heat transfer can be roughly approximated by using a two-resistance model, Frederick (1990a), Figure 2.7, model H2. In this model, the particle is assumed to be isothermal and also to have a surface temperature different from the bulk temperature. This approach is very attractive and can

also be used in CFD sub-models as no additional equations have to be solved. The heat transfer rate to the particle is calculated as

$$\dot{Q} = \frac{(T_g - T_b)A_s}{R_t} = \frac{h}{1+Bi}(T_g - T_b)A_s = h(T_g - T_s)A_s \qquad (2.3)$$

where

$$Bi = \frac{hd}{6l},\ h = h_c + h_r,\ h_c = \frac{Nu\, l_g}{d},$$

$$h_r = \frac{e\, s\,(T_g^4 - T_s^4)}{(T_g - T_s)} \text{ and } \frac{1}{R_t} = \frac{h}{1+Bi} = \frac{1}{1/h + d/6l}$$

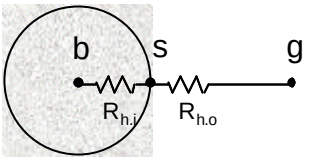

$$R_{h.o} = \frac{(T_g - T_s)A_p}{\dot{Q}} = \frac{1}{h},\ R_{h.i} = \frac{(T_s - T_b)A_p}{\dot{Q}} = \frac{\Delta r}{l}$$

Reactions are assumed to take place at the bulk temperature T_b. T_s is required for calculating the transport properties of gases for convection and the radiative heat transfer coefficient h_r, from Equation 2.3. Unfortunately, some iteration is required as the radiative heat transfer coefficient is non-linearly dependent on T_s. Heat that is delivered to the particle is consumed by reactions and affect the particle temperature.

$$\dot{Q} = \dot{m}\,\Delta h(T) + mc_p \frac{dT}{dt} \qquad (2.4)$$

The most simple model for the particle temperature is the isothermal particle assumption that corresponds to Equation 2.3 when $Bi = 0$. For thermally small particles, $Bi < 0.1$, $T_s \rightarrow T_b$, model H3 holds. This approach is very useful for thermally small particles or it can be used to solve particle temperature during char combustion, also for larger particles.

Simplifications for mass transfer

If the interactions of drying, devolatilization and char combustion are neglected, mass transfer does not need to be solved during drying and devolatilization. This is the case for all previous models developed for black liquor. For the char combustion stage, the particle is usually assumed to be isothermal, H3. For isothermal particles, an analytical solution exists for the internal reaction and diffusion case, when internal bulk flow is neglected. The rate for the kinetically controlled case, i.e. for the case where gas concentration in the particle is constant, is given as follows, Peterson (1965), Fogler (1992):

$$\dot{N}_i = \frac{h}{1 + h\frac{k_r''' d}{h_m 6}} k_r''' c_{i,\infty} V_p \qquad (2.5)$$

where $k_r''' = k_r S_a \rho_b$ is the rate per particle volume. S_a and ρ_b are the specific internal surface area and density of the particle, $V_p = \pi/6 d^3$ is the particle volume and $C_{i,\infty}$ is reactant bulk gas concentration. h_m is external mass transfer coefficient and D_e is the effective diffusion coefficient. The internal

effectiveness factor h for a sphere can be calculated from this, using the Thiele modulus f_1 for first order reactions:

$$h = \frac{3}{f_1^2}(f_1 \coth(f_1) - 1) \text{ where } f_1 = R\sqrt{\frac{k_r'''}{D_e}} \qquad (2.6\text{-}7)$$

If a particle is very dense, reactions take place only at the particle surface. Then, internal mass transfer can be neglected. The rate is then calculated from, Fogler (1992):

$$\dot{N}_i = \frac{h_m c_{i.\infty} A_p}{1 + \frac{h_m}{k_r}} \qquad (2.8)$$

and further, if the rate is very fast i.e. k_r (per external surface area) $\rightarrow \infty$, the mole fraction of the oxidizer equals zero at the particle surface and the diffusion control case is obtained:

$$\dot{N}_i = h_m c_{i.\infty} A_p \qquad (2.9)$$

As black liquor particles are very porous this model should be used with caution as it might overestimate the rate.

For black liquor, gasification rates are often expressed as Langmuir-Hinshelwood type of rate expressions, which means that they can not be directly applied to the pore diffusion model presented above. An approximate expression needs to be developed for Langmuir-Hinshelwood rate equations i.e. a linear model that describes the correct behavior:

$$R_i = k_i C_{char} \frac{c_i}{c_i + a c_j} \approx k_{r.i}''' c_i \qquad (2.10)$$

Here i refers to the gasifying species H_2O/CO_2 and j refers to the inhibiting species H_2 for H_2O gasification and CO for CO_2 gasification. For the case where the concentration of species j is negligible, following a zeroth order approximation is more recommendable. For this, an accurate analytical solution is available, Peterson (1965), and no approximation (2.10) is required.

$$R_i = k_i C_{char} \frac{c_i}{c_i + a c_j} \approx k_i C_{char} = k_{r.i}''' \qquad (2.11)$$

All the heat and mass transfer models described above are summarized in Figure 2.6. Application of these in different black liquor combustion models are presented in sections 2.3.1 and 2.3.2.

2.3.1 Available isothermal models for black liquor combustion

In these models a particle is assumed to be isothermal which means that only one equation is used to solve for the particle temperature. This approach is very useful for use in CFD calculations. However, as black liquor particles are thermally large, the isothermal assumption can be misleading

and a source of significant errors. Basically, non-isothermal models are reduced to this type if the number of intra-particle computational cells is reduced to one.

Merriam (1980) developed a comprehensive computer model of a kraft recovery boiler. The model divided the recovery furnace into 13 vertical zones where gas compositions were calculated via a thermodynamic equilibrium model. Interactions between the burning liquor and gas and also the char bed and gases were included. In-flight combustion of single particles was described by modeling the trajectory and combustion behavior of the particles. The single droplet combustion model was developed before any laboratory data was available. Therefore, this model did not fully succeed in describing the actual, later observed combustion behavior. Droplets were assumed to swell linearly during drying, although it was later observed that very rapid swelling takes place immediately after a droplet is exposed to a hot environment, Hupa *et al.* (1987). Devolatilization and char combustion models developed for coal were directly applied for black liquor. However, black liquor combustion behavior differs considerably from this. Although this model did not give a perfect description of the black liquor combustion processes, it was the first attempt to model the recovery furnace including the single particles. It was observed that this kind of tool could be very useful in engineering work and that more work should be concentrated on the subject.

Shick (1986) extended Merriam's droplet combustion and trajectory model. This model included the effect of changing particle size during on droplet trajectory. Shick's model did not consider the droplet-gas interactions or the characteristics of a liquor spray. In the model, swelling during drying was neglected. The rate of devolatilization was assumed to be a function of gas temperature. Char combustion was described by a empirical expression that did not give a perfect match with black liquor char combustion rate.

To further improve the description of single particle combustion, Walsh (1989a,b) presented a simple trajectory and combustion model TRAC for black liquor. There was also new experimental data available on single particle combustion and also on spray properties that made it possible to use these as more accurate initial data for simulations. This model was developed to effectively calculate the mass release, particle diameter and temperature along the flight path in a separate program assuming a fixed flow field. More importantly, the model was also implemented in FLUENT CFD software to solve interactions of particles and flow field. Droplet drying was assumed to be an external heat transfer controlled process, model H3, Figure 2.7, and particle temperature was assumed to be constant during drying. The devolatilization rate was calculated from a statistical expression as a function of initial dry solids content, particle mass, particle diameter and oxygen concentration. Particle diameter increases linearly during devolatilization as a function of devolatilization conversion. Particle temperature is set to increase from the boiling temperature to surrounding gas temperature as a linear function of devolatilization conversion. Char combustion is assumed to be a mass transfer limited process, model M3, Figure 2.7. Char may only react with oxygen, products being CO/CO_2. The volume of the particle is linearly dependent on the remaining mass of carbon. After all the char is burnt, the remaining inorganics may react with O_2, at a rate defined by external mass transfer as for char combustion. Although it is a simplified "earth, wind and fire" model, it can be very useful for predicting particle trajectories. For example, the role of in-flight and wall combustion can be specified. Also, as the interactions of droplets and gas flow field were considered, this model was a very important step towards more accurate recovery furnace simulation models.

Kulas (1990) presented a isothermal single particle black liquor combustion model that considered drying, devolatilization and char conversion reactions. Drying and devolatilization were assumed to be external heat transfer controlled processes, model H3, Figure 2.7. For isothermal char

conversion, the sulfide/sulfate cycle, carbon-O_2 oxidation by coal kinetics and char gasification by CO_2 were considered. Particle temperature during char conversion was obtained from experimental correlation. No gasification by H_2O was considered as it was not implemented in the reactor system used. During the char combustion stage, reactions were assumed to take place only at the droplet surface, this corresponds to model M2, Figure 2.7. As black liquor char is very porous, internal reactions and pore diffusion are both present and the assumption of a surface reaction might be too extreme. Also, as later observed, particles are non-isothermal and much too high drying and devolatilization rates might be predicted by isothermal assumption. The char burning model contained many simplifications that should be carefully evaluated, for example particle temperature should be solved from an energy equation in order to apply the model to typical recovery boiler conditions. It was suggested that more work on drying process should be done and black liquor swelling should be studied in greater detail. Also, the kinetic expression for volatiles evolution should be validated and more detailed and relevant model for char combustion implemented including gasification by H_2O.

Frederick (1990a) developed a simplified model for black liquor combustion. A large set of experiments were carried out to search for model parameters such as drying and devolatilization swelling and char size reduction. Intra-particle heat transfer was taken into account by using an internal thermal resistance model, model H2, Equation 2.3. Basically, this model is then not fully isothermal. This resistance model is very simple and can be effectively used also with CFD. Drying and devolatilization were modeled as limited heat transfer processes. Drying took place at the boiling point $T = 373 + 50\ y_s^{2.84}$ and devolatilization at a temperature between the ignition temperature and final temperature (typically 150°C below the surrounding gas temperature). Ignition takes place when a predefined solids content is reached, typically 90-95%, the corresponding temperature is solved from the boiling curve given above. For devolatilization swelling, an experimentally determined correlation was used to describe particle expansion as a function of devolatilization conversion, see Table 2.3. For char combustion, H_2O, CO_2 gasification and O_2 oxidation were assumed to be mass transfer limited, model M3, Figure 2.7. Particle volume was assumed to linearly decrease as a function of char conversion. Internal diffusion and reaction during char combustion were included later (Frederick *et al.* 1993), model M1, Figure 2.7. The total rate was calculated from:

$$\frac{1}{R_i} = \frac{1}{R_{i,m}} + \frac{1}{R_{i,c}h} \qquad (2.12)$$

where R_m and R_c are mass transfer and kinetic rates, respectively and h is the internal effectiveness factor that includes the effect of intra-particle diffusion and reaction, see Equation. 2.6-7. It was found that under typical recovery furnace conditions, char conversion is a film mass transfer limited process for char oxidation by O_2. For char gasification by H_2O and CO_2, intra-particle diffusion and reaction should also be considered.

Horton (1992, 1993) developed a single particle model to be used with fixed flow field calculations. Fixed flow field velocities were directly taken from CFD calculations. The furnace was assumed to be isothermal and homogenous in gas composition. As the objective of the work was to study the effect of black liquor spray parameters these simplifications were justified. One of the single particle combustion models used was based on the work of Frederick (1990a). This model was modified to take into account the radiation exchange between gases and particles. Also, a more detailed description on the char conversion processes was implemented, including the gasification reactions by H_2O/CO_2 as surface reactions, model M2, Figure 2.7. It was found that swelling strongly affects the flight path and release locations. It was suggested that gasification by H_2O/CO_2

may play a significant role in furnace conditions, since both H_2O and CO_2 are present in high quantities in the furnace. It was suggested that the kinetics for these reactions should be determined to find out whether these are mass transfer limited.

Thunman (1994) presented a single particle combustion model to be used with fixed flow field calculations. This model was based on Frederick's two-resistance model. Drying and devolatilization were assumed to be heat transfer controlled processes. A droplet was assumed to dry at the atmospheric boiling point $T = 373 + 50\ y_s^{2.84}$. During devolatilization an effective gas temperature was assumed to be defined by the oxidation of volatiles, a localized envelope flame then existed. A particle was assumed to swell as a function of devolatilization conversion, an experimentally determined correlation was used for this purpose, see Table 2.3. For char conversion, H_2O and CO_2 gasification, direct O_2 oxidation and sulfide/sulfate cycle were considered by kinetic expressions. The effect of internal mass transfer and reactions were modeled by using a Thiele modulus based pore diffusion/reaction model, Equations 2.6-7, 2.12. The changing internal reaction surface area was taken to be the random pore model.

Wåg (1995a, 1995b, 1997a) and Reis *et al.* (1995) presented an isothermal detailed char conversion model where char gasification by H_2O and CO_2, direct O_2 oxidation, inorganic reduction reactions of sulfates and carbonates were considered. The oxidation rates of CO and H_2 at the boundary layer were assumed to be infinitely fast. It was found that under typical recovery boiler conditions all O_2 is depleted in the boundary layer of the particle as long as carbon is present. No significant O_2 reactions take place at the particle's surface. The gaseous product of sulfate reduction was assumed to be CO_2, Grace *et al.* (1989). Then, in typical recovery boiler conditions the rate of carbon burn-up was given as:

$$R_C = R_{H_2O} + R_{CO_2} + 2R_{CO_3} + 2R_{SO_4} \qquad (2.13)$$

Rates R_i for char conversion by O_2, H_2O and CO_2 were calculated from Equation 2.12 to take into account the external mass transfer, pore diffusion and chemical reaction. The rate for reactions are presented later in this work, Table 5.1. Char oxidation by O_2 was assumed to be diffusion controlled, Wåg *et al.* (1995a). In the model presented by Reis *et al.* (1995), particle temperature was solved from the energy equation. Wåg (1997a) obtained particle temperature directly from an experimental correlation as a function of oxygen content. As this correlation was obtained in an O_2/N_2 environment, it should not be directly applied to a recovery boiler environment. It was found that char gasification by H_2O and CO_2 are the main routes for carbon consumption. As the O_2 does not reach the surface, char oxidation and sulfate re-oxidation are negligible. Sulfate reduction was found to be responsible for only a small part of the char carbon. The contribution of carbonate reduction on carbon consumption was not considered.

Grace *et al.* (1998) presented a combustion model for black liquor combustion that was based on the idea of presenting black liquor as a mixture of chemical species. This model also combined the knowledge obtained during development of the previous models presented above, Frederick (1990a, 1993) and Wåg *et al.* (1995a, 1995b, 1997a), Reis *et al.* (1995).

The properties of all these black liquor models presented here are summarized in Tables 2.2 and 2.3.

2.3.2 Non-isothermal black liquor combustion models

This type of model is usually very complex and a long time calculation is required in order to obtain its solution. Therefore, they are not usually suitable for CFD use, although Wessel *et al.* (1997) reported using their complex model in CFD furnace calculations. The best use of these models can be made by analyzing experimental single particle combustion data and using the model to obtain values for data that can not be measured.

Harper (1989) presented a detailed single particle combustion model for predicting the rate of devolatilization and sulfur release. Each particle was divided into 3 spherical concentric layers and the energy balances for these were solved. Internal thermal radiation was neglected. The energy balances for the layers were solved numerically and a non-uniform temperature distribution resulted, model H1, Figure 2.7. Drying was assumed to be a heat transfer controlled process taking place at 150°C. Mass transfer was not considered. Devolatilization was calculated from a statistical correlation determined from experiments as a function of initial diameter, dry solids content and temperature. Excellent correlation with internal and external temperature measurements was obtained. It was clearly observed that particles are non-isothermal. Unfortunately, only low temperatures (max 700 °C) were studied and the results were not applied to furnace conditions.

Manninen and Vakkilainen (1996) presented a single particle combustion model that combined the work of Frederick (1990a) and Harper (1989). For example, this model was used in fixed flow field calculations to study the effect of sulfur release (Manninen and Vakkilainen 1996) and liquor gun type (Järvinen *et al.* 1997). In this model, initial drying took place as an evaporating droplet. When a critical solids content is reached, ignition takes place and the non-isothermal model of Harper (1989) is applied. Drying and devolatilization were modeled as a heat transfer limited processes, model H1, Figure 2.7. Mass transfer during drying and devolatilization were not considered, for sulfur release a kinetic model of three parallel reactions was used and fitted to experimental data available. For char conversion, internal diffusion and the H_2O, CO_2 gasification reaction and O_2 oxidation were considered, model M1, Figure 2.7. Also inorganic reduction reactions by carbonates and sulfates were included.

Saastamoinen *et al.* (1984) presented a detailed combustion model for simultaneous drying and devolatilization of wood particles, model H1, Figure 2.7. This model is based on the numerical solution of energy and mass (water and dry solids) conservation equations. Instead of solving for temperatures in computational cells, the location of temperature isotherms were calculated. This approach is very useful as it automatically refines the computational grid where the gradients are the largest. This model was applied to black liquor combustion by Saastamoinen *et al.* (1993a, 1993b, 1996a). Droplets are first assumed to heat up isothermally to the atmospheric boiling point. During the initial stages of drying, droplets evaporate isothermally at the boiling point until a critical water content is reached. After this, the droplets start to behave as solids and a temperature gradient develops. The cooling effect of out-flowing water vapor and volatiles on internal heat transfer is considered. The reducing effect of the so-called Stefan blow (SB) is also considered in the effective convective heat transfer coefficient as follows:

$$h_e / h = \frac{\dot{C}'' / h}{\exp(\dot{C}'' / h) - 1} \qquad (2.14)$$

Where h_e and h are the corrected convective heat transfer coefficient and normal heat transfer coefficient, respectively. Drying was modeled to be a heat transfer controlled process. For

convective conditions, internal circulation during drying is considered. It will increase the drying rate by bringing water to the particle surface. This approach is questionable as a "skin" might easily form on the droplet surface preventing the formation of internal circulation. For devolatilization, there was no suitable data available for developing a kinetic expression and therefore devolatilization was modeled as a heat transfer limited process. Devolatilization kinetics were assumed to be infinitely fast and able to follow the thermo-gravimetric curve, $e(T)=m/m_0$=mass/initial mass for wood, determined by slowly heating the sample. Mass and mass release rate are then calculated as follows.

$$m = m_0 e(T), \dot{m} = -m_0 \frac{de}{dT}\frac{dT}{dt} \tag{2.15}$$

In Saastamoinen's model internal thermal radiation can be selected as an option. However, as there was no information on the pore size available, radiation was not included in the calculations presented. Swelling was described as a local process, where volume increases linearly as a function of devolatilization conversion. Saastamoinen (1996c) also studied char combustion by using a simple shrinking core model in a 20% O_2/N_2 environment. The effect of cenospheres and swelling (hollow particles) was studied and it was found that these both increase the rate of char conversion. Saastamoinen (1997) also implemented the reduction reaction of carbonates which are used to describe the release of sodium and potassium.

Another very similar model was presented by Verrill *et al.* (1995a). In this model, the energy equation for temperatures and condensed species conservation equations are solved by an implicit finite difference control volume method. Species conservation equations inside the particle are included for condensed species. For gaseous species, only the fluxes are solved from drying and devolatilization rates, no simultaneous solution of gas concentrations inside the particle is obtained. For the char combustion stage, an isothermal analytical pore diffusion and reaction model is applied, model M1, Figure 2.7. Time integration is done by a 2nd order accurate scheme with an adaptive time step to increase accuracy. A particle is divided into N computational layers of equal initial mass and volume. Surface conditions are represented by an infitesimal shell of zero mass, at the outer radius of the particle. The grid expands or contracts with the particle during swelling to conserve mass and material components within each shell. Internal thermal radiation heat transfer is considered by using the diffusion approximation for an optically thick media with a Rosseland mean absorption of 70 1/m at maximum porosity. Thermal radiation was the dominating internal heat transfer mode. The internal cooling effect of out-flowing gases is neglected but the effect of Stefan flow is considered for external boundary conditions. In the case of an oxidizing gas atmosphere an analytical envelope flame model is used as the boundary condition. This flame model is used when Re<1, the procedure for solving for the case Re>1 was not reported, Verrill *et al.* (1998). Black liquor composition was estimated from elemental analysis. Dry solids contains organic matter that form volatiles and char and inorganics Na_2SO_4, Na_2S, Na_2CO_3, K_2CO_3, NaCl and KCl. Devolatilization was described by 3 parallel reactions with different product yields, therefore, a temperature dependent product yield is considered. In this model, char conversion by H_2O/CO_2 gasification, direct oxidation by O_2, reduction of sulfates and carbonates were considered. Mass can also be released by physical ejection that is driven by the internal pressure gradient, Verrill *et al.* (1998). In this mechanism small particles are separated from the particles produced by the high flow rate of escaping gases. Verrill's model also includes the mechanisms for alkali and sulfur releases: these are not discussed here.

Table 2.2. Comparison of heat and mass transfer models

Researchers	*External heat transfer*	*Internal heat transfer*	*External mass transfer*	*Internal mass transfer*
Walsh *et al*., 1989a,b	HD + C + R	IT	D + C	-
Kulas, 1990	HD + C + R, combustion of volatiles at the surface	IT	D + C	-
Frederick, 1990a Frederick *et al*. 1993	HD + C + R, convective temperature during devolatilization $T_{g,eff} = T_g + 1980 \cdot x_{O2}$ Frederick (1990a)	IT, 2R	D + C	Neglected (1990a), PDR during char combustion (1993)
Horton et al., 1992, 1993	Frederick (1990a) + improved radiation model	Frederick (1990a)	Frederick (1990a)	-
Thunman, 1994	HD + C + R, convective temperature during devolatilization $T_{g,eff} = T_g + 1980 \cdot x_{O2}$, for char combustion $T_p=f(O_2,T_g)$	IT, 2R	D + C	PDR during char combustion, random pore model for internal surface area
Wåg *et al*., 1995a,b	Not solved, $T_p=f(O_2,T_g)$	IT, energy equation not solved	D + C	PDR during char combustion
Reis *et al*., 1995	HD + C + R	IT, T solved from energy equation	D + C	PDR during char combustion
Grace *et al*. , 1998	Frederick (1990a)	Frederick (1990a)	Frederick (1990a)	See Wåg *et al*. (1995a)
Harper, 1989	HD + C + R	NIT, particle divided into 3 concentric layers, HD	-	-
Manninen and Vakkilainen, 1996	HD + C + R, convective temperature during devolatilization $T_{g,eff} = T_g + 1980\, x_{O2}$	NIT, particle divided into 3 concentric layers, HD	D + C	PDR during char combustion
Saastamoinen *et al*., 1993a-1997.	HD + C + SB, R, convective temperature during devolatilization $T_{g,eff} = T_g + 1980 x_{O2}$	NIT, HD + C, numerical solution for energy equation, solved the position of temperature isotherms	D + C, SB	-
Verrill and Wessel, 1995-2000	HD + C + SB, R	NIT, HD + R, numerical solution for energy equation, solved temperatures in control volumes	D + C, SB, envelope flame as a boundary condition in oxidative condition when Re<1.	PDR during char combustion

C = convection
R = thermal radiation heat transfer
D = diffusion
HD = conduction (heat diffusion)
IT = isothermal
NIT = non-isothermal transfer resistances considered
2R = two resistance model, external and internal heat
PDR = analytical solution for pore diffusion and reaction
SB = Stefan blow effects considered, Eq. 2.12.

Table 2.3. Comparison of drying, devolatilization swelling and char conversion models

Researchers	*Drying*	*Devolatilization*	*Char conversion mechanisms*
Walsh, 1989a,b	eht, at a constant temperature 127 °C, swelling 1.5 d_0	Rate from a statistical, expression = f(m_0, $y_{s.0}$, d_p, x_{O2}) $(d - d_0) / (d_{max} - d_0) = X_P$	$C + O_2$? CO/CO_2 , emt
Kulas, 1990	eht, at the boiling temperature = f(y_s), swelling 1.5 d_0	Single 1st order reaction, $(d - d_0) / (d_{max} - d_0) = X_P$	$C + O_2$? CO/CO_2, emt/k $C + CO_2$? 2 CO, emt/k $2C + Na_2SO_4$? $2CO_2 + Na_2S$, k $Na_2S + 2\ O_2$? Na_2SO_4 , emt/k
Frederick, 1990a Frederick *et al*. 1993	ht, at the boiling temperature = f(y_s), swelling 1.5 d_0	ht, linear conversion as heat is delivered $(d - d_0) / (d_{max} - d_0) = X_P^{0.8}$	$C + O_2$? CO/CO_2, emt $C + H_2O$? CO + H_2, mt/k $C + CO_2$? 2 CO, mt/k
Horton et al., 1992, 1993	Frederick, 1990a	Frederick, 1990a	$C + O_2$? CO/CO_2, emt $C + H_2O$? CO + H_2, mt/k $C + CO_2$? 2 CO, mt/k
Thunman, 1994	ht, at the boiling temperature = f(y_s), swelling 1.54 d_0	ht, linear conversion as heat is delivered $(d - d_0) / (d_{max} - d_0) = X_P^{0.8}$	$C + O_2$? CO/CO_2, mt/k $C + H_2O$? CO + H_2, mt/k $C + CO_2$? 2 CO, mt/k $2C + Na_2SO_4$? $2CO + Na_2S$, k $Na_2S + 2\ O_2$? Na_2SO_4, emt
Wåg *et al*., 1995a,b Reis *et al*., 1995	-	-	$C + H_2O$? CO + H_2, mt/k $C + CO_2$? 2 CO, mt/k $C + O_2$? CO/CO_2, mt/k $2C + M_2SO_4$? $2CO_2 + M_2S$,k $M_2S + 2\ O_2$? M_2SO_4, emt $2\ C + M_2CO_3$? 3CO + 2M, k
Grace *et al*., 1998	Frederick (1990a)	2 parallel reactions with different product yields, linear volumetric swelling	See Wåg *et al*. 1995a,b
Harper, 1989	eht isothermal drying , at 150 °C, swelling 1.5 d_0	Rate from an empirical correlation f = (d_0, y_{s0}, T), swelling $(d^3-d_0^3)/(d_m^3-d_0^3) = (T-T_0)/(T_{max}-T_0)$	-
Manninen and Vakkilainen, 1996	eht isothermal drying till ignition, at boiling point T = $373 + 50\ y_s^{2.84}$, swelling 1.54 d_0	ht, linear conversion as heat is delivered $(d - d_0) / (d_{max} - d_0) = X_P^{0.8}$	$C + O_2$? CO/CO_2, emt $C + H_2O$? CO + H_2, mt/k $C + CO_2$? 2 CO, mt/k $2C + M_2SO_4$? $2CO_2 + M_2S$, k $M_2S + 2\ O_2$? M_2SO_4, emt $2C + M_2CO_3$? 3 CO + 2 M, k
Saastamoinen *et al*., 1993a-1997.	eht drying below transition water content, after that ht drying at 100 °C , swelling 1.54 d_0	ht, $m/m_0=e$(T) $\dot{m} = -m_0 \frac{de}{dT}\frac{dT}{dt}$ Linear local volumetric swelling	$C + O_2$? CO/CO_2, mt/k $2C + M_2CO_3$? 3 CO + 2 M, k
Verrill and Wessel, 1995-2000	Heat transfer controlled, at boiling point, swelling 1.54 d_0	3 parallel reactions with different product yields, physical ejecta during devolatilization $(d - d_0) / (d_{max} - d_0) = X_P^{0.8}$	$C + O_2$? CO/CO_2, emt $C + H_2O$? CO + H_2, mt/k $C + CO_2$? 2 CO, mt/k $2C + M_2SO_4$? $2CO_2 + M_2S$,k $M_2S + 2\ O_2$? M_2SO_4, emt $2C + M_2CO_3$? 3 CO + 2 M, k

mt = mass transfer controlled, ht = heat transfer controlled, emt = external mass transfer controlled, eht = external heat transfer controlled, k = kinetic expression used, X_p= devolatilization conversion, mt/k = mass transfer and reaction kinetics considered, M=Na/K

3 FOCUS OF THE PRESENT THESIS

As was shown in the previous chapter, there are many models already developed and available for single black liquor droplet combustion. Therefore, the rationale for this new work has to be well explained.

It was already observed by Frederick (1990a) that black liquor particles are thermally large and a non-isothermal model is required to accurately describe the combustion processes. Isothermal models are therefore not suitable for this purpose. These models can be effectively used for smaller particles such as pulverized coal particles or to describe the char combustion stage of larger droplets after the drying and devolatilization stages are completed.

Previously developed non-isothermal models reviewed above (Harper 1989, Saastamoinen 1993a and Verrill *et al.* 1995a) include the possibility of overlapping drying and devolatilization. Internal mass transfer was not modeled during drying and devolatilization. At combustion temperatures, the vapor pressure of water inside the particle is very high and it approaches the total pressure and therefore, drying can be assumed to be heat transfer controlled processes occurring at the boiling point. Drying can be modeled by only solving the energy and condensed species conservation equations. As the dependence of devolatilization reactions on gas partial pressures is very difficult to model, this connection is omitted. Devolatilization is usually modeled using first order reactions or assuming that devolatilization is a heat transfer controlled process. To solve the problem of simultaneous drying and devolatilization only the energy conservation equation needs to be solved, simultaneously with the conservation equations for water, pyrolysable matter and char. This was the approach in these previous non-isothermal models

For char combustion, the isothermal model presented by Wåg *et al.* (1995a,b) includes all the char conversion mechanisms presented previously and is adequate to describe the isolated char combustion stage. This has no interaction with the drying and devolatilization stage. However, as black liquor particles are thermally large ($Bi > 0.1$) a significant internal temperature gradient exists and at some point, the particle surface is pyrolysed and a char layer formed. As water vapor and CO_2 are simultaneously formed in the droplet interior, they have to pass through the surface layer. In theory, char conversion may take place at this point. CO_2 and H_2O have also access to the particles' surfaces during devolatilization from the localized flame around the particles and bulk gas. In furnace conditions where significant slip velocities exist, localized flames around the particles might not form and then, O_2 would have direct access to the char surface as well. In order to consider these processes and also to link all the interactions between combustion stages there is a need for modeling intra-particle mass transfer. This was the motivation for developing a completely new generalized combustion model that includes models for internal heat and mass transfer and all relevant reactions and conversion mechanisms. Also, the objective was to develop a model that could also be applied to other fuels and to study heat and mass transfer more generally (e.g. drying processes).

This thesis considers only the combustion processes of fully spherical particles, although it has been observed by Kankkunen *et al.* (2001) that a significant fraction of other shapes also exist. Combustion on the furnace walls or in the char bed is not considered here.

The primary objectives of this work were:

a) To develop a general detailed physical single particle combustion model for porous particles including intra-particle heat and mass transfer models and a description of the external heat and mass transfer
b) To implement relevant chemical reactions and experimentally observed physical combustion behavior e.g. black liquor swelling
c) To experimentally verify and validate this model in reactor conditions
d) By using the validated model, to compare char conversion mechanisms in reactor and furnace conditions for addressing the relevant reaction mechanisms needed to develop simplified particle combustion sub-models for CFD use in recovery furnace simulations

As part of this work, a new detailed single particle combustion for black liquor was developed. The interactions of drying, devolatilization and char conversion were studied. It was shown that for these thermally larger particles, a significant amount of char can be converted already during devolatilization by the gases escaping from the particle itself and also by the gases from the surrounding gas atmosphere. The role of localized gas oxidation around the particles and also inside the pores is studied and a relevant model to describe external heat and mass transfer in recovery furnace in-fight combustion is presented. Dominating char conversion mechanisms are identified and the key reactions isolated. The model was tested against available experimental data and also some new data was obtained for this purpose.

4 MODELING OF HEAT AND MASS TRANSFER IN 1D POROUS MEDIA WITH REACTING FLOWS

The purpose here is to develop a detailed heat and mass transfer model for porous spherical particles that is later to be applied to black liquor. Figure 4.1 shows the main mechanisms that are included and some principles of the model.

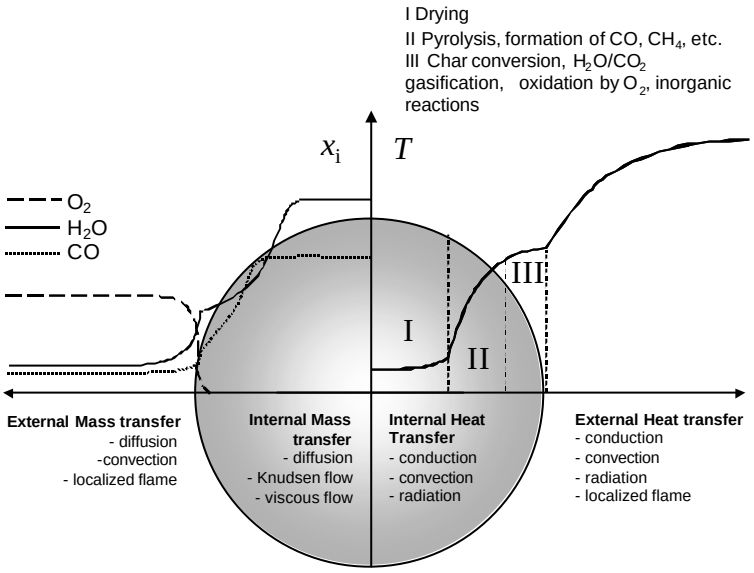

Figure 4.1. Processes to be considered for the combustion model.

Figure 4.1 shows the extreme case of simultaneous drying, devolatilization and char conversion. For this situation, internal and external mass transfer need to be modeled in addition to external and internal heat transfer. If the released gases are locally oxidized in an envelope flame, the external heat and mass transfer is more complex. The details of this model are discussed below.

4.1 Conservation equations and boundary conditions

The droplets are assumed to be spherical and are described by a 1-dimensional model. In principle, an infinite plate and cylinder can also be calculated using this same model with only small modifications. It was assumed there was local thermal equilibrium between different phases and species. The basic equations needed to model a chemically reacting system are the conservation equations of mass (1), chemical species (2) and energy (3):

$$\frac{1}{S}\frac{\partial}{\partial r}\left(\dot{m}\right)+\frac{\partial r}{\partial t}=0 \qquad (4.1)$$

$$-\frac{1}{S}\frac{\partial}{\partial r}\overline{\dot{N}}+\overline{\dot{c}}-\frac{\partial \overline{c}}{\partial t}=0 \tag{4.2}$$

$$-\frac{1}{S}\frac{\partial}{\partial r}\left(\sum_{j=1}^{n}\left\{\dot{N}_j H_{m,j}\right\}-lS\frac{\partial T}{\partial r}+\dot{Q}_r\right)-\frac{\partial}{\partial t}\sum_{j=1}^{n}\left\{c_j H_{m,j}\right\}=0 \tag{4.3}$$

where $H_{m,j}=H^{o}_{m,j}+\int_{T_0}^{T}C_{p,j}dT$, $S=4\pi r^2$

At the center of the droplet, the fluxes of heat and species are equal to zero due to symmetry. At the surface, the fluxes of heat and species $\dot{N}_j$ and $\dot{Q}$ depend mainly on the external conditions.

In this work two alternative flame structures for surface boundary condition were used. In the case of a low slip velocity, high O_2 concentration and high temperature, gases are oxidized in a thin reaction sheet. In the case of a high slip velocity, of lower temperature or in non-oxidizing conditions, no envelope flame will form. Gases will burn at the wake of the particle. These flame structures and corresponding models are illustrated in Figure 4.2. For non-stagnant flow conditions, thermal conductivity and diffusion coefficients were corrected for convection by multiplying them by *Nu*/2 and *Sh*/2, respectively Bartok and Sarofim (1991). The emissivity of the particle surface was calculated on the basis of measurement data by Wessel *et al.* (2000).

2-film model, Beck *et al.* (1990)	1-Film model
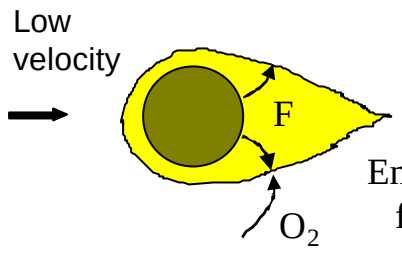	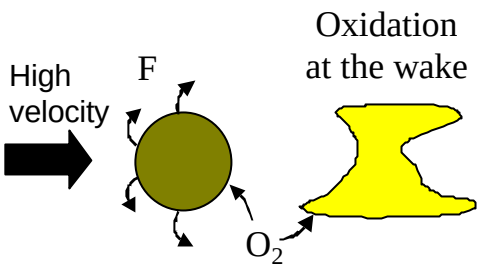
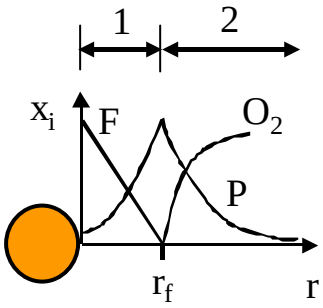	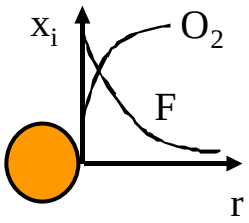
$\dot{N}_{j,1} = \frac{\dot{N}_{T,1}}{e^{B_{j,1}} - 1}\left(x_{j,s}e^{B_{j,1}} - x_{j,f}\right)$ $\dot{N}_{j,2} = \frac{\dot{N}_{T,2}}{e^{B_{j,2}} - 1}\left(x_{j,f}e^{B_{j,2}} - x_{j,\infty}\right)$ $\dot{Q}_1 = \frac{\dot{C}_{p,1}}{e^{B_1} - 1}\left(T_s e^{B_1} - T_f\right) + \dot{H}_1 + \dot{Q}_r - \dot{C}_{p,1}T_0$ $\dot{Q}_2 = \frac{\dot{C}_{p,2}}{e^{B_2} - 1}\left(T_f e^{B_2} - T_\infty\right) + \dot{H}_2 + \dot{Q}_r - \dot{C}_{p,2}T_0$ where $B_{j,1} = \frac{\dot{N}_{T,1}}{4\pi D_{j,1} Sh_j / 2}\frac{R_u T_1}{p_1}\left(\frac{1}{r_s} - \frac{1}{r_f}\right)$, $B_{j,2} = \frac{\dot{N}_{T,2}}{4\pi D_{j,2} Sh_j / 2}\frac{R_u T_2}{p_2}\frac{1}{r_f}$, $B_1 = \frac{\dot{C}_{p,1}}{4\pi\, l_1 Nu / 2}\left(\frac{1}{r_s} - \frac{1}{r_f}\right)$, $B_2 = \frac{\dot{C}_{p,2}}{4\pi\, l_2 Nu / 2}\frac{1}{r_f}$	$\dot{N}_j = \frac{\dot{N}_T}{e^{B_j} - 1}\left(x_{j,s}e^{B_j} - x_{j,\infty}\right)$, $\dot{Q} = \frac{\dot{C}_p}{e^{B} - 1}\left(T_s e^{B} - T_\infty\right) + \dot{H} + \dot{Q}_r - \dot{C}_p T_0$ where $B_j = \frac{\dot{N}_T}{4\pi D_j Sh_j / 2}\frac{R_u T}{p}\frac{1}{r_s}$, $B = \frac{\dot{C}_p}{4\pi\, lNu / 2}\frac{1}{r_s}$
$\dot{C}_p = \sum_{j=1}^{n}\left\{\dot{N}_j C_{p,j}\right\}$, $\dot{N}_T = \sum_{j=1}^{n}\dot{N}_j$, $\dot{H} = \sum_{j=1}^{n}\left\{\dot{N}_j H^o_{m,j}\right\}$ and $\dot{Q}_r = s e_s 4\pi r_s^2 (T_s^4 - T_\infty^4)$	

Figure 4.2. Description of the flame models, F = combustible gas, P = oxidation products CO_2 or H_2O.

Flame temperature in the 2-film model can be calculated by equating $\dot{Q}_1 = \dot{Q}_2 = \dot{Q}$. $\dot{N}_{j,2}$ is calculated from $\dot{N}_{j,1}$ and the stoichiometry of oxidation reactions of gases flowing out of the particle. When $\dot{N}_{j,2}$ is known, the gas composition at the flame can be calculated directly from Equation 5. Molar fluxes through the surface and the surface mole fractions $x_{j,s}$ need to be solved iteratively, simultaneously with the numerical solutions for particle interior.

4.2 Modeling of energy flux

Flow of sensible and formation enthalpy, thermal conduction and thermal radiation are considered as fluxes in the energy equation. Kinetic energy is neglected as gas velocities are small here. It is assumed that there is local thermal equilibrium, this means that the temperature of all phases are equal. This requires that the gases are effectively dispersed in porous media, no channeling may occur. However, for black liquor, this may occur in some cases, Saastamoinen (1996a), this will be discussed later.

As presented above, the contribution of the internal thermal radiation was lumped into the effective thermal conductivity l_e. The coupling can be modeled in many ways. Two approaches were used in this work: A diffusion approximation for cube pores and an opaque cube pore model. In the diffusion approximation, used here, Equation 4.4, Siegel *et al.* (1992), Verrill *et al.* (1995a).

$$l_e = l_s(1-f^{2/3}) + \frac{f^{2/3}}{\frac{1-f^{1/3}}{l_s} + \frac{f^{1/3}}{l_g}} + \frac{16 s T^3}{3 a_R} f \qquad (4.4)$$

where a value 850 1/m was used for the Rosseland mean absorption coefficient a_R, Paper V. In this model, we assume that the porous structure is formed of cubical pores surrounded by a char matrix. According to the diffusion model thermal radiation is directly additive to heat transfer by molecular conduction. Another model for internal radiation was presented by Saastamoinen and Richard (1996b). It assumes that pore walls are opaque and that thermal radiation only takes place in the gas pores.

$$l_e = l_s(1-f^{2/3}) + \frac{f^{2/3}}{\frac{1-f^{1/3}}{l_s} + \frac{f^{1/3}}{l_g + \frac{4 s T^3 L_g}{2/e - 0.13}}} \qquad (4.5)$$

The pore size L_g in this model needs to be defined experimentally. For large black liquor droplets, pore size needs to be in the order of 1-5 mm in order to have a correlation with experimental devolatilization data, Paper V. A large fraction of the particles are smaller than this pore size. This large pore is then physically impossible, and it is better to use model (4.4). Theoretically, both models can be used to give the same value of effective thermal conductivity by iterating the values for a_R and L_g.

4.3 Modeling of gas fluxes

Fluxes of solid and liquid species are assumed to be equal to zero. Fluxes of gases in a multi-component gas mixture in a porous medium are given by the Stefan-Maxwell diffusion equations combined with the viscous contribution and Knudsen flow, Equation 4.6, Mason *et al.* (1983):

$$\mathbf{A}\,\overline{\dot{N}''} = \overline{b} \quad \text{where} \quad A_{i,i} = \frac{1}{D_{K,i}} + \sum_{\substack{k=1 \\ k\neq i}}^{n_g} \frac{c_k / c}{D_{i,k}}, \quad A_{i,j\neq i} = -x\,\frac{c_i / c}{D_{i,j}}$$

$$\text{and } b_i = -\frac{\partial c_i}{\partial r} - \frac{c_i}{D_{K,i}} \frac{B_0}{m} \frac{\partial p}{\partial r} \tag{4.6}$$

Effective diffusion parameters, effective Knudsen flow parameters and permeability coefficients are calculated as $D_{i,j} = Đ_{i,j}\,\varepsilon / t^2$, $D_{K,i} = Đ_{K,i}\,\varepsilon / t^2$ and $B_0 = d^2\,\varepsilon /(32\ t^2)$, respectively, Mason *et al.* (1983). The gaseous species H_2O, CO_2, CO, H_2, CH_4, C_2H_2, O_2, Na, K and N_2 were included in the calculations. Binary molecular diffusion coefficients $Đ_{i,j}$ were calculated using the Chapman-Enskog theory, Gardiner (1984), Geankoplis (1972). Knudsen diffusion coefficients were given by $Đ_{K,i} = 48.5\ d\ (T/M_j)^{0.5}$, McCabe *et al.* (1993). For tortuosity the value t = 1.41 was used, Mason *et al.* (1983). A better estimate for the permeability coefficient B_0 and Knudsen flow parameter D_K would be obtained from direct measurements, Mason *et al.*(1983), but since no such data is currently available, we estimated the pore size, *d*, from the measured internal surface area to be *d* = 1 µm, van Heiningen *et al.* (1992). A very common assumption made when solving Equation 4.6 is that the non-diagonal elements of the coefficient matrix **A** are neglected, i.e. $x = 0$, Salmi and Wärna (1991), Fott *et al.* (1984). Usually, the diffusion matrix **A** is diagonally dominant and this simplification does not cause any significant error. In this work the complete system is considered for solving the fluxes in Equation 4.6, i.e. $x = 1$. For the numerical solution, a Newton-like method is used, where the calculation of the full Jacobian determinant is rather complex. The derivates of fluxes with respect to partial pressures must then be calculated. For this purpose, the value $x = 0$ was used to greatly simplify the solution, which has no effect on the physical model.

4.4 Reactions source terms

For a number of n_R reactions and *n* species, the source term vector of the species $\overline{\dot{c}}$ in Equation 4.2 is obtained from the reaction rates of the key components and stoichiometry, Equation 4.7, Salmi and Wärna (1991).

$$\overline{\dot{c}} = \mathbf{a}^T \overline{R} \text{ or by using summations } \dot{c}_j = \sum_{k=1}^{n_R} a_{k,j} R_k \text{ for } j = 1, n \tag{4.7}$$

Here, **a** is the stoichiometric matrix and $\overline{R}$ denotes the column vector of the reaction rates of the key components, as listed in Table 5.1. Cell $a_{i,j}$ denotes the stoichiometric coefficient of species j in the i:th reaction. A negative coefficient indicates that the species is consumed. For example, for drying

$a_{i,j}$ is equal to –1 and 1 for liquid water and water vapor, respectively. This approach is very useful in computer modeling as the matrix presentation can be effectively manipulated by numerical algorithms.

4.5 Modeling of structural parameters of porous media

Modeling of structural parameters in porous media is very difficult. For some applications such as paper drying and low temperature applications, properties such as permeability and effective thermal conductivity can be measured. Here, experimental determination of these is very difficult or even impossible as particle size is small, temperatures are high and the time scale of the processes is very short.

For black liquor, particle swelling is a very important phenomenon. Swelling opens pore volume for mass transfer, for internal reactions and also for internal thermal radiation. Although these parameters are very difficult to measure and are scarcely available, they are very important factors affecting the processes studied. In this work, we had to use very rough approximations for some of these parameters, for example pore size that is used in the mass transfer model, was approximated on the basis of measured internal surface area. The role of these parameters will be examined in section 6 by means of sensitivity analysis to give some estimate on the effect of these on combustion behavior. The internal structure of a swollen particle was roughly studied in Papers II and V. Figure shows an example on how a particle looks inside.

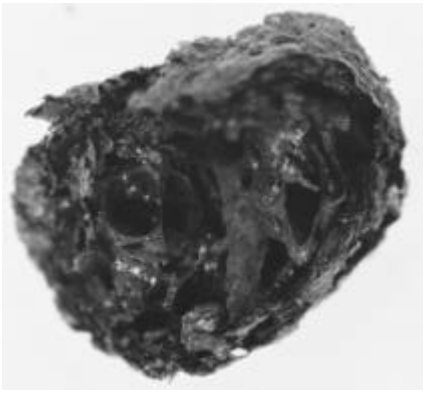

Fig. 4.3. Internal structure of a swollen kraft black liquor char particle, pyrolyzed at 700 °C in N_2, Paper V

Fig. 4.4. Edited version of 4.3, horizontal size ~ 5 mm, Paper V

As Figures 4.3 and 4.4 show, the internal structure of swollen black liquor char particles seem to be very non-homogenous. Pores up to few mm can be observed in the center region of the particle. Near the surface, the structure seems to be more compact, showing a “corn flakes”-type of matrix. To get a better picture of the internal structure of a char particle at different conditions, more detailed research on pore properties of chars should be done. From these results, we may only estimate the magnitude of the largest pores and a general impression of the pore matrix. However, this information is very valuable in developing a detailed combustion model.

4.6 Numerical solution

An implicit control volume method was used in this work, Ferziger and Peric (1997). The droplet was divided into a sufficient amount of spherical concentric computational cells, see Figure 4.5. Boundary conditions for the center and surface were given by ghost cells and a numerical grid. Conservation equations were written for each of these cells and discretized for the node values to be solved. We first also tested an explicit method for time integration (Paper I), but it was found very unstable as the system is very stiff (different time scales exist). The benefit of an implicit method is that it is stable on time integration and the time steps are limited only the physical processes. A droplet was divided into a sufficient number of spherical concentric computational cells of equal radial thickness. Diffusion and convection terms were approximated by a 2^{nd} order schemes, Ferziger and Peric (1997). A three time-level approximation of the time differentiate was used to obtain a satisfying 2^{nd} order accuracy , Ferziger and Peric (1997). The very first time step was calculated using a 1^{st} order backward scheme.

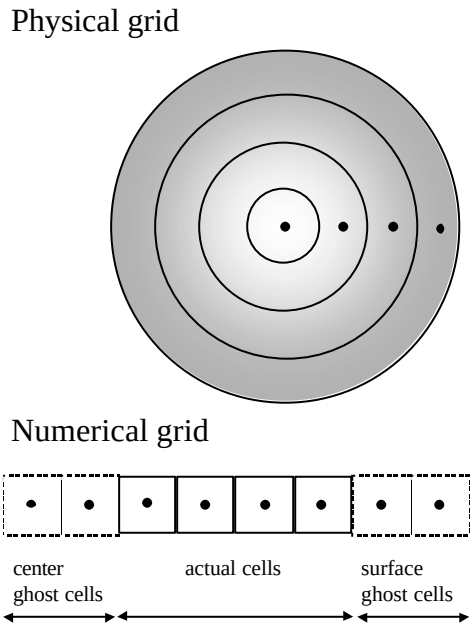

Figure 4.5. Physical and numerical calculation domains

The discretized algebraic conservation equations for every time step were solved by linearizing all the fluxes and source terms of the discretized conservation equations and presenting the solution in *delta form* that gives the corrections that are needed to approach the correct solution, Equation 4.8, Ferziger and Peric (1997).

$$\mathbf{J}_n \Delta x_n = G_n \qquad (4.8)$$

where **J** is the Jacobian matrix, Δx is the correction vector needed in variables and G is the residual function vector that is to be iterated to zero, i.e. the right hand sides of Equations 4.2 and 4.3. n

refers to the current iteration step. This tri-diagonal linearized system of equations can effectively be solved by the Thomas algorithm, Tannehill *et al.* (1984). Then new, corrected values for variables follow from $x_{n+1} = x_n + \Gamma \Delta x_n$. Γ is the under-relaxation variable that can be used in highly non-linear problems to damp numerical oscillations, values Γ = 0.5, 0.7 and 1.0 were used for partial pressures, temperature and concentrations of condensed species, respectively.

The calculation of the full Jacobian requires complex algorithms in the case of the complex relation of fluxes and gradients of concentrations and total pressure according to the dusty gas model. In our work, a different approach was used. The diffusion matrix **A**, Equation 4.6, is usually diagonally dominant, Salmi and Wärna (1991). Therefore, we may use the diagonal approximation i.e. $x = 0$ in calculating the Jacobian, and a simple form was obtained for differentiation of the fluxes because the strong coupling between the fluxes of different species disappears. The chemical reaction rate source terms, Equation 4.7, are linearized according to Equation 4.9:

$$\dot{c}_j^{n+1} = \dot{c}_j^n + \sum_{k=1}^{n_R} \left\{ \min\left(a_{k,j} \frac{\partial R_k^n}{\partial c_j}, 0 \right) \right\} \Delta c_j \qquad (4.9)$$

Superscript *n* refers to the current iteration step. The min() function is used here to consider only the negative slopes of the source terms in order to increase the value of the diagonal of the Jacobian and obtain an adequate under-relaxation effect.

The convergence of discretization was studied by refining the spatial and time increments until the result remained unchanged. Convergence of iteration inside every time step was checked, for L_2-norm of 10^{-8} K, 10^{-8} Pa and 10^{-8} mole/m^3 for the energy conservation equation, gaseous species conservation equation and condensed species conservation equations were used, respectively. This resulted in a varying number of iterations inside every time step, depending on the dominating reactions and mechanisms.

4.7 Limitations of the 1D model

The one dimensional model developed here can be used for modeling heat and mass transfer in a plate, cylinder or spherical geometry. In reality, cases are often 2- or 3-dimensional. The one-dimensional sphere model was used here for its reasonable simplicity and because it is a fair approximation of the observed geometries of black liquor particles in combustion experiments. One-dimensional problem is also much simpler and can be solved quicker. In fact, there is no sufficient experimental data available on internal particle structure for validating a 2- or 3-dimensional models.

Even in fully spherical particle combustion applications where slip velocity is high, the problem is not necessarily symmetrical and one-dimensional as the external flow field is highly distorted. For example, conditions at the stagnation point, at the wake side or at the side location are totally different. A one-dimensional approach may be justified by effective rotation of the particle in the flow field. When it comes to defining the boundary conditions the 1D model has some limitations, for example only symmetrical BC's can be used. This may lead to significant errors, for example, the modeling of internal thermal radiation heat transfer is not always straightforward.

5 APPLICATION OF THE HEAT AND MASS TRANSFER MODEL FOR BLACK LIQUOR COMBUSTION

5.1 Estimation of physical and thermodynamical properties

A typical elemental composition for black liquor used in this work is 39.8%-wt C, 4.2% H, 0.1% N, 15.5% Na, 0.07 % K, 3.97% S, 0.33% Cl and 36.03% O (by difference), Frederick *et al.* (1993). Based on this data, chemical composition can be roughly estimated, Adams *et al.* (1997). The Na content of black liquor used here is as high as 15.5%. However, for black liquors this is near the lower limit. The Na content may be as high 20% for some liquors, Adams *et al.* (1997). The large amount of inorganic matter in black liquor makes its gasification reactivity very high when compared with other fuels.

The basic idea in estimating the compositions was that we first assume the species present in addition to pyrolysable matter (here Na_2S, K_2S, Na_2SO_4, K_2SO_4, Na_2CO_3, K_2CO_3, NaCl, KCl). The ratio of sulfide sulfur to total sulfur was specified, here a value of 0.95 was typically used. It was also assumed that sulfur is bonded by Na_2S and K_2S in proportion to the mole amounts of elemental Na and K. All N was assumed to be organic. Based on these, the composition of the assumed species and also, the modeling composition and the amount of pyrolysable matter (for one carbon atom) can be solved.

Molar heat capacity, molar heat of formation and density of species were obtained from the database of the HSC software, HSC (1994). From these and the estimated composition, the total density (kg/m^3) and specific heat capacity (J/kgK) were calculated as follows

$$\frac{1}{r_{BL}} = \sum_{j=1}^{n} \frac{y_j}{r_j} \tag{5.1}$$

$$c_{p,BL} = \frac{\sum_{j=1}^{n} \{c_j C_{pm,j}\}}{r_{BL}} \tag{5.2}$$

Where y_j = mass fraction of species, r_j = density of species j (kg/m^3), c_j = molar concentration of species j (mol/m^3), and $C_{pm,j}$ = molar heat capacity of species j (J/molK). r_j and $C_{pm,j}$ for pyrolysable matter were calculated from the measured values, Adams *et al.* (1997) and equations 5.1 and 5.2, respectively. The heat capacity of gases was calculated from NASA polynomials, Gardiner (1984). Thermal conductivity and dynamic viscosity were presented as 3rd and 2nd order polynomials, respectively, fitted to values obtained from the kinetic gas theory, Gardiner (1984). The thermal conductivity of black liquor was calculated by $l_s = 1.44 \cdot 10^{-3} \cdot (T - 273.15) + 0.58 - 0.335\, y_s$, where y_s is the mass fraction of dry solids in liquor, Adams *et al.* (1997).

5.2 Intrinsic reactions for black liquor combustion modeling

It was assumed that the combustion stages are locally sequential in the droplet i.e. only drying, devolatilization or char conversion may occur at the same location r inside the particle. The reactions considered are given in Table 5.1. Arrhenius' expressions were used for the specific reaction rate constants k_i. Drying was modeled as a heat transfer limited process, where the local boiling temperature during drying was assumed i.e. $T = T_b(y_s)$, Clay *et al.* (1984). It was assumed that when the water content of liquor is high, the droplet behaves as a liquid particle during the initial stages of drying, Saastamoinen (1996a). The critical water content was assumed to be 10%-wt: below that droplet behaves as a solid fuel and temperature gradients may arise in the droplet.

When this study was initiated, devolatilization was modeled by a set of decomposition of functional groups (aliphatic carboxylic acids, lignin), Alén *et al.* (1996). This type of model is successfully used by Solomon and Colket (1979) for coal and also lignin, Avni *et al.* (1985). It was assumed that each of these groups acts independently of each other. Also carboxylic acids are assumed to be fully volatilized and lignin is the only char forming component. Rates for these reactions were roughly estimated from Shricharoenchaikul *et al.* (1995). It was found that this model does not work well. No correct amount of char can be formed under these assumptions. Also, as it was found by Alén *et al.* (1996) that inorganic matter strongly affects the total yield and decomposition, so this model was rejected.

As it was found that the functional group model did not work well, a more simple model was selected. Devolatilization was describe by a single first order reaction, kinetic parameters were approximated from Sricharoenchaikul *et al.* (1995). The problem with this model was still a lack of proper experimental data and it was impossible to define accurately the kinetic parameters and also devolatilization heat. The conclusion was then that there was currently no reliable devolatilization data (i.e. simultaneous particle temperature and mass loss data with a small time resolution) available for determining the kinetic parameters. It had earlier been observed by Sricharoenchaikul *et al.* (1995) that devolatilization proceeds as fast as heat is delivered to the particles. Based on this, we used here the model proposed by Saastamoinen for heat transfer controlled devolatilization of wood, Saastamoinen *et al.* (1996b) and black liquor, Saastamoinen (1993a), Equation 11.

$$m = m_0 e(T), \quad \dot{m} = m_0 \frac{de}{dT}\frac{dT}{dt} \tag{5.3}$$

where m_0 is the initial mass of the sample and $e(T) = m/m_0$ is determined by slowly heating the sample. Alén *et al.* (1996) determined a curve for $e(T)$ for 2 types of black liquor with heating rate of 20 °C/min, this data was used here.

Pyrolysable matter was described here as $P = CH_nO_oS_pNa_qK_rN_s$, where coefficients n, o, p, q, r and s were solved simultaneously with dry solids composition estimation. For the composition showed in section 5.1, n=1.32063, o=0.55484, p=0.03727, q=0.10640, r=0.00028 and s=0.00226. As shown by, Li and van Heiningen (1990a), the organic part of the char also contains O and H in addition to carbon. For simplicity, it was assumed that the organic char composition equals the initial organic composition of the pyrolysable matter P, being CH_nO_o (Paper VI), or only carbon n = 0, o = 0 (other papers). Devolatilization S- and Na-releases were taken to be 30% and 15%, respectively, for all cases, Frederick *et al.* (1992). Mass loss of pyrolysable matter at 700-900°C was taken from the experimental data. Carbon loss and stoichiometry of the devolatilization products could be calculated on the basis of this information. The rate of devolatilization is here defined by the

devolatilization heat and heat transfer. For large particles, the ratio of internal to external heat transfer is small. Effective thermal conductivity then greatly affects the devolatilization rate. Values for devolatilization heat and effective thermal conductivity were obtained by fitting the model carbon release rates to experimental data, Paper V.

TABLE 5.1. Reactions, rate of key components and rate constants (Units m, s, mole, K, Joule), R=8.314 J/moleK.

No.	Reaction	Reaction rate expression, R_i mole/m^{3}s		A_i 1/s	E_i J/mole	Ref.
				-	-	-
1	$H_2O(l) \rightarrow H_2O$	Heat transfer controlled, latent heat 2250 kJ/kg				
2a	Reactions of the functional groups, aliphatic carboxylic acids, lignin.	First order kinetic model, used in Paper I	Kobayashi model parameters			
			1. Y = 0.3	2.00×10^{0}	1.8×10^{4}	
			2. Y = 0.5[b]	5.00×10^{5} [b]	8.0×10^{4} [b]	
			3. Y = 1.0	1.60×10^{13}	2.2×10^{5}	
2b	$P \rightarrow CH_nO_o(s), H_2O, CO, CH_4, C_2H_2,$ Na, $M_2S(s), M_2SO_4(s), M_2CO_3(s)$	First order kinetic model, used in Papers II-IV		3.78×10^{3}	4.70×10^{5}	-
2c	$P \rightarrow CH_nO_o(s), H_2O, CO, CH_4, C_2H_2,$ Na, $M_2S(s), M_2SO_4(s), M_2CO_3(s)$	Heat transfer controlled, devolatilization heat 800 kJ/kg, used in Papers V-II		8		-
3	$C(s) + H_2O \rightarrow CO + H_2$	$k_3 A_s [C] c_{H_2O} / (c_{H_2O} + 1.42 c_{H_2})$ [b]		1.60×10^{7}	2.10×10^{5}	[d]
4	$C(s) + CO_2 \rightarrow 2\ CO$	$k_4 A_s [C] c_{CO_2} / (c_{CO_2} + 3.4 c_{CO})$ [b]		3.94×10^{8}	2.50×10^{5}	[e]
5	$H_2 + 0.5\ O_2 \leftrightarrow H_2O$	$k_5 c_{H_2}^{0.5} c_{O_2}^{2.25} c_{H_2O}^{-1}$		1.41×10^{14}	1.67×10^{5}	[f]
6	$CO + H_2O \leftrightarrow CO_2 + H_2$	$k_6 (c_{H_2O} c_{CO} - 1/K_{eq} c_{H_2} c_{CO_2})$		2.75×10^{6}	8.37×10^{4}	[f]
7	$CH_4 + H_2O \rightarrow CO + 3\ H_2$	$k_7 c_{CH_4} c_{H_2O}$		3.00×10^{5}	1.26×10^{5}	[f]
8	$CH_4 + O_2 \rightarrow CO + 2\ H_2$	$k_8 c_{CH_4}^{0.5} c_{O_2}^{1.25}$		2.47×10^{9}	1.26×10^{5}	[f]
9	$C(s) + 0.5\ O_2 \rightarrow CO$	$k_9\ A_s [C]\ p_{O_2}$ [b]		3.00×10^{3}	1.80×10^{5}	[g]
10	$M_2S(s) + 2\ O_2 \rightarrow M_2SO_4(s)$	$k_{10}\ A_s [M_2S]\ p_{O_2}$ [b, c]		0.75×10^{3}	1.80×10^{5}	[g]
11,12	$M_2CO_3(s) + 2\ C(s) \rightarrow 2\ M + 3\ CO$	$k_{11} [M_2CO_3]$		1.00×10^{9}	2.44×10^{5}	[h]
13,14	$Na_2SO_4(s) + 2\ C(s) \rightarrow Na_2S(s) + 2\ CO_2$	$k_{13} [x_{M_2SO_4}]^{1.4} [C]$ [a]		3.79×10^{3}	7.81×10^{4}	[i]

[a] $x_{M_2SO_4}$ = [M_2SO_4] / [M_2SO_4 + M_2S + M_2CO_3], M = Na or K, [b] A_s = specific surface area, 160 m^2/g, [c] it is assumed that oxygen reacts with char and M_2S in proportion to the mole amounts of these present locally, [d]Li and van Heiningen 1991, [e]Li and van Heiningen 1990a, [f]Jones and Lindstedt 1988, [g]Smith 1982, [h]Li et. al l990b, [i]Wåg *et al.* 1995b

[b] only reaction 2 is used to describe the decomposition of the aliphatic acids, assuming no char formation (Y = 1), for char forming lignin, reactions 1-3 are used to have temperature dependent char yield

The data from Li and van Heiningen (1991) and Li van Heiningen (1990a) were used for H_2O and CO_2 gasification reactions R.3. and R.4, respectively. The specific surface area in these experiments were 160 m^2/g. This value was also used in this work and A_s was assumed to be constant for all cases studied here. Chapter 6 also gives a sensitivity analysis with this parameter to determine its importance for conversion mechanisms. Usually, surface area is not constant and it changes with char conversion. However, as there is no better information available, the assumption of a constant internal surface was used here. These same rate equations are also used in most of the other models developed for black liquor, and therefore it is well justified to use then.

In all the previous models for black liquor combustion the role of intra-particle gas reactions during devolatilization is neglected. Here, for intra-particle gas oxidation, the simplified methane oxidation scheme of Jones and Lindstedt (1988) was used, R.5-8. Basically, if no CH_4 is present and CO is still present, this model will work as CO oxidation pathway, and its relevancy should be tested at the specific conditions studied here. Also, if both CH_4 and O_2 are absent, the CO-water shift reaction remains, which will control the composition of gas species in the particle. It is well known that gas reactions are effectively catalyzed by char surfaces. This should be the case also here, but since we could no find any better information, these gas phase rate equations were used.

If O_2 reaches the char surface a fast and exothermic reaction will take place, R.9. There are currently no data available on this for black liquor. It is known that the reaction with O_2 is much faster than H_2O/CO_2 gasification. Here, the data from Smith (1982) for activated carbon was used. Black liquor also contains sulfide that gets very easily oxidized when it comes into contact with O_2. As there was no data available for this reaction either, some relevant approximation was required. It was assumed that O_2 reacts with char and Na_2S in proportion to amounts of these present. If CO is assumed to be the product of carbon oxidation, then $A_{10} = 0.25\ A_9$ and $A_{10} = 0.5\ A_9$ for product CO_2, see Table 5.1.

For the carbonate reduction reactions R.11-12, a model presented by Li and van Heiningen (1990b) was used. The same rate coefficients were used for carbonates of Na and K. This reaction is the path for Na/K vapor release. However, there are no further reactions of alkali vapors included in this work. This reaction releases char carbon without any additional oxidizer. It was shown by Wåg et al. (1997b) by molecular beam mass spectrometry (MBMS) that CO is the main product of this reaction, only a small amount of CO_2 was detected. Based on this, CO was assumed to be the only product here. In theory, any C released from carbonate reduction reaction as CO_2 will be available for char CO_2 gasification. However, in typical furnace conditions where the concentration of water vapor is high, char gasification by CO_2 has a minor role. Therefore, whether CO or CO_2 is the product, has only a minor effect. After devolatilization, in reactor conditions in pure N_2 atmosphere, carbonate reduction reaction and CO_2 gasification are the only mechanisms available for char conversion. In this case, the char gasification by CO_2 (coming from the carbonate reduction) might be important. The role of this hypothetical reaction path was tested by varying the product gas composition from CO to CO_2, in pure N_2, at 900 - 1200 °C. It was found that CO_2 from carbonate reduction will be effectively converted by char during CO_2 gasification. This means that if CO_2 is the product of carbonate reduction, the CO_2 formed will be partly converted and CO is formed. In the case of high temperature and large particles, CO_2 conversion in gasification is high, and at maximum, CO would be the main gas species leaving the droplet as experimentally observed by Wåg at el. (1997b). This mechanism should be further studied experimentally. For example, by varying the particle size and temperature, this additional auto-gasification mechanism can maybe identified.

For sulfate reduction reactions, R.13-14, models presented by Wåg *et al.* (1995b) were used. In this model the activation energy was corrected from the original model presented by Grace *et al.* (1989). This reaction together with the sulfide re-oxidation R.10. forms the well known sulfide-sulfate cycle. Cameron and Grace (1985) found that CO_2 is the main product of this reaction. Therefore, no CO was assumed to be formed in the reactions R.13-14.

5.3 Modeling physical combustion behavior

One of the specific combustion characteristics of black liquor is its swelling behavior. The diameter of the droplet may increase by a factor of 3 or more during devolatilization, Frederick *et al.* (1994c). Swelling of the droplet was modeled using a uniformly stretching grid and an overall swelling coefficient that could be experimentally determined. Volumetric swelling parameter was defined as $b_i = V_i / V_i^{t=0}$, where i refers to a single computational cell. A volumetric swelling coefficient, *ß*, was calculated from Equation 13:

$$b = \underbrace{1 + f_1(X_{dry})\,(b_{dry} - 1)}_{(a)} + \underbrace{f_2(X_P)(b_P - b_{dry})}_{(b)} \qquad (5.4)$$

where b_{dry} and b_P are the volumetric swelling coefficients during drying and devolatilization, respectively. The terms (a) and (b) describe the volume increase during drying and devolatilization, respectively. *f(X)* is the function that describes the volume increase on conversion of the different processes. Here, $f_1(X_{dry}) = 1$ and $f_2(X_P) = X_P$. Here, the values b_{dry} = 3.65, Frederick (1990a) and b_P = 27 were used. As the char conversion in a computational cell reaches a critical value, X_{cr}, the cell is removed and particle size is decreased stepwise. The material left in the removed cell is transferred into the other cells in proportion to cell volumes, Paper III. Figure 5.1 shows an example of how this critical char conversion value, X_{cr}, affects the shrinking of the particle diameter in gasification conditions. Best correlation is obtained for $X_{cr} = 0.8$.

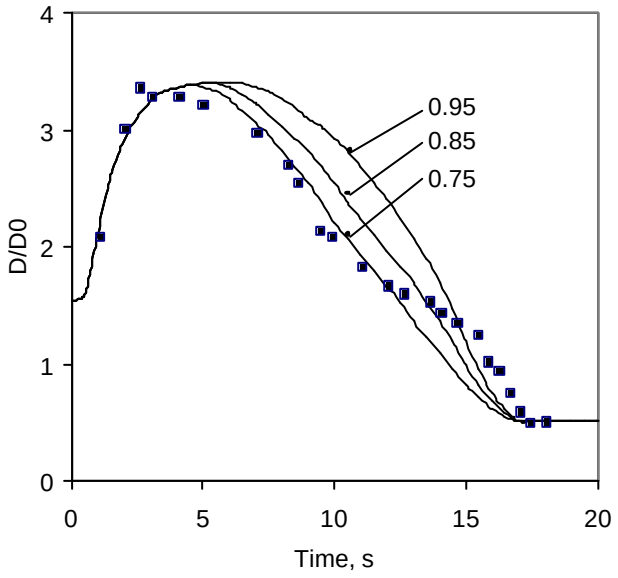

Figure 5.1. Effect of critical collapse conversion of char, in a 20% H_2O, 4% CO, N_2 environment, experimental data from Frederick (1990b).

6 SENSITIVITY ANALYSIS

The objective of this chapter is to study the effect of model parameters that can not be accurately measured. For example, the internal mass transfer in black liquor combustion was modeled in detail in this work but the related parameters are not available. Table 6.1 presents all the parameters studied, the typical values used in simulations and the range that has been studied. The numerical model solution parameters such as relaxation parameters, grid/time resolution etc., are not discussed here.

Table 6.1. Model parameters

Parameter	***Definition***	***Range/used value***	***Source***
b_{dry}	Swelling coefficient during drying	1.2-1.54 / 1.54	-
b_{dev}	Swelling coefficient during devolatilization	1.54-3 / 1.54	-
$y_{s.cr}$	Critical dry solids content, if $y_s<y_{s.cr}$ droplet dries as an evaporating droplet, if $y_s>y_{s.cr}$, as a solid	0.7-1 / 0.9	Paper III
X_{cr}	Local collapse conversion of char, -	0.75-0.95 / 0.8	Paper III
j	Diameter ratio of cenospheres, -	0-0.875 / 0	Paper II
a_R	Rosseland mean adsorption coefficient, 1/m	100-10000 / 850	Paper V
DH_p	Devolatilization heat, kJ/kg	200-1200 / 800	Paper V
A_s	Internal reaction surface area, m^2/g	16-1600 / 160	Here
d	Mass transfer pore size, μm	0.31-3.1 / 1	Here
t	Tortuosity, -	1-3 / 1.41	Here
h_R	Reduction efficiency, ratio of sulfide sulfur to total sulfur		Järvinen *et al.* (1999)

As drying and devolatilization are both usually considered to be heat transfer controlled processes, the swelling coefficients b_{dry} and b_{dev} play an important role. For char combustion, typically considered to be a mass transfer controlled process, a larger external surface area means a higher rate. External surface area increases in proportion to d^2, i.e. b^2. For drying, b is roughly 1.2 at its minimum and 1.54 at its maximum, Frederick (1990a). The drying rate is then 1.6 times greater in the latter case. For the devolatilization of an isothermal particle the rate is 3.8 times greater for the maximum case (3 vs. 1.54). For mass transfer limited char combustion, the rate is much higher for the more swollen droplets.

As the droplet is exposed to a hot environment, it will first heat up to the atmospheric boiling point. Then it starts to evaporate vigorously, bubbling also from the interior. As its water content decreases, the viscosity of the liquor increases and finally, when a certain value of viscosity is reached no bubbles can be formed, and the droplet starts to behave as a solid fuel and an internal temperature gradient develops. The value of dry solids content at which this transition takes place is used as a free parameter, determined from experiments. Typically, a value of $y_{s.cr}$ = 0.9 gives a sufficient correlation with experimental data, Paper III. It was shown by Frederick *et al.* (1993), that critical water content (usually referred to as the dry solids content at ignition) is a function of gas temperature. As shown by Kulas (1990), swelling data for 2 mm droplets do not work with larger particles and apparently, particle size will also affect this parameter. This parameter should be further studied experimentally, including the effect of internal water transport mechanisms during drying.

In all previously developed black liquor combustion models, it is assumed that particle volume decreases linearly as char carbon is converted *i.e.* particle size decreases while *char carbon* mass concentration remains constant. Total density of the particle is not constant as the amount of inorganics does not change accordingly. In the new model presented here, as the char conversion in a computational cell reaches a critical value, X_{cr}, the cell is removed and particle size is decreased stepwise. Therefore, all char that is converted does not decrease the particles external volume continuously. The material left in the removed cell (i.e. 20% of the char left and inorganic species) is transferred into the other cells in proportion to the cell volumes. This model was already presented in Figure 5.1. and it was found that best correlation with experimental shrinking data was obtained with a value of 0.8 for X_{cr}, which means that the supporting char structure will collapse locally when 80 % of the char matrix is consumed.

As was observed in Paper II and by Saastamoinen (1996c), black liquor particles may be hollow i.e. they are cenospheres. Compared to fully homogeneous particles, the surface region is much more dense in these and the porosity is smaller too. This affects the internal heat and mass transfer rates. For cenospheric particles conduction by the internal heat transfer is more effective, whilst mass transfer is less effective due to their smaller porosities. As it was already shown in Paper II, drying and devolatilization rates are faster for cenospheres. Because the internal heat transfer is more effective for cenospeheres, surface temperature will be lower, which decreases the effect of auto-gasification. The auto-gasification mechanisms was observed to be very sensitive to the internal structure and therefore, more work on this should be done.

As mentioned above, thermal conductivity not only strongly affects the rate of drying and devolatilization but also the degree of overlapping of char combustion and devolatilization. Thermal radiation heat transfer was modeled by the diffusion approximation, using Rosseland mean absorption coefficient a_R. Thermal radiation is then directly added to molecular conduction. The mean radiation attenuation distance is inversely proportional to a_R, Siegel and Howell (1992). The greater the value for a_R the shorter the distance radiation will penetrate the structure. The effect of internal heat transfer was studied in detail in Paper V. The best correlation with experimental carbon loss data was obtained for roughly a_R = 850 1/m. This means that radiation loses most of its intensity within a distance of 1 mm. In the model used by Verrill *et al.* (1995a), a_R was taken to be equal to 70 1/m. According to this, significant attenuation takes place at 14 mm which is far greater than the particle dimensions. In Paper V different thermal conductivity models were compared. Verrill's (1995a) model gave higher rates for devolatilization char release than measured due to a more effective internal heat transfer. In addition to internal heat transfer, devolatilization heat is a very important parameter that defines the rate of devolatilization. Therefore, a_R and devolatilization heat DH_p were simultaneously varied over relevant ranges. The best correlation with experimental data was obtained with a_R = 850 1/m and DH_p = 800 kJ/kg. For comparison, in Saastamoinen's model (1996a) $a_R = \infty$, DH_p = 610 kJ/kg and in Verrill's model (1995a) a_R = 70 1/m, DH_p = 83 kJ/kg.

All the parameters discussed above were already studied in the appendix papers. As well as these parameters, internal surface are A_s, mass transfer pore size d and tortuosity t are also studied here. The internal reaction surface area typically varies between 10 and 200 m^2/g , van Heiningen *et al.* (1992). Here, the theoretical range 16-1600 m^2/g was considered for model performance. Figure 6.1 shows the effect of internal reaction surface area on carbon release rate for 0.5-2 mm particles burned *in-flight* (initial slip velocity 14 m/s) at 1200°C, 20% H_2O, 12% CO_2, 3% O_2 and N_2.

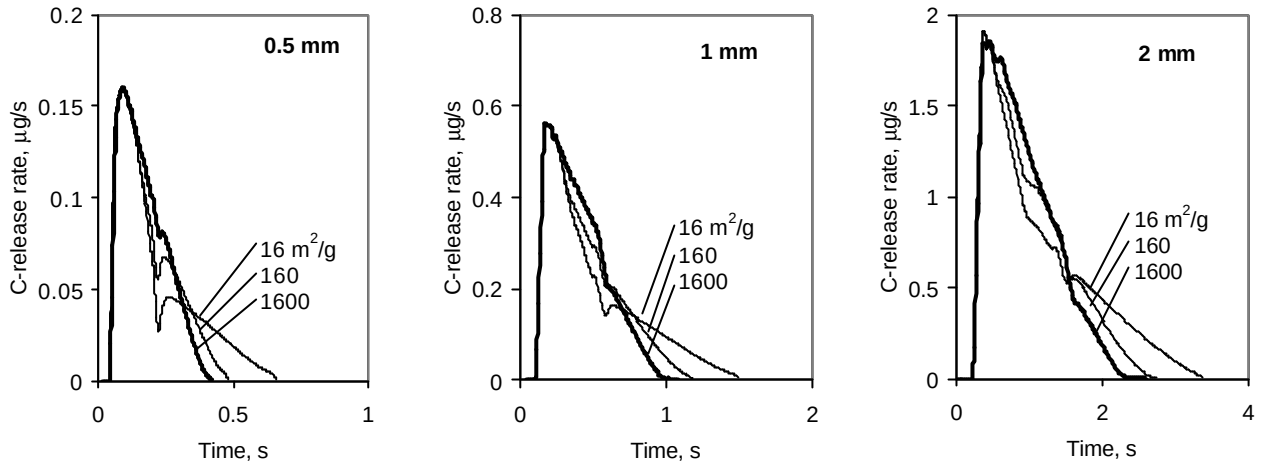

Figure 6.1. The effect of internal reaction surface area on C-release rate during in-flight combustion, note the different axes.

As Figure 6.1. shows, internal reaction surface area has a significant effect on char conversion during devolatilization. As A_s increases, the auto-gasification mechanism becomes more important *i.e.* the released H_2O and CO_2 are more effectively converted by gasification as they flow out through the char surface layer. This can be seen as a larger area under the devolatilization peak (larger amount of carbon release in devolatilization).

What is important, is that the effect of flow channeling is not considered in the model. (Flow channeling means that instead of flowing out uniformly through the porous matrix, most gases are escaped through a single blow hole.) This means that all gases released are available for heterogeneous reactions. In reality, if all gases are released through a large single hole, no internal gasification takes place. As the fraction of char converted already during devolatilization increases there is less char left for the char combustion stage. Therefore, carbon release rates *during char combustion* are not fully comparable.

For the mass transfer pore size, a value of 1 µm was used for all cases studied in the appendix papers. This parameter primary defines the internal mass transfer mechanism. The effect of pore size on effective diffusivity D_e, a combination of molecular diffusion and Knudsen diffusion, Equation 6.1, is presented in Figure 6.2.

$$\frac{1}{D_e} = \frac{1}{D_K} + \frac{1}{D_{AB}} \tag{6.1}$$

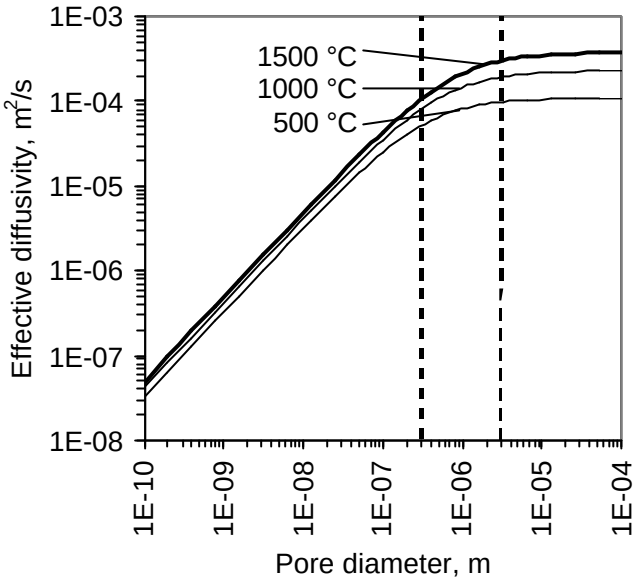

Figure 6.2. The effect of pore size on effective diffusivity of H_2O in air, 800-1200 °C, studied range 0.3-3 mm is showed.

As Figure 6.2 shows, for pore sizes smaller than 10^{-7} m, Knudsen diffusion dominates. If the pore size is larger than 10^{-5} m, molecular diffusion is the controlling factor. Here, pore sizes is in the range where both mechanisms are present, see Figure 6.2. During devolatilization, the devolatilization rate is heat transfer limited, an internal pressure gradient develops and the viscous contribution becomes important. The permeability is proportional to d^2, which means that if the pore size increases by a factor of 10, permeability increases by a factor of 100. In order to maintain the same flow rate, the pressure gradient needs to be 99% smaller. Typically, for a 1 µm pore size, total pressure at the particle's center is less than 1.1 times the atmospheric pressure. If a pore size of 0.1 µm is used the internal pressure will be very large, it would break the droplets. This has not been observed in experiments, so pore sizes should be larger than this. Because of this, the pore size range 0.31-3.1 µm was used, resulting in 10 times larger and smaller permeability than the reference case. Figure 6.3 shows the effect of pore size on carbon release rate.

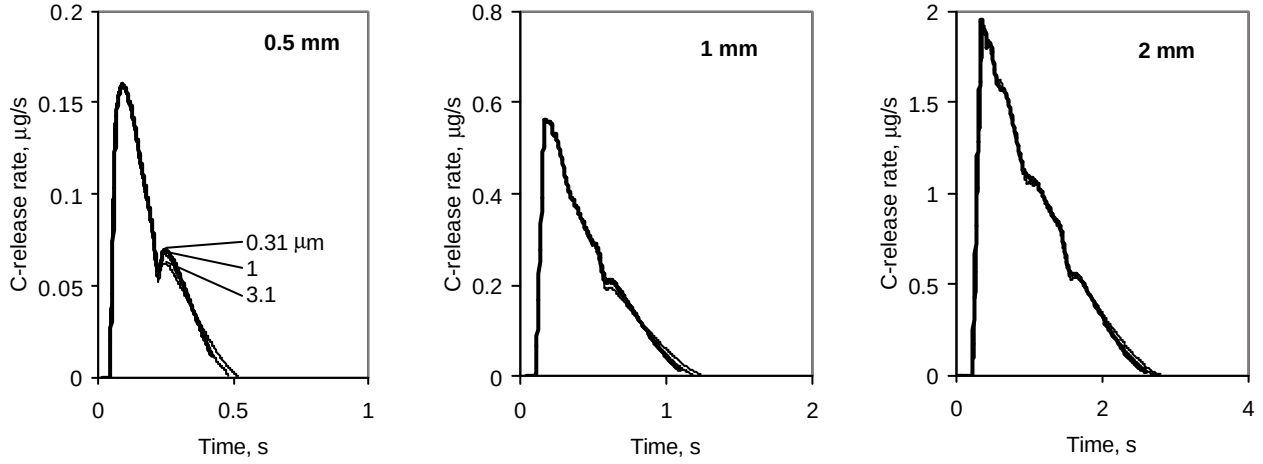

Figure 6.3. The effect of mass transfer pore size on C-release rate during in-flight combustion, note different axes.

The change from 0.31 to 1-3.1 µm in pore size has a negligible effect on the auto-gasification mechanism. For the char combustion stage, the smaller the pore size, the lower the rate of char conversion. Generally, pore size had a negligible effect of carbon release rate over the studied range.

The tortuosity was assumed to be 1.41, which corresponds to a "zig-zag"-channel bent at an angle of 90 °. Here values from 1 to 3 were studied that correspond to a decrease in effective diffusion coefficients and permeabilities with a factor of 0.1 at the maximum. Figure 6.4 shows the effect of tortuosity on carbon release rate for 0.5-2 mm particles burned in-flight at 1200°C, 20% H_2O, 12% CO_2, 3% O_2 and N_2.

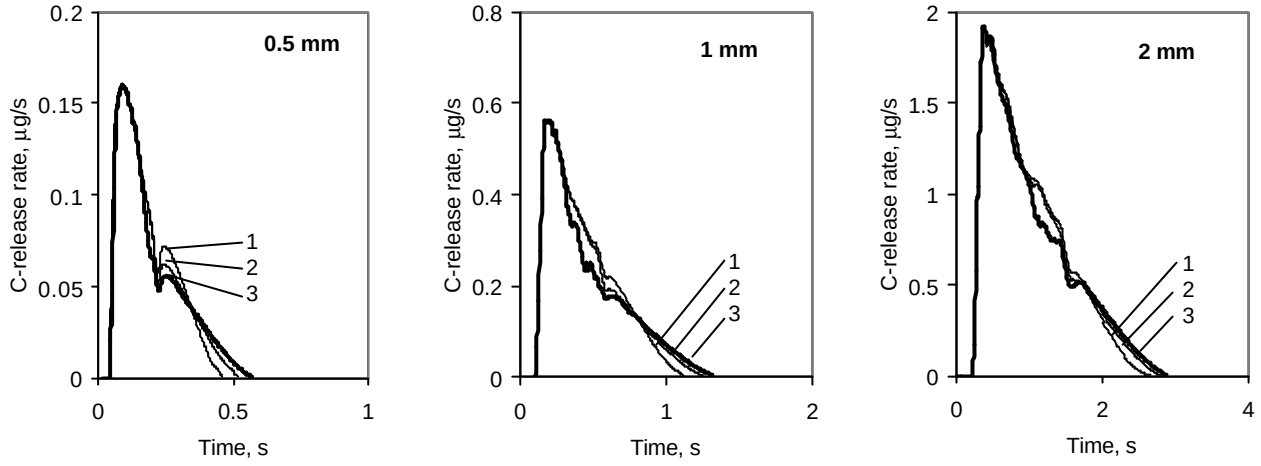

Figure 6.4. The effect of tortuosity on C-release rate during in-flight combustion, note different axes.

As the tortuosity increases, so does the internal mass transfer resistance. This can be clearly seen as a lower rate of carbon release during the char combustion stage. For a tortuosity of 3, model had convergence problems during drying and devolatilization.

Only a rough analysis of the importance on different parameters was made here. It was found that internal structural parameters are important for the char conversion processes. For the new internal auto-gasification mechanism, these parameters are of great importance as here the gasifying agents originate from the droplet itself while the external mass transfer resistances are absent. However, the flow channeling effects should be further studied and also the fraction of dead pore volume, Bear (1972) identified.

One of the model parameters is the reduction efficiency that defined the amount of reactive sulfur. The effect of the reduction efficiency for sulfate was studied by Järvinen *et al.* (1999). The reduction efficiencies of 0 and 95% were compared. It was found that if all sulfur is initially in the form of Na_2SO_4 (*e.g.* reduction efficiency is 0%), sulfate reduction is an important char conversion mechanism that competes with auto-gasification. In the modeling calculations presented here, it is assumed that the total sulfur reduction efficiency is equal to 95%. In non-oxidizing conditions *i.e.* in 100% N_2 environment 5% sulfur in sulfate is then insufficient to have any contribution to char conversion. Also, in typical furnace conditions with 3% O_2 in the gas, the sulfate-sulfide cycle has no significant effect on char conversion for the initial 95% reduction efficiency. Figure 6.5. shows an approximate calculation of the effect of sulfate reduction on carbon loss.

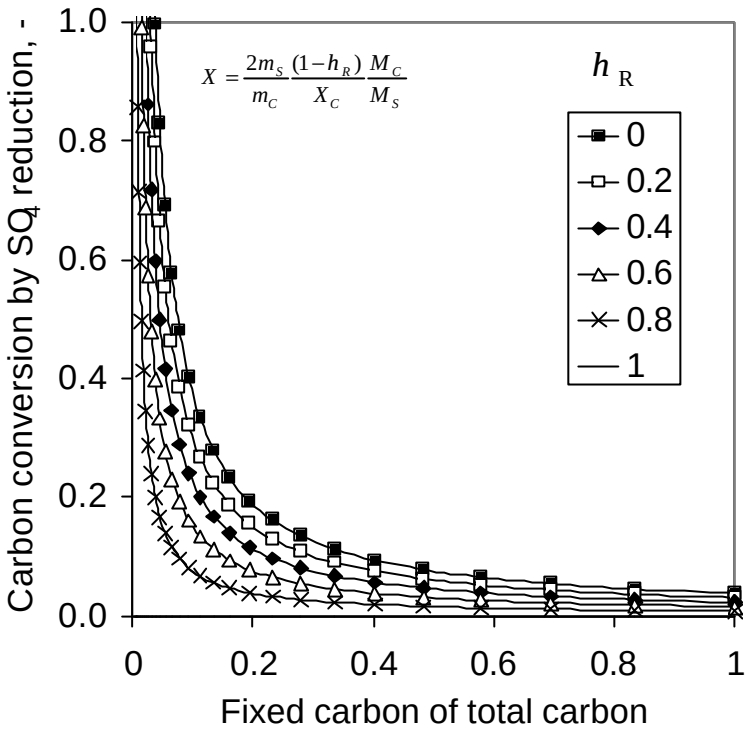

Figure 6.5. The effect of fixed carbon and sulfate reduction efficiency on char conversion, m_S/m_C = 0.1.

As Figure 6.5 shows, sulfate reduction can be very important mechanism for char conversion when the amount of fixed carbon is small and most sulfur is in the sulfate form. In this work, reduction efficiency is 95% which means that the role of sulfate is negligible for the typical values of fixed carbon of 0.3-0.5.

7 EXPERIMENTAL VALIDATION

7.1 Mass loss and carbon release

In order to accurately calculate the flight path of the droplet and the gas mass source terms for flow field simulations, particle mass needs to be correctly estimated. Therefore, it is of great importance to validate this for the model developed. In a model where solids are described by a combination of chemical species formed from elements, also elemental balance needs to be satisfied. In this work, since the focus was in the modeling of devolatilization, char reactions and related physical mechanisms, and not the mechanistic modeling of sulfur and sodium release. Sulfur and sodium losses during devolatilization were taken from typical experiments and assumed to be constant for all cases to have their contributions in the total mass loss.

Mass loss is the most important output from the model. There are two main possibilities to experimentally validate the mass loss predictions:

a) continuously weighting the particle (*in situ* measurement) or
b) by varying the particle residence time in reactor conditions

For option a), significant additional forces may by introduced to the microbalance by the ejecting gases that are release from the particle. Therefore, this method is not used for rapid heating rate tests. For option b), two different methods can be applied: b1) a particle can be suspended into a thin metal hook and inserted into a furnace for a predetermined time or b2), a drop tube furnace can be used, were the residence can be controlled by adjusting the length of the particle flight path. In both of these methods (b1 or b2), only one temporal value can be obtained for each droplet. Data for this same particle can not be obtained at any other moment. As swelling or other properties may differ from droplet-to-droplet, this method gives only an average description of the process.

Figures 7.1 and 7.2 shows a model comparison with experimental devolatilization mass loss data in N_2, 700-1200 °C, 2 mm particles, 40% initial water content for 5 and 10 s residence times, Frederick *et al.* (1994b). The experimental data was obtained from the literature, the measurements were made in a muffle furnace reactor where the droplet was suspended to a thin platinum wire. The reactor gas atmosphere was very close to stagnant and the temperature of the gas and surrounding reactor walls can be assumed to be equal. As the dimensions of the furnace are much larger than the droplets, reactor can be assumed to be a black enclosure. The suspended and weighted droplet is lowered into the furnace for a predetermined time (here 10 s data was used) and lifted up into a nitrogen quench to stop further reactions. After this, particle dimensions, mass and elemental balance for carbon were determined.

Figure 7.1 shows the temporal variation of the mass compared with experiments at 5 s intervals. Final yield on devolatilization can be validated using these results, Figure 7.2, predicted contributions of different reactions on mass and carbon losses are also shown.

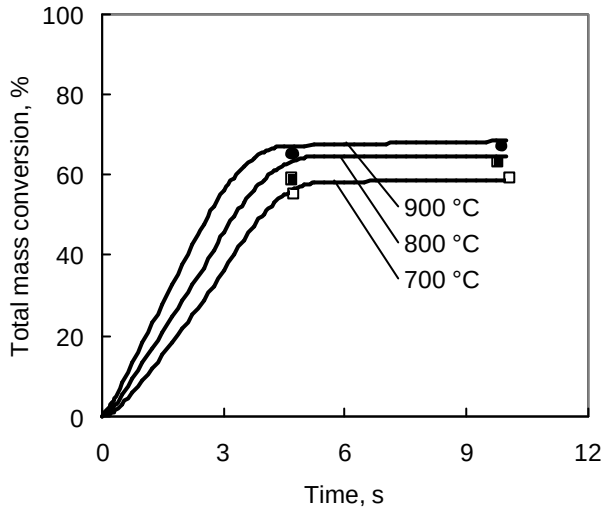

Figure 7.1. Total mass conversion, ds = 60%, 2 mm, muffle furnace, 0 m/s. 700 °C open square, 800 °C filled square, 900 °C filled circle. 95 % N_2, 5 % CO, exp. data from Frederick *et al.* (1994b)

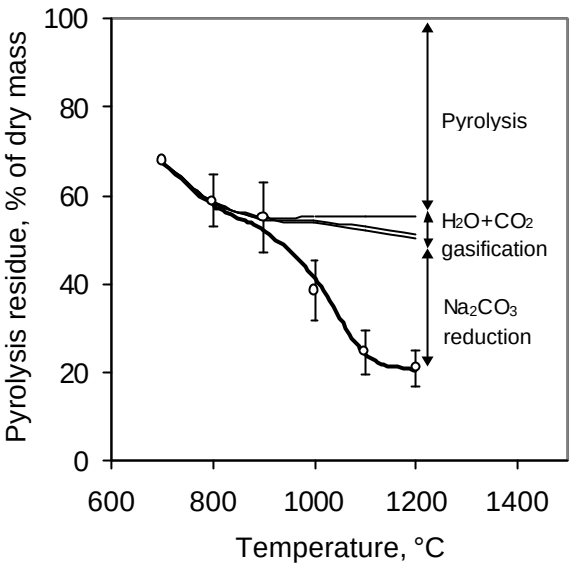

Figure 7.2. Devolatilization residue, 10 s residence time, ds = 60%, 2 mm particle, error bars indicate ± 1 standard deviation, ? experimental data, Frederick *et al.* (1994b)

As can be seen, 5 s is far too large a time step to really determine the rate for devolatilization, no accurate validation can be obtained based on this. In Paper II, a shorter residence time was tested (1s) but it was not sufficient for fast devolatilization stage. As can be seen from Figures 7.1 and 7.2, the model succeeds very well in predicting correct trends for mass loss. Final yield predictions are within the limits of ± 1 experimental standard deviation (which covers ~75 % of measurement points). This type of a contribution analysis is very useful in understanding the role of char conversion mechanisms and also, to see what mechanisms need to be further studied or may be omitted.

Carbon loss can be analyzed from the same experiments as was done for mass loss. However, the determination of the carbon release rate by this technique is very difficult. Currently, there are more accurate on-line techniques available for analyzing CO/CO_2 release from the particle. Figure 7.3 shows the measured and predicted carbon yields after 10 s and Figure 7.4 shows the on-line carbon release curve. Figure 7.3 also shows the contributions of different reactions responsible for carbon release.

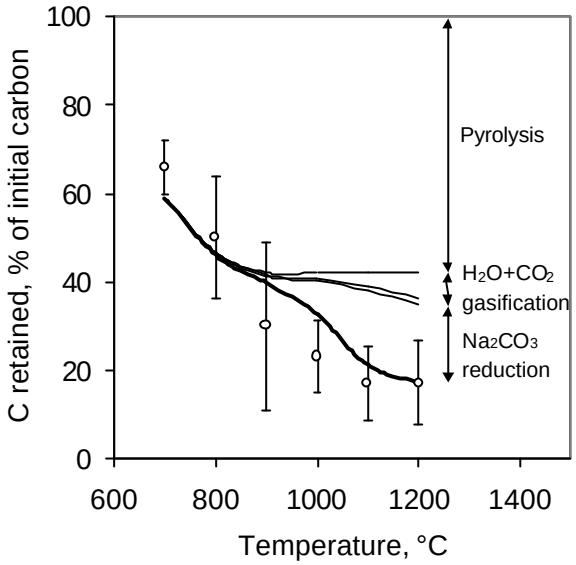

Figure 7.3. Carbon retained in char, 10 s residence time, ds = 60%, 2 mm particle, error bars indicate ± 1 standard deviation, ? experimental data, Frederick (1994b)

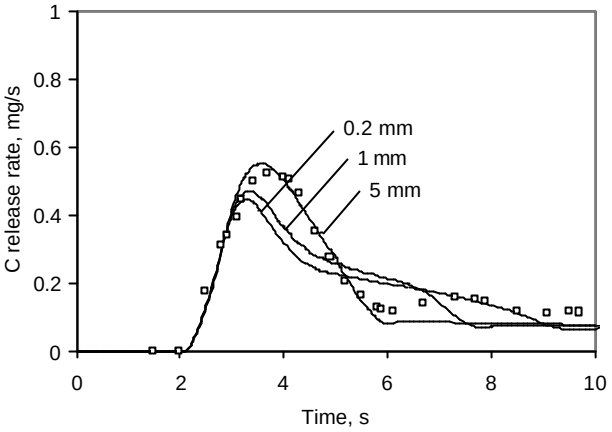

Figure 7.4. Carbon release rate, 2.5 mm particle burned in 3% O_2, 900 °C, apparent pore size 0.2, 1 and 5 mm, Paper V.

As Figure 7.3 shows, below 900 °C roughly all carbon and mass is released by devolatilization as the rates of gasification and inorganic reactions are too slow to make any contribution. In pure N_2, no H_2O gasification takes place after drying and devolatilization. Some CO_2 gasification might take place as carbon dioxide is formed by reduction reactions. Therefore, mass and carbon losses after devolatilization are mainly due to Na_2CO_3 reduction. Reduction of Na_2SO_4 is not seen here as the amount of sulfate was assumed small. Although this kind of data does not give information about the rate of the processes, it is very useful in understanding the relevant mechanisms.

Much more valuable information can be obtained from on-line release data, Figure 7.4. For example, the parameters for heat transfer controlled devolatilization model were extracted i.e. a value for devolatilization heat and a parameter for the internal thermal radiation model. It was found that for a correct rate of devolatilization, significant internal heat transfer by thermal radiation must occur. The apparent 5 mm pore size obtained corresponds to 50-70% of the swollen particle diameter, being far greater than the dimensions of a single computational cell used. In comparison with experimentally observed pore sizes, 5 mm is much larger than experimentally observed by Miller *et al.* (1989), Whitty (1997) and Saviharju *et al.* (1995). Pore sizes observed visually in Paper V were in the range of a few millimeters. When using the diffusion approximation, Eq. 4.4, a 5 mm pore size in Eq. 4.5 corresponds to a Rosseland mean absorption coefficient value a_R = 850 1/m (fitting range: porosity 0.5-0.99, temperature 100-1200 °C).

The new online method was also used to test the model for both devolatilization and char combustion (Paper IV). At this point, only initial results were obtained and swelling was the only parameter fixed for calculations. Figures 7.5 and 7.6 show the carbon release and diameter change for a sulfate liquor droplet. For carbon release, devolatilization release and char conversion are separated.

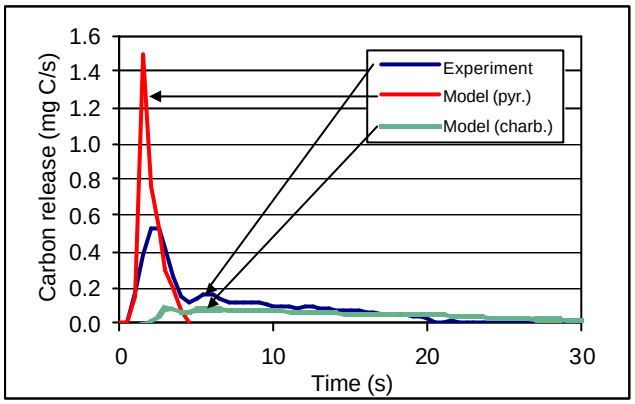

Figure 7.5. Experimental and modeled carbon release divided into release during devolatilization and char burning (900°C, 3.0% O_2, 11.9 mg, sulfate black liquor), Paper IV.

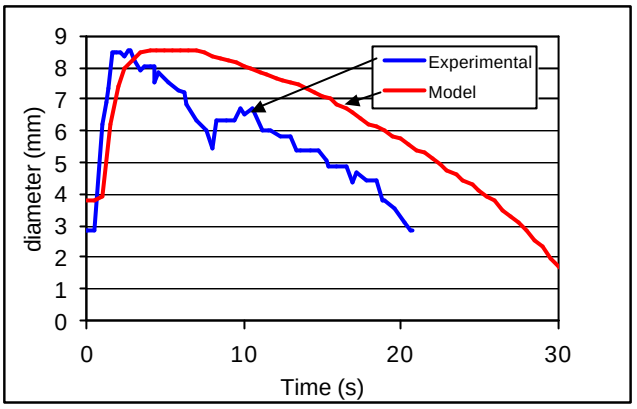

Figure 7.6. Experimental and modeled diameter of particle (900°C, 3.0% O_2, 11.9 mg, sulfate black liquor), Paper IV.

As can be seen form Figures 7.5 and 7.6, the model succeeds in predicting the duration of devolatilization stage but predicts a too large value for maximum rate. One reason for this is that the amount of volatile carbon used in the model was too large, the predicted peak has a much larger area. Also, the kinetic model for pyrolysis and intra-particle thermal conductivity was not fixed for the specific liquor used. For char combustion, predicted rate is slower than measured. This can also be seen in the delayed size reduction. The model was also tested for lower-swelling sulfite liquor, Figure 7.7 shows the carbon release rate.

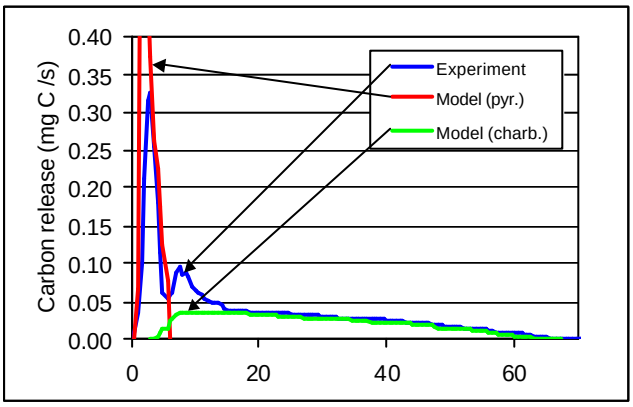

Figure 7.7. Experimental and modeled carbon release divided into release during devolatilization and char burning (900°C, 3.0% O_2, 11.9 mg, sulfite black liquor), Paper IV.

As Figure 7.7 shows, the devolatilization peak is also too high here, duration is correctly predicted. For char combustion, a good prediction is obtained. This is due to a too large amount of pyrolysis carbon used in the model. As sulfite liquor swells less, the shape of the particles remain much more spherical and therefore, the model used also works much better for this case. The porosity for lower-swelling liquor is also smaller so the internal mass transfer is less effective. These mechanisms may be studied in greater detail in future studies, also more simple models will be used for comparison.

When studying the new results from the online gas analyzers, shown in the Paper IV, it should be noted that the modeled system and the actual reactor conditions are not always fully identical. The

1-dimensional model used is only a rough approximation of the actual case. For example, black liquor particles are not fully spherical and boundary conditions in the reactor are not symmetrical. Also, the sub-models used for pyrolysis, thermal conductivity, swelling etc. are approximates. The possible in-accuracy in the measurement system should be studied in detail. A proper error analysis of the measurement system and also, the de-convolution procedure should be done. However, despite of these sources of errors, model predictions are very close to measured ones.

7.2 Temperatures

Particle temperature defines the particle heat flux (sink/source in flow field) and also the rate of reactions. Temperature is solved from the energy equation. Interaction between the particle and bulk gas takes place through the particle surface. This means that to correctly predict the heat flux, the surface temperature needs to be correct. If the particle is thermally large/non-isothermal, reactions take place at different temperatures in the particle. But even if the surface temperatures are correct it does not necessarily mean that the rates will be correctly predicted. This case could be verified only by simultaneously measuring the surface temperature, swelling and release rates for different species. No such data is currently available.

In order to test char chemistry models we need accurate temperature estimate data. Here, we compare the model with temperature measurement data obtained at different oxygen concentrations, 5.3-21% O_2, for particle sizes, 1.5-3.2 mm, Frederick *et al.* (1994a). Swelling was assumed to be 1.54 and 3.0-3.73 (at 21-5.3% O_2) times the initial diameter during drying and devolatilization, respectively. Figure 7.8 shows the maximum temperature differences measured between the particle surface and the environment.

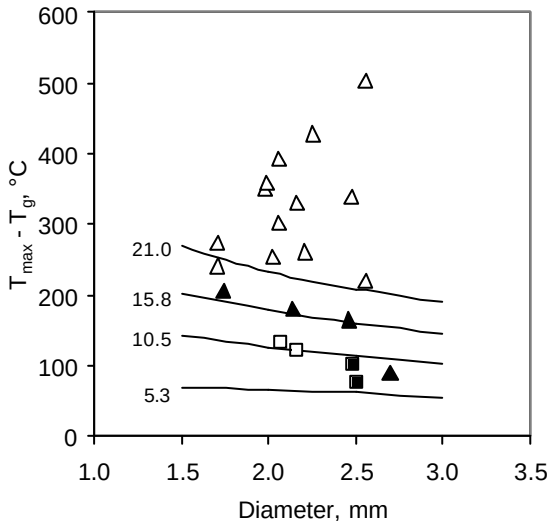

Figure 7.8. The maximum temperature differences between the particle surface and the environment, T_g = 800 °C O_2/N_2 environment, solid line = model, measurements, Frederick *et al.* (1994a), ■ 5.3 %, □ 10.5 %, ▲ 15.8 % and △ 21 % O_2, Paper III.

The model and also the experiments show that the smaller the particle size and the higher the oxygen concentration, the larger the temperature differences. This is a typical trend for diffusion

controlled oxidation. Maximum surface temperatures are well predicted although large deviation exists in the experimental data at the highest level of O_2.

7.3 Swelling and size reduction

Swelling and particle size reduction is probably the most important parameter that affects both the flight path of the particle and the rate of combustion, as external surface area is proportional to the second power of particle diameter. It is important that this parameter is well predicted by the model. Unfortunately, black liquor particles are initially often far from fully spherical when suspended from the metal hook and as they swell, even greater geometrical deviations can be seen. Because of this, modeling and validation of swelling models is very challenging.

Figure 7.9 shows an example of the measured and predicted rate of swelling in the tube furnace. The data in Figure 7.9 is not directly comparable with the modeling results because the particles were not filmed inside the tube furnace environment and the earlier reported by Frederick *et al.* (1994c) value of 1.54 for the diameter ratio during drying can not be seen.

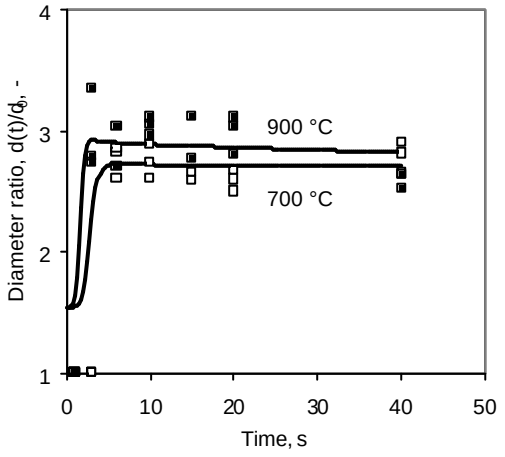

Figure 7.9. Experimental and predicted swelling, ds=83 %, 2.3 mm, tube furnace, 0.2 m/s, 700 °C open square, 900 °C filled square. 100 % N_2, Paper II

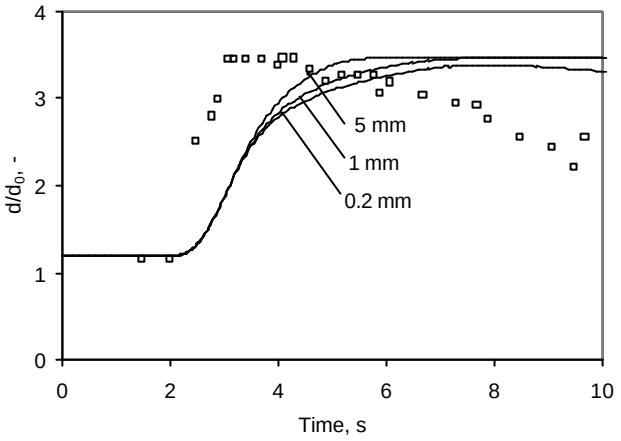

Figure 7.10. Swelling for 2.5 mm particle burned in 3 % O_2, 900 °C, Paper V.

In Figure 7.9 the value for diameter ratio was measured to be 1 for the short residence times. In the early stages of combustion (1-3 s) the water in the droplet evaporates by rapid boiling and the bubbles that are formed increase the droplet diameter. When the droplet is removed from the hot furnace, the heat flux is cut off and the vapor bubbles collapse because no rigid matrix has yet been formed that could support the bubble structure. From this, it can be concluded that continuous data on swelling should be available. Much better information can be obtained from a muffle furnace where droplet combustion is video-recorded and from this, a continuous swelling profile can be determined.

Figure 7.10 shows the continuous swelling curve measured and predicted for a 2.5 mm particle burned in 3% O_2 at 900 °C. This curve corresponds to the carbon release rate shown in Figure 7.4. Figure 7.10 shows a good agreement for the rate of diameter increase, although the position of swelling curves is shifted with respect to time. Partly because of this, particle shrinkage during char conversion is also delayed. One possible reason for these deviations is that in the experiments the swelling of the droplet during combustion is finished when the outer layer loses its plasticity, while the devolatilization can still continue inside the droplet and be seen as flames surrounding it. This possibility was not included in the current model. Also the synchronization of carbon release and swelling is still in progress and these results should be considered as preliminary ones.

One critical feature of the combustion model is the particle shrinking model. As the conversion in a computational cell reaches a critical value X_{cr}, the cell is removed and the material in it is transferred to other cells in proportion to cell volumes. To study the effect of this parameter, the model is tested against experimental data for 9 mg droplet gasified in 900 °C, 20% H_2O, 4% CO, Frederick and Hupa (1990b). The model was very sensitive to the parameter X_{cr}. The best correlation was obtained for the value X_{cr} = 0.8, see Figure 5.1. By using this value, we can test the model against some other cases in a H_2O/CO environment, see Figures 7.11-12.

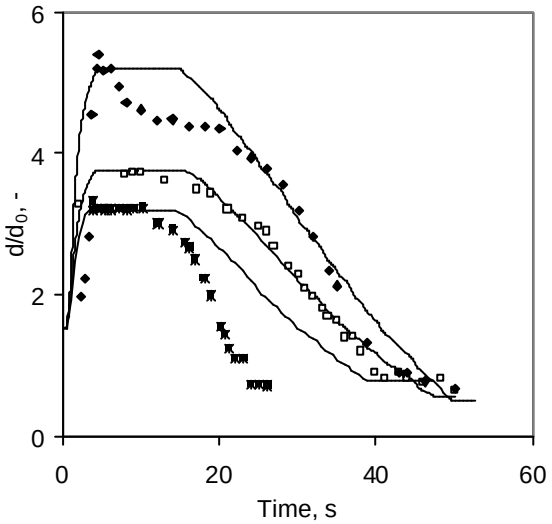

Figure 7.11. Relative swelling in 20 % H_2O, 4% CO, rest N_2, 800 °C, ■ 4.2 mg, □ 8.6 mg, ◆ 17.4 mg, Paper III, Frederick and Hupa (1990b)

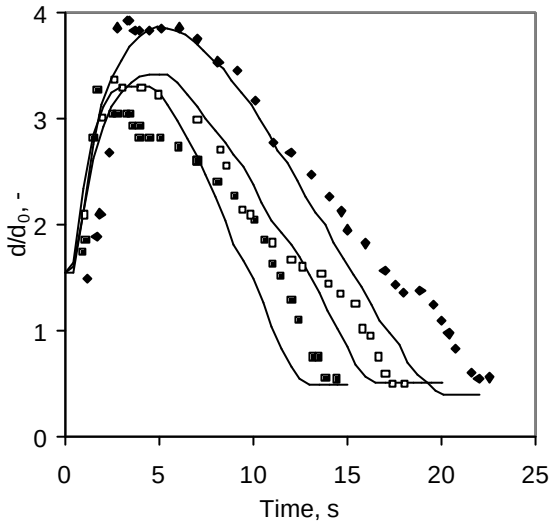

Figure 7.12. Relative swelling in 20% H_2O, 4% CO, rest N_2, 900 °C, ■ 4.1 mg, □ 8.1 mg, ◆ 17.2 mg, Paper III, Frederick and Hupa (1990b)

Generally, the model succeeds well in predicting the particle shrinking behavior in a H_2O/CO environment. For a small 4.2 mg particle at 800 °C, the correlation is worst. The model was also tested in a CO_2/CO environment, but a poor correlation was obtained. In the case of small particles, lower temperatures and lower rate CO_2 gasification, we lie near the kinetically controlled regime: particle shrinking is then very difficult to predict. In furnace conditions where H_2O is always present, the model will perform properly since H_2O gasification dominates. Making experimental swelling measurement is very difficult, and this has to be kept in mind when comparing these results.

8 CHAR CONVERSION MECHANISMS

8.1 Auto-gasification

In the case of thermally large and wet fuel particles, the stages of drying and devolatilization occur simultaneously during combustion, Saastamoinen *et al.* (1984). At some point the devolatilization at the surface is completed and a char layer remains. H_2O and CO_2 are simultaneously released during drying and devolatilization at the inner parts of the particle. These pass through the char surface layer as they flow out from the droplet. If the temperature of the char layer is high enough, gasification reactions may take place, converting the char into gaseous species, see Figure 8.1. Preliminary results for this mechanism were presented in Paper I, other papers study this mechanism in greater detail or as a part of other mechanisms. In the case of high surface temperature, gasification rates are very fast and the rate of carbon consumption is limited by H_2O and CO_2 availability. As these come from the droplet interior, the external mass transfer resistances are absent and therefore, this can be a very effective mechanism for different droplet sizes and temperatures. Figure 8.2 shows the calculated internal reaction profiles for a 5 mm droplet at the moment of maximum char conversion.

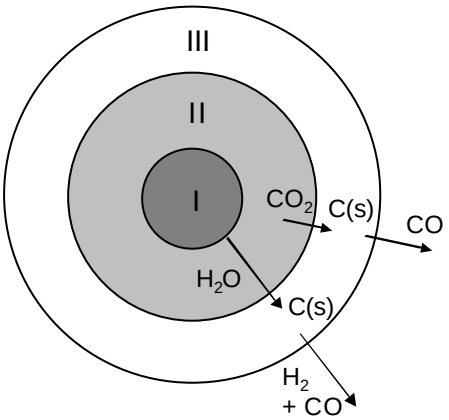

I. Drying zone
II. Pyrolysis zone
III. Char conversion zone

Figure 8.1. Principles of the auto-gasification mechanism inside the particle, Paper VI

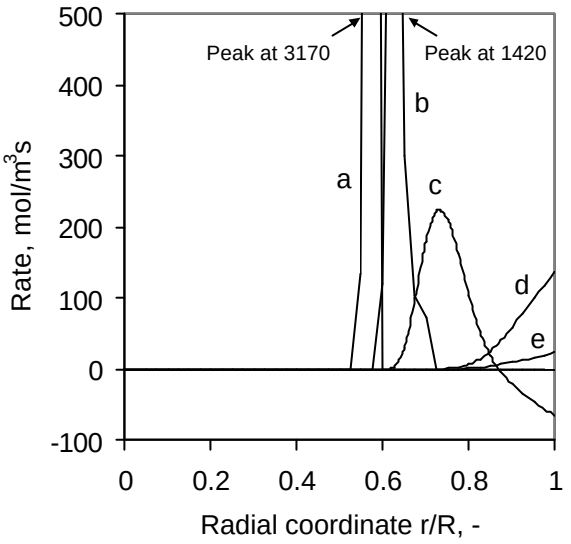

Figure 8.2. Calculated rate of reactions (mol/m^{3}s) as a function of radial position inside a 5 mm particle, moment of maximum char conversion rate (t = 6.1 s), T_g 1100 °C, 20 % initial water content, a = H_2O formation from drying, b = CO formation from devolatilization, c = CO_2 formation from CO-water shift reaction, d = char conversion by H_2O gasification, e = char conversion by CO_2 gasification, Paper VI

As Figure 8.2 shows, drying (a) and devolatilization (b) both occur as thin reaction fronts close to each other. Drying takes place at the boiling temperature. Devolatilization reactions are completed at 600 °C. H_2O and CO formed in these flow outwards, heat up, and react to form CO_2 and H_2 by the CO-water shift reaction (c). After this, H_2O and CO_2 will gasify the char at the droplet surface, (d) and (e), respectively. Clearly, internal gasification play an important role during devolatilization and a significant char conversion rate is obtained. Also, CO-water shift reaction (c) plays a very important role. To summarize, Figure 8.3 shows the effect of particle size and gas temperature on auto-gasification.

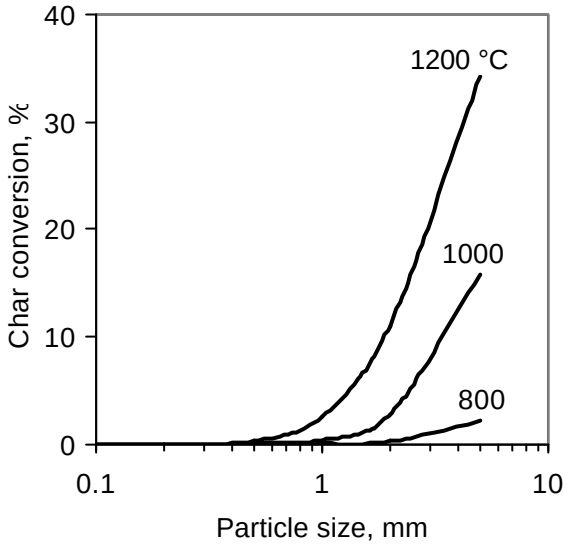

Figure 8.3. Calculated effect of particle size on char conversion during devolatilization, 800, 1000 and 1200 °C, 20% water content, 100% N_2 environment, β_{dry}=3.65, β_{dev}=27, Paper VI

It was found that the larger the particle and the higher the temperature, the higher was the degree of char conversion already during devolatilization. Black liquor particles are wet and large, and BL char is very reactive i.e. it has all the properties that favors this mechanism.

The internal structure of the swollen char particles were roughly examined, Paper II. The volume fraction of large gas voids was roughly determined, it was typically over 50%. This means that particle is not homogenous internally and large pores occupy a significant fraction of the particle volume. For modeling purposes, it was first assumed that only a single large gas void exists in the particle, see Figure 8.4. Fifty percent of the particle volume corresponds to a gas void of 80% particle outer diameter. This can be considered as an extreme case, in reality, pores are much more evenly distributed, Paper II. For the auto-gasification mechanism, it was found that the swelling and internal geometric structure of particle has a significant effect, as can be seen in Figures 8.5. As has already been show in the section 6.1. "Sensitivity analysis", the internal reaction surface area also plays an important role. We will examine the effect of swelling for 3 different cases here. These are: 1) no additional swelling during devolatilization s = 0, 2) slight swelling, s = 1 and 3) strong swelling behavior s = 2. In addition to these, the effect of particle morphology was examined, four different cases were calculated 1) no cenosphere j = 0, 2) j = 0.5, 3) j = 0.75 and 4) j = 0.875.

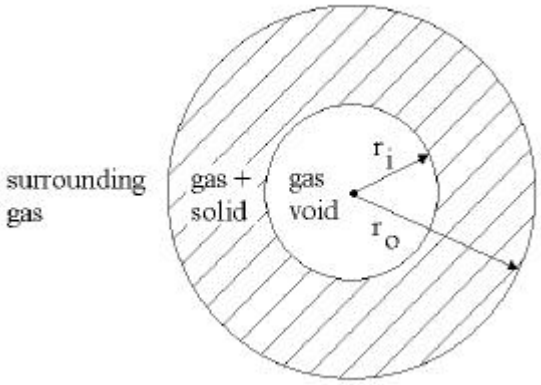

Figure 8.4. Cenosphere dimensions in the droplet, Paper II

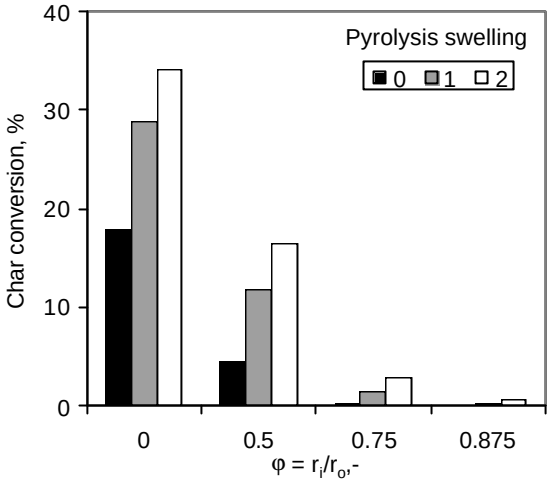

Figure 8.5. Char conversion after complete drying and devolatilization, 2 mm, dry solids 70 %, 0.2 m/s, 1200 °C, 100 % N_2, Paper II.

Based on Figure 8.5, char conversion after complete devolatilization and drying is greatly affected by the swelling and formation of cenospheres. Auto-gasification mechanism (mainly by H_2O gasification) is the dominating char conversion mechanism. The greater the swelling and the smaller the cenospheric fraction, the larger the conversion of char will be at the end of devolatilization. For the extreme case of a single 50% gas void, auto-gasification would be negligible. In reality, the situation is not this ideal.

The effect of internal gas flow channeling was not studied in this paper. Flaming gas jets appear is some cases during the devolatilization stage indicating that internal channeling can take place. Naturally, if the gases escape the droplet through a single hole, the effect of auto-gasification is significantly reduced. Also, the amount of dead pore volume should be determined. These mechanisms should be further studied for validating the auto-gasification mechanism for black liquor combustion.

Attempts were also made to validate this auto-gasification mechanism, see Figures 7.2 and 7.3. However, as the experimental deviation was very large, (Frederick *et al.* (1994b), no hard proof was obtained from these attempts. As there are new on-line gas analyzing techniques becoming available, the validation of this mechanism can be further studied later work.

8.2 Simultaneous devolatilization and char conversion in oxidizing conditions

In addition to auto-gasification, char gasification or oxidation may take place also by the surrounding gases H_2O, CO_2 or O_2. Here the structure of localized flame plays a significant role. It was already found by Hupa *et al.* (1987) that a clearly visible envelope flame surrounds the particles when they are burned in oxidizing conditions. In the case of an intense envelope flame, oxygen is consumed in the boundary layer of the particle and no heterogeneous char oxidation may take place. This is the case in close-to-stagnant reactor conditions. In a furnace, there are high slip velocities that may strip the flame away from the surface, and the oxygen may have access to the particle surface.

Based the data of Kulas (1990), a flammabity map was constructed for black liquor, Figure 8.6. Based on this work, the Damkohler number for CO oxidation was calculated. For the situation studied here, the Damkohler number is then defined as the ratio of gas residence time around the particle $t_R = d/|u\text{-}u_g|$ and chemical reaction time for CO oxidation $t_{CH} = c/R_{CO}$, Dryer and Glassman (1986), Dwyer and Sanders (1973).

$$Da = \frac{t_R}{t_{CH}} = \frac{d}{|u - u_g|} 3.981 \times 10^{14} \exp(-20143/T)\, c_{CO} c_{H2O}^{0.5}\, c_{O2}^{0.25} c^{-1} \qquad (8.1)$$

with units [c] = mol/cm^3, [d] = m and [u] = m/s. The Damkohler number during in-flight combustion of 0.5-4 mm particles was calculated to see how these results are related to the determined ignition criteria in Figure 8.7.

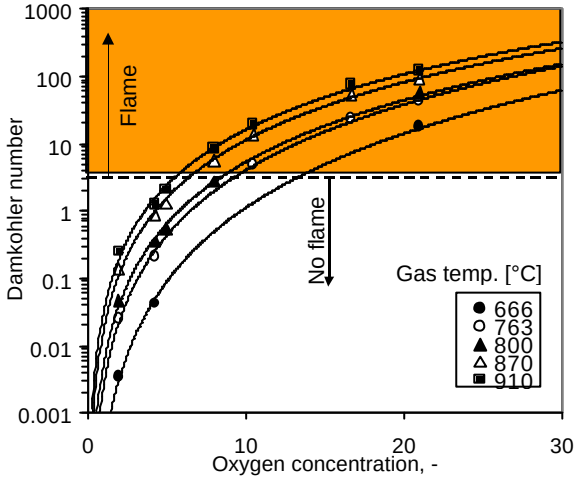

Figure 8.6. Calculated maximum Damkohler number for CO oxidation during devolatilization, rate calculated at the non-adiabatic flame temperature, see Figure 2, *Re* = 20-60, broken line shows the approximate limit of flame formation, Kulas (1990), Paper VII

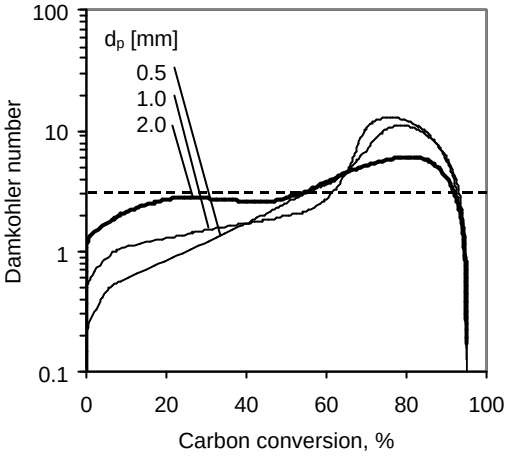

Figure 8.7. Damkohler number for 0.5-2 mm particles during in-flight combustion, 1200 °C, Paper VII.

Based on Figure 8.6., flame appears when Da>3. As can be seen from in-flight simulations, Figure 8.7. Da is below the ignition criteria, no significant localized devolatilization gas oxidation takes place in the furnace. Therefore, it was assumed that no localized gas oxidation takes place during in-flight combustion. Figure 8.8 shows the calculated contributions of char conversion mechanisms during in-flight devolatilization.

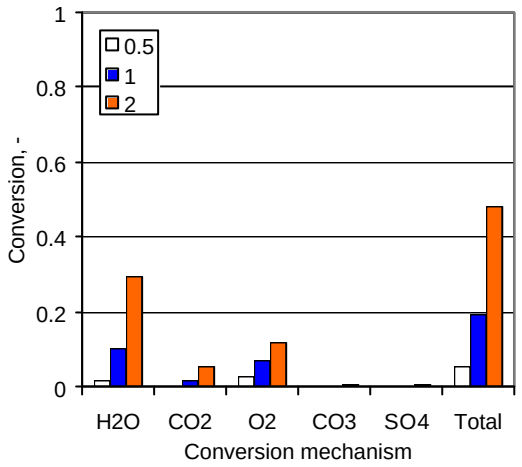

Figure 8.8. Contributions of char conversion mechanisms during devolatilization, X_P = 100%, 0.5-2 mm, 1200°C, 20% H_2O, 12% CO_2 and 3% O_2, Paper VII.

As Figure 8.8 shows, H_2O gasification is the dominating char conversion during devolatilization of 2 mm particles. What is important, significant O_2 oxidation takes place too. This means that even if the auto-gasification mechanism would not be present, significant char conversion takes place during devolatilization. For smaller particles, the effect of auto-gasification is smaller and as external mass transfer is effective, direct oxidation takes place.

8.3 Char combustion stage

After all volatiles are released, the H_2O source disappears from the particle. Some auto-gasification may still take place, as CO_2 is formed in sulfate reduction reactions. According to calculations done for this work, this plays a negligible role. Please note that the oscillations are due to numerical model and the finite number of computational cells used.

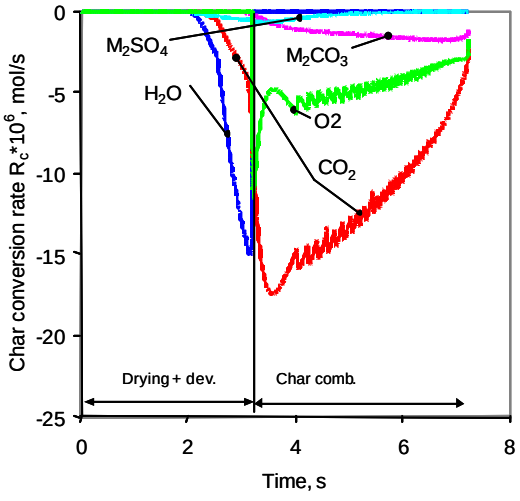

Figure 8.9. Rate of char conversion, 800 °C dry air, 2 mm droplet, Järvinen *et al.* (2000).

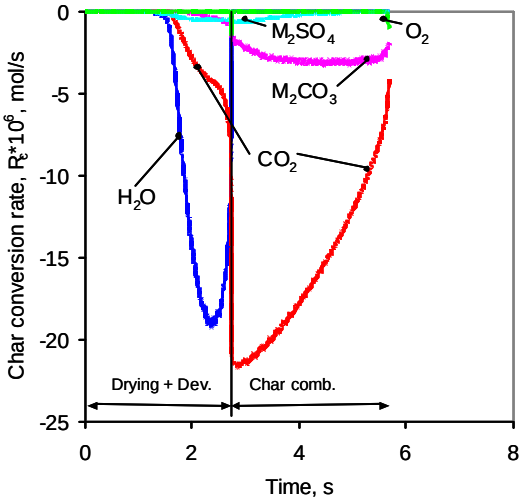

Figure 8.10. Rate of char conversion, 1000 °C dry air, 2 mm droplet, Järvinen *et al.* (2000).

The rate of gasification reactions is very high for black liquor. Even at relatively low temperatures, the flame will be lifted off the particles surface. Basically, char is converted by gasification reactions as the flow of the oxidized gasification products CO and H_2 will prevent flames from reaching the surface. In stagnant conditions, where the envelope flame surrounds the particle, char combustion stage is actually a gasification process. Figures 8.9-10 presents a contribution analysis for combustion of 2 mm particles in air at temperatures of 800 and 1000 °C. When the temperature is increased from 800 to 1000 °C, flame lift off takes place and oxygen will reach the surface only after all carbon is depleted.

Under furnace conditions, high slip velocities exist, and the localized flame gets easily stripped away from the surfaces of particles. Here, if no gas phase reactions take place and the "bulk flow" of gaseous products is too weak to overcome the inward diffusion of O_2, O_2 will reach the particles surface and react heterogeneously. For black liquor, as it swells significantly, drag forces during in-flight combustion increase, and therefore, slip velocity will decrease. This may have a significant effect of localized gas oxidation and on the formation of an envelope flame as was already shown in Figure 8.7. Figure 8.11 presents temperature profiles during char combustion and also profiles for char conversion reactions for initially 0.5 and 2 mm particles.

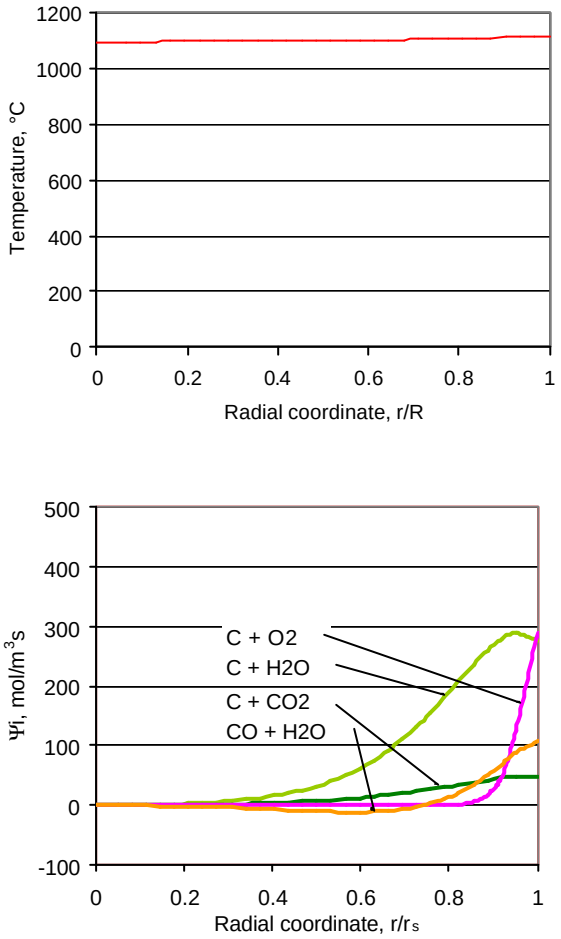

Figure 8.11. 0.5 mm particle, in-flight combustion, 1200 °C, temperature profiles during char combustion (X_C=0.7) (top), reaction rates inside the particle during char combustion (bottom), Paper VII

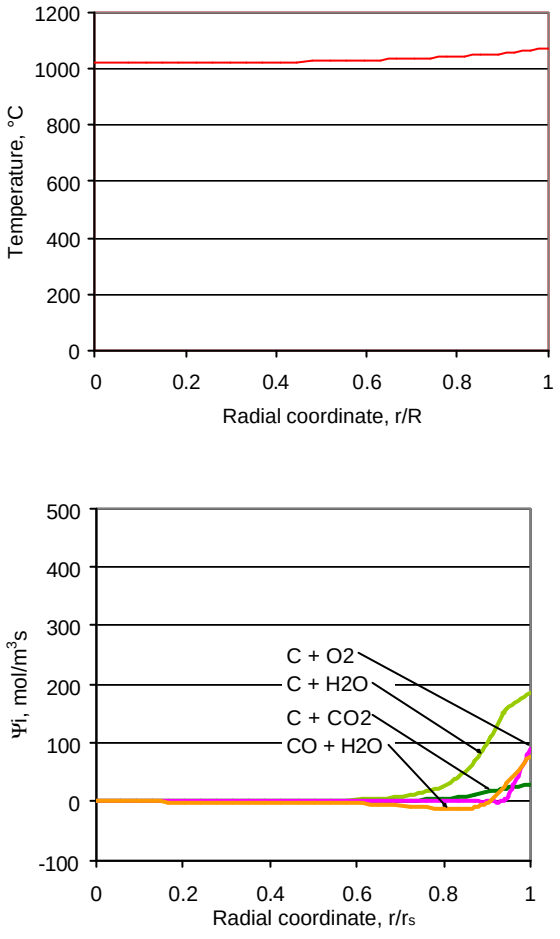

Figure 8.12. 2 mm particle, 1200 °C, in-flight combustion, temperature profiles during char combustion (X_C=0.7) (top), reaction rates inside the particle during char combustion (bottom), Paper VII

Char will be consumed mainly by H_2O gasification. Although not shown in Figures 8.11-12, the inorganic reduction reaction R.11. also plays some role in this. As the particle internal temperature profile is uniform here, the isothermal particle assumption would apply for developing simplified CFD sub-models. As the internal mass transfer resistance is higher for a large particle, reactions take place closer to the particle surface. For smaller particles reactions take place more evenly inside the particle. Figure 8.13 shows the total contributions of different char consuming reactions during char combustion.

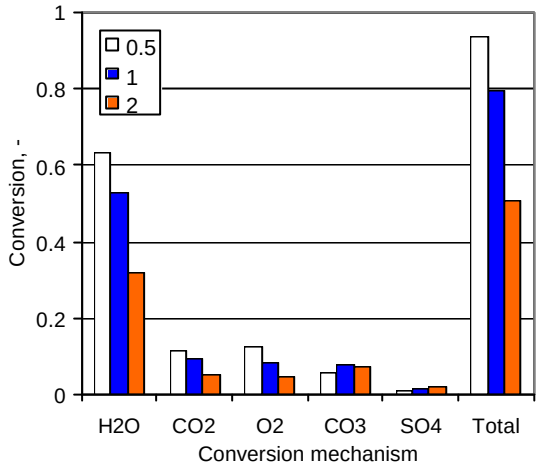

Figure 8.13. Total contributions of char conversion mechanisms during char combustion, X_{char} = 100 %, 0.5-2 mm, 1200°C, 20% H_2O, 12 % CO_2 and 3 % O_2, Paper VII.

H_2O gasification is the dominating char conversion mechanism. Char oxidation by O_2 and CO_2 play a minor role but they can not be neglected. Sulfate reduction can be neglected. For large particles, a significant fraction of char is converted during devolatilization by "auto-gasification", and less char is left to be gasified after that.

9 CONCLUSIONS

Drying, devolatilization and char conversion mechanisms were studied by means of detailed numerical modeling. All black liquor combustion models developed prior to this work neglected the possibility of gas-char interaction already during devolatilization. In this work, a new detailed physical model was developed where internal mass and heat transfer were modeled in detail, also during devolatilization to solve for interactions of water vapor, volatiles and char.

In the case of large and wet fuel particles, the drying and devolatilization stages of combustion overlap. At some point the devolatilization at the surface is completed and a char layer remains. In this work, it was found that this char layer may be converted already during devolatilization by three different main mechanisms.

1. H_2O and CO_2 that are released during drying and devolatilization in the inner parts of the particle pass through the char surface layer as they flow out from the droplet. If the temperature of the char layer is high enough, gasification reactions may take place converting the char into gaseous species. This mechanism was referred as auto-gasification in this work. For this mechanism to be significant, the surface temperatures of the particles have to be exceed 800 °C during devolatilization.
2. H_2O, CO_2 and also O_2 may reach the char surface also from the bulk gas or from the localized enveloped flame that surrounds the particle. This mechanism does not require that the auto-gasification mechanism is present and valid. It was found that a significant fraction of the char can be consumed by this single mechanism.
3. For black liquor, as the amount of Na_2CO_3 is significant, char conversion by Na_2CO_3 reduction may take place in the char surface layer during devolatilization. However, as the temperature needs to very high for effective conversion, this reaction plays a minor role in devolatilization.

Based on detailed numerical simulations which could be verified with experiments, the auto-gasification mechanism seems to be important when the ratio of chemical char conversion time to devolatilization time is small. This requirement is fulfilled for large particles (long devolatilization time) with reactive char (short char conversion time). As the gasifying agents CO_2 and H_2O come from the particle interior, external mass transfer resistances are absent. All gases that are released during devolatilization must eventually escape the particle. As the rate of devolatilization is high, volatilized gases are pushed effectively towards the hot particle char surface. Final char conversion after completed devolatilization and drying is greatly affected by swelling and formation of larger voids. The greater the swelling and the smaller the cenospheric volume fraction, the larger the conversion of char at the end of devolatilization. Some experimental validation for this mechanism was done. However, as there is a limited data suitable for this purpose, no hard proof could be obtained. More work should be concentrated on this, as this mechanism could be important also for other fuels such as wood (burnt as logs) and the combustion of bioslugde. For wood and other fuels the char gasification rate is much lower than for black liquor. Much larger particle sizes and longer devolatilization times are required then for this mechanism to take place. Coal and peat are usually burnt as small particles, d_p <1 mm, and this mechanism does apply in these cases. For wood combusted as large wood logs, devolatilization time is in the order of 1000 seconds, and the auto-gasification mechanism should be considered. This may be part of future studies.

For char combustion, under a *stagnant* recovery boiler furnace gas atmosphere, the modeling results suggest that a 3 mm particle does not react heterogeneously (char oxidation and sulfide re-oxidation) with oxygen as long as char is present. Partly similar results were obtained by Wåg, *et al.*

(1995a). The gasification reactivity of black liquor is high, and the flow of the gasification products H_2 and CO will prevent oxygen from reaching the particle surface even at lower temperatures. For less reactive fuels such as coal, this mechanism might take place at higher temperatures.

In a recovery furnace, the particle environment is far from stagnant. As the slip velocity is high, combustible gases may be stripped away from the particle surface and burnt in the bulk gas. This means that the localized heat and H_2O/CO_2 source and O_2 sink would be absent. The ignition and combustion of black liquor particles were also studied by means of detailed numerical simulations. A critical Damkohler number for the formation of a localized CO flame was determined from experimental data found from the literature and the in-flight combustion of 0.5-4 mm particles was simulated. Based on the calculated Damkohler number during in-flight combustion, a general trend seen was that the role of local gas oxidation outside the particle surface during devolatilization is small but increases as swelling takes place and slip velocity decreases. For 0.5-2 mm spherical particles that are burnt fully in-flight, the maximum Damkohler number during devolatilization will be below the critical value for envelope flame formation, indicating that the particle will act only as a source of combustible gases, and gas oxidation takes place mainly in the bulk gas. This will be an very important for developing simplified single particle combustion models for CFD purposes. To verify this, experiments at higher temperature and higher slip velocities would be required. It was found that under typical recovery furnace conditions, char is mainly consumed by H_2O gasification *during devolatilization*, but also char conversion by O_2-oxidation, CO_2-gasification and carbonate reduction takes place. Calculations showed for initially 2 mm particles that a significant fraction of the CO is oxidized locally by H_2O *inside* the particle, while the role of CH_4 oxidation is negligible. For initially 0.5 mm particles, internal gas reactions can be neglected. After the particle is pyrolyzed, char is mainly converted by H_2O gasification, while CO_2 gasification, O_2 oxidation and inorganic reactions play a minor role.

For thermally large particles, thermal conductivity is one of the most important parameters that affects the rate of particle heating rate and consequently, processes controlled by the heat transfer rate, such as drying and devolatilization. For char combustion that is usually considered to be a mass transfer limited process the temperature profile is more uniform in the particle and the role of thermal conductivity is smaller. A numerical combustion simulation sensitivity analysis showed that in order to have reasonable agreement between experimental and modeled carbon release rates, a significant addition of internal thermal radiation heat transfer must be included. Surprisingly, there are only a few studies available concerning the physical properties of porous black liquor char, such as pore size, size distribution and thermal conductivity. Especially, the size of large pores and voids, and the internal *macroscopic* structure of the swollen particles in general, are not well characterized. On the basis of available data, pores and voids up to mm in size can exist in the particles. Thermal radiation becomes important in the porous structure if pore size is larger than 100-500 μm.

It was found that this kind of detailed combustion model can be a very useful tool for theoretically studying the processes taking place during single particle combustion. Also, single particle combustion processes and mechanisms can be effectively studied, also for other fuels such as coal and wood. By using this model, data that may not be measured can be obtained and models for different mechanisms can be developed. Also, completely new mechanisms can be isolated. It was found that the development of this type of models requires a broad understanding of numerical methods, physical heat and mass transfer mechanisms and chemical kinetics.

Most of time used for this work was spent on numerical model development as the solution of a stiff system of partial differential equations (i.e. a very broad range of different time scales exists) is

not straightforward. However, the numerical method is only the tool to solve the physical and chemical models that actually describe the system. Surprisingly, it was found that there is only a limited amount of data on the internal structure (pore surface area, pore structure geometry, pore size etc.) of black liquor available for combustion applications. As this data is essential for accurate results, there is a huge amount of work still to be done to obtain these parameters. A sensitivity analysis was carried out for the parameters that could not be measured.

9.1 Contribution of the work

A detailed single particle combustion model was developed in this work. Unlike the models developed prior to this study, in the current model, drying, devolatilization and char combustion stages may overlap in the particle if physical and chemical processes allow. In order to consider these, internal mass and heat transfer needed to be modeled in detail. An implicit control volume method was selected to solve the non-linear stiff differential equations. This model was developed also to be used for other fuels than black liquor and also for studying heat and mass transfer in porous media more generally. The simulation program is based on modules that are fuel/problem-independent. Therefore, the implementation of additional chemical species or chemical reactions is simple and requires only small changes in the program and initial files.

A new theoretical char conversion mechanism was presented in this work, referred to as auto-gasification. As this mechanism was observed to be very effective, it should be considered also when studying the combustion of other fuels burnt using large particle size or having extremely reactive char. This mechanism was found to be very sensitive to effective thermal conductivity, swelling, internal structure (i.e. surface area via reaction rate). In contrast to previous black liquor combustion models, it was also found that even if the auto-gasification mechanism is not present (for example by flow channeling), significant overlap between devolatilization and char conversion may take place as H_2O, CO_2 and O_2 reach the particle surfaces from outside. In order to consider these mechanisms intra-particle mass transfer needs to be studied during devolatilization. This significantly complicates the model. A new general model for this purpose was developed. The model can also be used for studying the combustion behavior of other fuels, general mass transfer phenomena etc.

In stagnant oxidative conditions, at relatively high temperatures, no direct char oxidation takes place. The rate of gasification reactions is very high and the flow of oxidized gasification products (CO/H_2) will keep the flame of the particle surface. For convective conditions, the released gases tend to be stripped away from the surface. This means that the droplets only act as a source of combustible gases, while the main oxidations takes place at the bulk gas. In CFD calculations, the modeling of the gas combustion is then handled by the CFD software routines.

The detailed model developed in this work was also extensively compared with available experimental data. Also, some new data was obtained for this purpose. It was found that the model well succeeds in predicting measured release rates, surface temperatures and particle swelling/size reduction behavior. Also, some model parameters such as the parameters for heat transfer controlled devolatilization model were obtained by roughly fitting the model to measured data. There in only a limited amount data that can be measured from combustion experiments. A detailed model can be effectively used for obtaining the missing data that can not be experimentally obtained. The model can also be used to extrapolate combustion to conditions that can not be reach experimentally.

9.2 Recommendations and future work

For developing CFD sub-models for furnace calculations, some simplified model that considers non-isothermal devolatilization and overlapping combustion stages should be used. Also, as H_2O, CO_2 and O_2 will reach the particle surface during devolatilization, the development of simplified single particle CFD sub-model is very challenging. During char combustion, the particle can be assumed to be isothermal. Therefore, char conversion processes could be easily described for CFD purposes by a simplified pore diffusion model, e.g. Peterson (1965), combined with a proper description of dominating reaction chemistry. Parameters and relevant mechanisms for these simplified model can be effectively obtained by the detailed model. One option could be that different models were used for different particle sizes.

The model developed was validated in stagnant laboratory conditions. A good correlation with experimental data was obtained. The model was also extended to furnace conditions that require the extrapolation of many parameters, for example, no information on the swelling behavior is available for convective conditions (slip velocity > 1.7 m/s up to 15 m/s) at high temperatures (> 1200 °C). These should be further studied experimentally.

In this work, the particles were assumed to be fully spherical and symmetrical. As observed by Kankkunen *et al.* (2001) most particles are initially non-spherical and even greater shape deviations exists during combustion, Hupa *et al.* (1987). The effect of this on particle geometry will be studied in the future work during 2002-2004 and a proper model for these shapes will be developed.

In order to more efficiently use and further develop the detailed combustion model, internal structural parameters such as internal reaction surface area, pore size distribution and radial changes in the pore structure should be determined. This data is available for other fuels such as coal, and the techniques used for these could be applied to black liquor char.

REFERENCES

Adams, T. N., Frederick, J. M., Grace, T. M., Hupa, M., Iisa, K., Jones, A. K. and Tran, H., (1997) *Kraft Recovery Boilers*, Tappi Press, Atlanta

Alén, R., Kuoppala, E. and Oesch, P., (1996), Thermogravimetric behavior of black liquors and their organic constituents, *J. Anal. App. Devolatilization*, 36: 137

Asplund, D., (1997) *The Status and Development Possibilities of Bioenergy in Energy Industry*, Ministry of Trade and Industry, Energy Department, Finland

Avni, E., Coughlin, R. W., Solomon, P. R. and King, H. H. (1985) Mathematical modeling of lignin devolatilization, Fuel 64, pp. 1495-1501.

Bartok, W. and Sarofim, A, F., (1991) *Fossil Fuel Combustion,* Whiley & Sons, New York, USA p. 607

Bear J. (1972) Dynamics of fluids in porous media, American Elsevier, USA, p. 47.

Beck, N. C. and Hayhurst, A. N., (1990) *Combust. Flame*, 79:47

Cameron, J. H. and Grace, T. M. (1985) Kinetic Study of Sulfate Reduction with Kraft Black Liquor Char, Ind. Eng. Chem. Fundam. 24, pp. 443-449.

Clay, D. T. and Grace, T. M., (1984) *Tappi Journal* 67:92

Clay, D. T., Lien, S. J., Grace, T. M., Macek, A., Semerjian, H. G., Amin, N. and Charagundla, S. R. (1987) Fundamental studies of Black Liquor Combustion, Report No. 2-Phase I for the Period Octobed 1984-1986, DOE Report DOE/CE/40637-T2, USA.

Dryer, F. L. and Glassman, I., (1973) *Fourteenth Symposium (Int.) on Combustion*, The Combustion Institute, Pittsburgh p. 987-1003

Dwyer, H. A. and Sanders, B. R., (1986) A detailed study of burning fuel droplets, *Twenty-first Symposium (Int.) on Combustion*, The Combustion Institute, Pittsburgh p. 633-639

Ferziger, J. H. and Peric, M., (1997) *Computational Methods for Fluid Dynamics*, Springer, Heidelberg, Germany

Fogler, H. S., (1992) Elements of Chemical Reaction Engineering, Prentice Hall Inc., USA.

Fott, P. and Schneider, P., (1984) Chem. Eng. Sc. 39:643

Frederick, W. J., (1990a) *Combustion Processes in Black Liquor Recovery: Analysis and Interpretation of Combustion Rate Data and an Engineering Model*, DOE Report DOE/CE/40637-T8, USA

Frederick, W. J. and Hupa, M. (1990b) Report 90-12, Gasification of Black Liquor at Elevated Pressures, Part 2. Rate Data with CO_2 and Water Vapor, *Combustion Chemistry Research Group Report*, Åbo Akademi, Turku, Finland.

Frederick, W.J., Forssén, M., Hupa, M. and Hyöty, P. (1992) Sulfur and sodium volatilization during black liquor devolatilization, Proceedings of the 1992 International Chemical Recovery Conference, Tappi Press, pp. 599-608.

Frederick, W. J. and Hupa, M., (1993) *Combustion Properties of Kraft Black Liquors, Report 93-3*, Åbo Akademi University, Finland

Frederick, W.J., Hupa, M., Stenberg, J. and Hernberg, R. (1994a) Optical Pyrometric Measurements of Surface Temperatures During Black Liquor Char Burning and Gasification, *Fuel* 73(12): 1889-1893

Frederick, W. J., Hupa, M. and Uusikartano, T., (1994b) Volatiles and char carbon yields during black liquor devolatilization, Bioresource technology 48, pp. 59-64

Frederick, W.J. and Hupa, M. (1994c) The Effects of Temperature and gas Composition on Swelling of Black Liquor Droplets During Devolatilization, Journal of Pulp and Paper Science 20(10) p. J274-279.

Gardiner, W. C., (1984) *Combustion chemistry*, Springer-Verlag, New York

Geankoplis, C. J., (1972) *Mass Transport Phenomena*. 6th printing, Edwards Brothers, USA

Grace, T. M., Cameron, J. H. and Clay, D. T. (1989) Role of sulfate/sulfide cycle in char burning-experimental results and implications, 1989 Kraft recovery operations, Tappi seminar notes, pp. 159-167

Grace, T. M., Frederick, W. M., Iisa, K., (1998) New Black Liquor Drop Burning Model, 1998 International Chemical Recovery Conference, Tappi Proceedings, Tappi Press, USA p. 257-270.

Harper, F. D. (1989) Sulfur release during the pyrolysis of kraft black liquor, Doctors Thesis, Institute of Paper Chemistry, USA

Horton, R. R., Grace, T. M. and Adams, T. N. (1992) The effect of black liquor spray parameters on combustion behavior in recovery furnace simulations. International Chemical Recovery Conference, Seattle, June 7 - 11, pp. 85 - 99.

Horton, R. R. and Vakkilainen, E. K., (1993) Comparison of simulation results and field measurements of an operating recovery boiler, TAPPI Engineering Conference, Orlando, September. pp. 20 - 23. 1993

HSC Chemistry for Windows Ver. 2.0, Outokumpu Research Ltd., Finland, (1994)

HUPA, M.. SOLIN. P. AND HYÖTY. R, Combustion Behaviour of Black Liquor Droplets, *J. Pulp Paper Sci.* 13(2) :J67-J72 (1987).

Jones, W. P. and Lindstedt, R. P., (1988) *Combustion and Flame*, 73:233

Järvinen, M. P., Vakkilainen, E. K. and Kankkunen, A. (1997) Effects of Liquor Gun Type on Black Liquor Combustion, Tappi Engineering Conference, October 6 - 9, 1997. Nashville, TN, USA

Järvinen Mika, Zevenhoven Ron, Vakkilainen Esa, (2000) Rate Controlling Mechanisms During Black Liquor Char Conversion-Effect of Particle Size and Temperature. Nordic Seminar - Thermochemical conversion of biofuels, Trondheim.

Järvinen, M., Zevenhoven R. & Vakkilainen, E. (1999) Auto-gasification Phenomena in Black Liquor Combustion, Nordic Seminar-Single Particle Conversion, Trondheim, 21.10.1999

Järvinen Mika, Zevenhoven Ron, Vakkilainen Esa. (2000) Rate Controlling Mechanisms During Black Liquor Char Conversion-Effect of Particle Size and Temperature. Nordic Seminar - Thermochemical conversion of biofuels, Trondheim, 21.11.2000

Kankkunen, A., Miikkulainen, P. and Järvinen, M., (2001) *2001 International Chemical Recovery Conference*, Whistler, BC, Canada, June 11-14, 2001, PAPTAC, Canada pp. 51-54

Kochesfahani, S. H., Tran, H. (2001) Formation of intermediate sized particles (ISP) during black liquor combustion, presented in International Chemical Recovery Conference, Chateau Whistler Resort, Whistler, BC, Canada, 11-14 June 2001

Kulas, K. A., (1990) An overall Model of the Combustion of a Single Black Liquor Droplet of Kraft Black Liquor, Doctors Thesis, Institute of Paper Science and Technology, USA

Li, J. and van Heiningen, A R. P., (1990a) Kinetics of CO_2 gasification of fast devolatilization black liquor char, *Ind. Eng. Chem. Res*. 29:1776

Li, J. and van Heiningen, A. R. P., (1990b) *Tappi Journal.,* 73:213

Li, J. and van Heiningen, A. R. P., (1991) Kinetics of gasification of black liquor char by steam, *Ind. Eng. Chem. Res*., 30:1594

Macek, A., (1999) Research on combustion of black-liquor drops, *Progress in Energy and Combustion Science* 25:275

Manninen, J., Vakkilainen, E. (1996) Reduction of sulphur emissions from kraft recovery furnace with black liquor heat treatment. 29th Latin American Congress for Pulp and Paper. Sao Paulo, Brasilia , Associacao Brasileira Technica de Delulose e Paper

Mason, E. A. and Malinauskas, A. P., (1983) *Gas Transport in Porous Media: The Dusty Gas Model*. Elsevier, New York, USA

McCabe, W. L., Smith, J. C. and Harriot, P., (1993) *Unit Operations of Chemical Engineering*. McGraw-Hill, USA p. 839

McKeough, P. M., Arpiainen, V., Venelampi, E. and Alén, R. (1994) Rapid devolatilization of Kraft Black Liquor. Part 1. Release of carbon, Paperi ja Puu 76(10), 650-656.

Merriam, R. L. (1980) Kraft, version 2.0: Computer model of a kraft recovery furnace. American paper institute, Cambridge, MA

Miller, P. T., Clay, D. T., and Lonsky, W. F. W. (1989) The Influence of Composition on the Swelling of Kraft Black Liquor During Devolatilization, *Chem. Eng. Comm*., 75: 101-120.

Petersen, E. E., (1965) Chemical Reaction Analysis, Englewood Cliffs, N.J. Prentice Hall

Reis, V. V., Frederick, W. J., Wåg. K. J., Iisa, K. and Sinquefield, S. A. (1995) Effects of temperature and oxygen concentration on potassium and cloride enrichment during black-liquor combustion, Tappi J. 78(12), pp. 67-76.

Saastamoinen, J. J. and Aho, M. (1984) The simultaneous drying and devolatilization of single wood particles and pellets made of peat, American Flame Research Committee, 1984 International Symposium on Alternative Fuels and Hazardous wastes, October 9-11th, Tulsa, USA. Paper 2.1.

Saastamoinen, J. J., (1993a) Modelling of black liquor devolatilization, Nordic Seminar on Biomass and Gasification, NTH, Trondheim, Norway 30th August

Saastamoinen, J. J. and Kymäläinen, M., (1993b) Simultaneous drying and devolatilization of black liquor droplets, Swedish-Finnish Flame Days 1993, Gothenburg, Sweden, 7-8th September.

Saastamoinen, J. J., (1996a) Modelling of drying, devolatilization and swelling of black liquor droplets, AIChE Symposium Series 92: 311 74

Saastamoinen, J. J., and Richard, J. R., (1996b) Simultaneous drying and devolatilization of solid fuel particles, *Combust. Flame* 106:288

Saastamoinen, J. J., (1996c) Formation and Combustion of char cenospheres from black liquor droplets, Nordic seminar on thermochemical conversion of solid fuels, Institute of Thermal Energy and Hydropower, Norwegian University of Science and Technology, NTH, Trondheim, Norway, 4-5th December.

Saastamoinen, J. (1997) Black liquor combustion model (In Finnish: Mustalipeän vapautumismalli), Liekki 2, Yearbook 1997, p. 823-832.

Saastamoinen, J. J. (2000) Combustion of a pulverized wood particle – a modeling study, Nordic Seminar - Thermochemical conversion of biofuels, Institute of Thermal Energy and Hydropower, Norwegian University of Science and Technology, 21th November 2000, Trondheim, Norway.

Salmi, T. and Wärnå, J. (1991) *Computers & Chemical Engineering* , 15: 715

Saviharju, K., Moilanen, A. and Heiningen, A. R. P. (1995) New High Pressure Gasification Rate Data on Fast Devolatilization of Black Liquor Char". *1995 International Chemical Recovery Conference, Toronto, Ontario, Canada*, Tappi Press, A237-243.

Shick, P. E. (1986) Predictive simulation of recovery furnace processes on a microcomputer. Tappi 1986 Recovery Operations Seminar, Orlando, FL, pp. 121-133

Siegel, R. and Howell, J. R. (1992) Thermal Radiation Heat Transfer. Third Edition. Taylor & Francis, Washington, pp. 286-303, pp. 821-841

Solomon, P. R. and Colket, M. B. (1979) Coal devolatilization, 17th symposium (International) on combustion, the combustion institute, Pittsburgh, PA 131.

Sricharoenchaikul V., Frederick, W.J. (1995) Thermal Conversion of Light Gases During Black Liquor Devolatilization, In: 1995 International Chemical Recovery Conference, Toronto, Ontario, Canada, p. A209-A216

Tamminen, T. Kiuru, J., Kiuru, R., Janka, K. and Hupa, M. (2001) Dust flue gas chemistry during rapid changes in boiler load – full scale mill studies, presented in International Chemical Recovery Conference, Chateau Whistler Resort, Whistler, BC, Canada, 11-14 June 2001

Tannehill, J. C., Anderson, D. A. and Pletcher, R. H, (1984) *Computational Fluid Mechanics and Heat Transfer*. Taylor & Francis, USA, p. 715.

Thunman, H. (1994) Combustion of black liquor droplets in a recovery boiler (In Swedish: Förbränning av svartlutsdroppar I en sodapanna), Chalmers University of Technology, Sweden.

van Heiningen, A. R. P., Arpiainen, V. T. and Alén, R., (1992) Effect of liquor type and devolatilization rate on the steam gasification reactivities of black liquors, *1992 International Chemical Recovery Conference*, Westin Hotel, Seattle, WA, June 7-11, Tappi Press, Atlanta pp. 641-649

Verrill, C. L., Nichols, K. M. (1994) Inorganic Aerosol Formation During Black Liquor Drop Combustion, Advances in Forest Products Environmental and Process Engineering, AIChE Symposium Series, 302, Vol. 90, pp. 55-72.

Verrill, L. V. and Wessel, A. R., (1995a) Sodium Loss During Black Liquor Drying and Devolatilization - Application of Modeling Results to Understanding Laboratory Data. *1995 International Chemical Recovery Conference*, Toronto, Ontario, Canada, Tappi Press, Atlanta, pp. B89-B103.

Verrill, C. L., McIlroy, R. A., Southards, W. T., Wessel, R. A. and Clement, J. L. (1995b) Recovery Furnace Simulator – Design and Modeling, *1995 International Chemical Recovery Conference*, Royal York Hotel, Toronto, Ontario, Canada, Tappi Press, Atlanta (1995) pp. A111-122

Verrill, L. V. and Wessel, A. R., (1998) Detailed Black Liquor Drop Combustion Model for Predicting Fume in Kraft Recovery Boilers, *Tappi J.* 81:9, 139

Walsh, A. R. A (1989a) Computer Model for In-Flight Black Liquor Combustion in a Kraft Recovery Furnace, Doctors Thesis, Institute of Paper Chemistry, USA.

Walsh, A. R. and Grace, T. M., (1989b) TRAC – A Computer Model to Analyze the Trajectory and Combustion Behavior of Black Liquor Droplets, J. Pulp and Paper Sci. 15:3, 84

Wessel, R. A., Parker, K. L. and Verrill, L. C. (1997) Three-dimensional Kraft Recovery Furnace Model: Implementation and Results of Improved Black Liquor Combustion Models, *Tappi J.* 80:10, 207.

Wessel, R. A., Denison, M. K. and Samretvanich, A., (2000) The effect of fume on radiative heat transfer in kraft recovery boilers, *Tappi J.* 83

Whitty, K., (1997) Devolatilization and Gasification Behavior of Black Liquor under Pressurized Conditions. PhD thesis, Report 97-3, Åbo Akademi University, Turku, Finland.

Wåg, K. J., Reis, V. V., Frederick, W. J. and Grace, T. M. (1995a) Release of inorganic emissions during black liquor char combustion: A predictive model, 1995 Engineering conference, TAPPI Proceedings, Tappi Press.

Wåg, K.J., Grace, T.M. and Kymäläinen, M., (1995b) Sulfate reduction and carbon removal during kraft char burning, 1995 International Chemical Recovery Conference, Royal York Hotel, Toronto, Ontario, Canada, Tappi Press, Atlanta pp. B35-B50.

Wåg, K. J., Reis, V. V., Frederick, W. J. and Grace, T. M. (1997a) Mathematical Model for the Release of Inorganic Emissions During Black Liquor Char Combustion, Tappi J. 80:5 135

Wåg, K. J. Frederick. W. J., Dayton, D. C. and Kelley, S. S. (1997b) Characterization of Black Liquor Char Gasification Using Thermogravimetry and Molecular Beam Mass Spectrometry, AIChE Symposium Series, No. 315, Vol. 63, p. 67-76

Zevenhoven, R. and Hupa, M. (1997) Characterization of Solid Fuels for Advanced Pressurized Combustion and Gasification, *Proceedings of the 14th International Conference on Fluidized Bed Combustion*, ASME, New York, USA, 1997, pp. 213-227.